Biological/chemical sensing system based on degradable hydrogel with fiber optics or microfluidics

By

Xiudong Wu

A dissertation submitted in partial fulfillment of

the requirements for the degree of

Doctor of Philosophy

(Electrical and Computer Engineering)

at the

UNIVERSITY OF WISCONSIN – MADISON

2017

Date of final oral examination: 08/07/2017

The dissertation is approved by the following members of the Final Oral Committee:

Hongrui Jiang. Professor, Professor, Electrical and Computer Engineering

Nader Behdad. Professor, Professor, Electrical and Computer Engineering

Zongfu Yu. Professor, Assistant Professor, Electrical and Computer Engineering

Xudong Wang. Professor, Associate Professor, Materials Science and Engineering

Sangkee Min. Professor, Assistant Professor, Mechanical Engineering

ABSTRACT

We developed a prototype of PAAm-based sensor platform which can be used to detect chemical- and bio- agent with low-cost, easy-to-use, fast screening, and in-site detecting tool. By changing the crosslinker of the hydrogel, various agents could be detected. We also introduced microfluidics and fiber-optics together to improve the sensitivity of the sensor. So far, we had realized detecting chemical agent, DTT, and especially the most natural toxic substrate, BoNT.

First, we fundamentally proved an idea: the PAAm-based degradable hydrogel could be used to detect chemical- and bio-agent. By exchanging the cross-linkers, various related target regent could be detected through the degradable PAAm hydrogel. In this work, DTT and BoNT were selected as agents, and the related cross-linkers for these two agents were N, N' – bis(Acryloyl) crystamine and modified SNAP 25-mer peptide. Through the detection of the two agents, the idea was fundamentally proved. During this process, we also found the flow control was important to the degradation of the hydrogel and could be used to enhance the sensitivity and speed up the detecting process.

Second, we introduced a microfluidic structure to our sensing system, and developed a new microfluidics-based PAAm hydrogel sensor, which incorporates a modified SNAP-25 peptide for the detection of BoNT/A. The BoNT/A can be detected by direct observation of the morphology change of the hydrogel. The best response of the BoNT/A sensing hydrogel we achieved within 22 h at 45 μg/mL of LC, and the lowest LC concentration of 4.5 μg/ in 90 h, with hydrogel post 200 μm in

diameter and 50 μm in thickness. The hydrogels remained intact in both control buffer and DTT solutions.

Third, the mechanism of the above detecting was only based on naked human eyes, and almost all the hydrogel needs to be cleaved by target agent to allow the obvious changes that could be observed by naked human eyes. Once the target agent contacted the hydrogel, the change of the hydrogel would start. Therefore, we introduced the fiber-optics to further improve the sensitivity of our device. The optic fiber FPI device significantly improved the detection sensitivity and efficiency of biological and chemical sensors based on the degradation of hydrogels. The hydrogels that we used belong to PAAm hydrogel. By introducing the interfering optics shown in this work, such changes can be detected as the evidence of hydrogel cleavage. Our FPI device increased the detection sensitivity of DTT by 2000 times, and greatly reduced the detection period by several times in comparison with the previous work. We demonstrated a low concentration of detection of 50 mM of DTT within 36 min. In the future, we will explore to further improve the sensitivity and the detection speed by reducing the thickness of the hydrogel to accelerate the liquid diffusion and hydrogel reaction process. The centimeter-sized FPI sensors are promising for high-precision, ultra-sensitive, and fast in-field detection of biological and chemical agents. Finally, by combining the fiber optics with microfluidics, we fundamentally confirmed the combination can increase the detecting speed for our biological/chemical sensing system based on degradable hydrogel. We also believe it could enhance the sensitivity of our sensing system. Specifically, the LC of 4.5 μg/ml was detected in 24 hours. In comparison with the previous detecting time of 90 hours, the detecting speed was enhanced by around 4 times. By following on this research,

we believe it could further enhance the sensitivity and detecting speed of our sensing system.

ACKNOWLEDGEMENTS

I would like to thank all the people who have supported me and helped me during this amazing journey pursuing my PhD degree. My research was performed under the guidance of Professor Hongrui Jiang. I appreciate the opportunity and enjoy the journey of working in his lab as a research assistant. His kindness, integrity, diligence, and wisdom enlightened me over the past several years and will continue to enlighten the rest of my life. Especially, it is one saying he told to me that I would keep in my heart for ever: now we are advisor-student relationship, and after you graduated, we would be friends, and I hope we are friends forever. Actually, limited by English, I could not repeat the words exactly, but the meaning of the saying had engraved on my mind. It is my honor and luck to be one of the students of Prof. Hongrui Jiang.

I am also grateful to my committee members - Professor Nader Behdad, Professor Zongfu Yu, Professor Sangkee Min, and Professor Xudong Wang, for their suggestions.

It is a great pleasure to work with my labmates, collaborators classmates, such as Chi-Chieh Huang, Yen-Sheng Lu, Xuezhen Huang, Hewei Liu, Xi Zhang, Hao Bian, Yinggang Huang, Ye Liu, Chensha Li, Bader Aldalali, Chenhui Li, Jayer Fernandes, and Yuelin Peng, Xuan Zhang. They helped me so much on academic and courses. Six years before, one of my labmates had a saying to me. She thought any of my successes or achievement would base on others' help. I really feel that her saying is definitely true and I really think that the cooperation with others is one of the most important factors to realize any achievement. Thanks again for those persons helped me to achieve my PhD. Without your help, I could not reach this point. Here, I would

like to mention my previous advisor, Shengyong Xu, during my master at Beijing University in China. Actually, he did not give me any help directly for my PhD, but during the three years, he served as my advisor for my master in China, he taught me so much. The learning I got from him helped me so much during my PhD in US. I really feel I am a lucky guy, as so far I already had two wonderful advisors in my life, Hongrui Jiang and Shengyong Xu. Thanks a lot!!!

Finally, we would appreciate my family, the most important person in my life. My wife, my son, my parents, and my brother, they are my powerful backing, and they could always give me immediately help. Thanks again for all the persons who offer their favor. Without your kindness, I could not realize any achievement.

Contents

LIST OF FIGURES

CHAPTER 1. INTRODUCTION

1.1 Hydrogel and polyacrylamide (PAAm) hydrogel

Hydrogel could be regarded as one large molecule on the macroscale with cross-linked 3-D hydrophilic polymer network containing significant amounts of water (70-99 %wt) [1-4]. Moreover, due to its physiochemical similarity with the native extracellular matrix in both compositionally and mechanically, hydrogel has a great biocompatibility [5]. Great efforts have been made in this area, in which the first research on hydrogels could be traced back as early as as 1960s to a poly (2-hydroxyethyl methacrylate) related paper by Wichterle et al [6]. To date, due to its intrinsic half-liquid and half-solid characteristic, hydrogel was used in a broad range of applications such as pharmaceutical and biomedical [7-12], soft electronics, soft robotics and machines [12, 13]. In order to satisfy the requirement in various applications, a large number of hydrogel had been developed, like agarose [14-16], hydroluronic acid [17-19], alginate [20-22], Polyhydroxyethylmethacrylate (pHEMA) [23-25],Poly ethyleneglycol (PEG) [26-28], and Poly vinylalcohol (PVA) [29-30].

Based on the different types of cross-linking, those hydrogels can be classified into two categories: the physically cross-linked hydrogelandchemically cross-linkedhydrogel. Physically cross-linked hydrogel refers to the absence of cross-linkers for synthesis. These hydrogels are cross-linked by physical interactions, such as hydrogen bonds [31-32], crystallization [33], ionic interactions [34, 35], or protein interaction [36, 37]. In the network structure of physically cross-linked hydrogel, the transient junctions, referring to various physical interactions mentioned above are involved. All of these physical interactions are reversible, and the status of these

hydrogel could be affected by the variation of physical conditions such as temperature, pH, application of stress, or ionic strength. Based on this principle, lots of related sensors were developed, such as temperature sensor [38], pH sensor [39], stress sensor [40], solvent composition and specific ions [41, 42]. Chemically crosslinked hydrogel refers to hydrogel 3D network structure with permanent junctions and/orcovalent linkages. These chemical hydrogels are formed by adding a cross-linking reagent to a polymer through a chemical reaction, such as adding complementary group to cross-link polymer chains under high energy radiation [43, 44]. The related chemical cross-linkages are based on covalent bonds. Covalent bond is a permanent junction, and is irreversible for the change of the shape or other features of these hydrogels resulting from breaking down of the cross linkage, such as the change of refractive index based on the cleavage of the cross-linker of the hydrogel [45]. Chemical cross-linking makes the hydrogel really stable with excellent mechanical strength [46]. In conclusion, the physical properties, such as the shape and the refractive index, of the hydrogel could be mainly affected by the chemical linkage density, while they could be only slightly affected by physical conditions, such as temperature, pH, or pressure.

Among tons of chemical hydrogels, PAAm is one of great popular, and has been used in a large number of applications [47-54]. The PAAm hydrogel is made of acrylamide (AAm) monomers. The monomer consists of a $CONH_2$ group and a carbon double bond, which makes it extremely suitable to cross-link many other monomers. Therefore, the property of the hydrogel can be varied by adjusting the synthesis conditions, by copolymerization with other monomers and/or cross-linkers, or through chemical modification of the synthesized hydrogel [55-57]. Because the

PAAm hydrogel is one of chemical hydrogels with covalently cross-linkage, it has good mechanical strength, and these chemical cross-linkages could be made to be biodegradable or chemical-degradable. The density of the cross-linkage is one of the overwhelming determinant factors, which could affect the physical property of the hydrogel. The cross-linker itself would determine the chemical property of the hydrogel [58]. Specifically, the cross-linker cross-linked the hydrogel monomers polymer chains, and the hydrogel became a solid gel status from its previous liquid status. When the cross-linker in the hydrogel matrix was cleaved by the target agent, the network structure of the hydrogel broke down, meanwhile the hydrogel became pasty and laterly totally water-soluble. During this cleavage process, the density of the cross-linkage would decrease, while the corresponding physical properties of the hydrogel, such as morphology, and refractive index of the hydrogel, would change. By taking a special agent as the cross-linker which could be cleaved by a related target chemical- or bio-agent, the hydrogel could be potentially used to detect the target agent, due to its dramatically morphology change or other physical property changes of the hydrogel resulting from the degradation. Based on this feature, several types of sensors had been developed [52, 59].

1.2 The detection of biological agents, and PAAm-hydrogel-based biological agent detection

The detection of biological agents, especially biotoxins, plays a crucial role in a broad range of applications related to biodenfense, environmental monitoring, food safety and public health [60], [61]. A large variety of detection schemes based on different principles have been developed, such as mouse lethality assay [62], enzyme-

linked chemiluminescence assay [63-67], electrochemiluminescence [68], immune/real-time-polymerase chain reaction (PCR) [69], [70], cell culture assay [71-72], surface plasmon resonance (SPR) [62, 73], and mass-spectrometry [74]. Despite their high sensitivity, these methods generally require time-consuming sample preparation or long incubation time, high-cost, complicated instrument and skilled personnel, hereby they are generally not suitable for in-field detecting [73]. In addition, some of these methods, such as mass-spectrometry, cannot distinguish between active and inactive biotoxins [74]. However, swift in-field testing is often of utmost importance in biodefense [75]. Therefore, there is enormous demand for a low-cost, easy-to-use, fast screening tool that allows for rapid in-field detection of active biotoxins with high sensitivity and specificity.

Sridharamurthy et al. [59] previously reported on an autonomous sensing mechanism based on a polyacrylamide (PAAm) hydrogel. In this method, a cross-linker cross-links water-soluble acrylamide chains to water insoluble network hydrogel (Fig. 1.1 (a, b)). The cross-linker can be cleaved by a specific agent. The hydrogel thus degrades and becomes water-soluble after the cleavage, revealing the presence of the toxin in the sample (Fig. 1.1 (c, d)). Various biological agents could be detected by utilizing different cross-linkers. This approach exploits the intrinsic protease activity of the corresponding enzyme and thereby leverages the inherent amplification function associated with the target enzyme. Therefore, the potential sensitivity and specificity of this method could be extremely high. In addition, it is well suited for detecting biotoxins, because many of them are proteases. For example, active botulinum neurotoxins (BoNT) could be detected with this method using a synaptosomal-associated protein (SNAP) 25-mer peptide as the cross-linker [52].

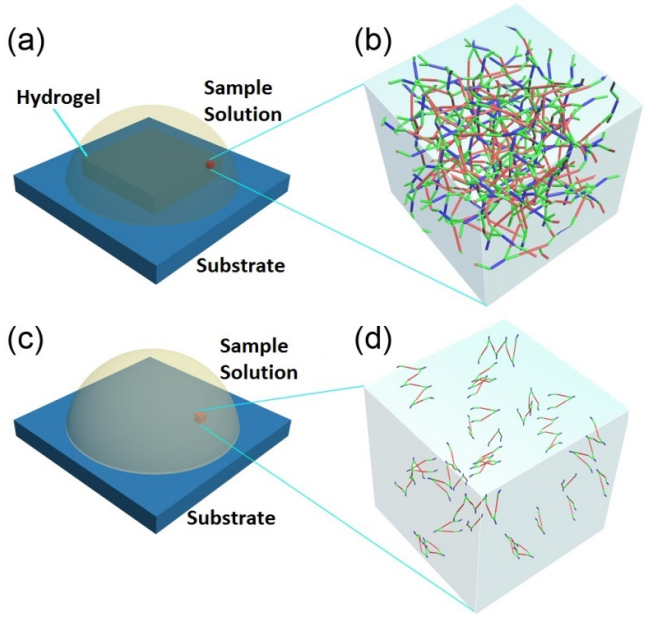

Fig. 1.1: Schematic of the cleavage of hydrogel by BoNT/A toxin. (a, b) The original network structure of the hydrogel. (c, d) The degraded hydrogel network in the sample solution after cleavage.

1.3 Clostridium botulinum Neurotoxins (BoNTs) and related detecting methods

1.3.1 BoNTs and current detecting methods

BoNTs, the most toxic substance known to humans with a median lethal dose (LD50) of approximately 1 ng/kg body weight, have attracted much attention in the last few decades due to their potential use as a bioterrorism agent [52, 76-79]. BoNTs have traditionally been immunologically distinguished into seven serotypes (BoNT/A–G), among which BoNTs A, B, E and F are known to cause human botulism [80, 81]. An accidental or deliberate release of BoNTs in civilian population, especially in food supply, would seriously threaten human health and may cause panic

resulting in large economic losses. Especially, it would be used by terrorists as bioweapon [66, 82]. Actually, the attempts for using BoNT as bioweapon by terrorists have been done for several times [67, 68]. Moreover, early detection is significantly important, particularly early detection in the first 72 hours would avoid 2/3 casualties [73].

Therefore, highly sensitivity and facile assays in the early stage are essential to harness outbreak or controlled distribution of BoNTs. The current gold standard for detection of the seven serotypes of Clostridium botulinum neurotoxin (BoNT/A-G) is the mouse bioassay [83, 84]. Due to the high cost, low throughput and the need for highly trained personnel and large number of animal sacrifices, a practical alternative to the mouse bioassay is needed.

To date, much efforts have been made to improve the technologies to sense the presence of BoNTs either in vivo (testing in animals) or in vitro, such as enzyme-linked immunosorbent assay (ELISA) [63, 69, 85], immune/real-time-polymerase chain reaction (PCR) [86, 87], mass spectrometry [88], cell culture assays [89, 90], as well as others [91-93]. These tools generally require complex instrumentation and are not suitable for in-field testing. Furthermore, some of these assays are not able to distinguish between active and inactive BoNTs.

1.3.2 Previous PAAm hydrogel-based BoNTs detecting sensor and its drawbacks

An alternative highly efficient toxin-screening approach developed by M. Frisk et al. [52] used a PAAm-based hydrogel with a synthetic synaptosomal-associated protein of 25-kDa (SNAP-25) substrate peptide as cross-linker to detect BoNT/A.

Peptide integrated hydrogels had been used as sacrificial structures by decomposition in the presence of a stimulus, such as an enzyme. SNAP-25 is one of the three synaptic proteins recognized by the 50-kDa light chain (LC) of BoNT/A in the proteolytic activity leading to paralysis [94, 95]. Thus the decomposition of a hydrogel combined with SNAP-25 modified cross-linker in the presence of BoNTs provides a rapid and accurate detection for the active BoNTs [52].

Although the polyacrylamide (PAAm) hydrogel with SNAP 25-mer (sequence: CGGGSNRTRIDEANQRATR{Nle}LGG- GC) containing a cross-linker developed in the previous work [52] showed sensing capabilities with both LC and BoNT/A, the disulfide bonds in the hydrogel were not stable under reducing conditions and could cause a false positive alert, which limits its application as an on-site sensor for BoNT/A. This is particularly problematic *in vitro* since BoNT/A requires reduction for full activity in substrate cleavage assays. In addition, PAAm SNAP peptide hydrogels without disulfide bonds were investigated to detect BoNT/A. The poor degradation of gels observed was associated with the conjugation points that seemed to prevent the cross-linked portion from being cleaved by BoNT/A [52]. To develop an on-site BoNT hydrogel sensor with higher accuracy, it is important to develop a new SNAP-25 peptide hydrogel without disulfide bonds, where the SNAP-25 has optimized conjugation sites for the cross-linker such as acryloyl-PEG-NHS (APN) to anchor.

1.4 Microfluidics

Microfluidics refers to creating structures and patterns with dimensions of tens to hundreds of microns, and transporting or manipulating small amount of fluids. During

the last three decades, microfluidics has triggered a wide range of scientific investigations, and achieved many applications in many of areas, such as micromechanical vavels and micromixers [96, 97], micropumps [98], chromatography [99], electrophoretic separation systems [100], electro-osmotic pumping systems [101], diffusive separation systems [102], cytometers [103], chemical microreactors [104], drug development [105], and bioanalyses [106]. Especially, it shows a number of useful capabilities in the field of chemical- and bio-analysis, such as short-time analysis, fluid-flow control, usage of very small quantity of samples, low cost, and minimization of the device size [107].

Novo et al. reported a microfluidics system based point-of-care prototype system [108]. This system integrated capillary microfluidics with chemiluminescence ELISA, microfabricated photodiode array and electronic instrumentation into a hand-held unit, and realized a related detection with limit-of-detection of 2 nM, which is a great performance comparable to a traditional bench-top instrumentation. Due to the introduction of microfluidics, it miniaturizes the biosensor, and enables a development of a point-of-care device. The microfluidics also offered the device with some added advantages, such as reduced time and low cost, in comparison with the traditional laboratory techniques. Specifically, capillary microfluidic structures were integrated to the device to control fluid flow autonomously and sequentially, including the average fluid velocity at any giving point of the device.Fig. 1.2 shows the schematics of such device.

In addition, some of the research achievement had been commercialized in the market. For example, the company Biosite has developed a commercial system that

could take only one drop of blood from a patient to analyze the blood. The Biosite device not only enables the blood analysis portable, but also significantly reduce the time of blood analysis in 15 min, while traditional system needs several hours [109].

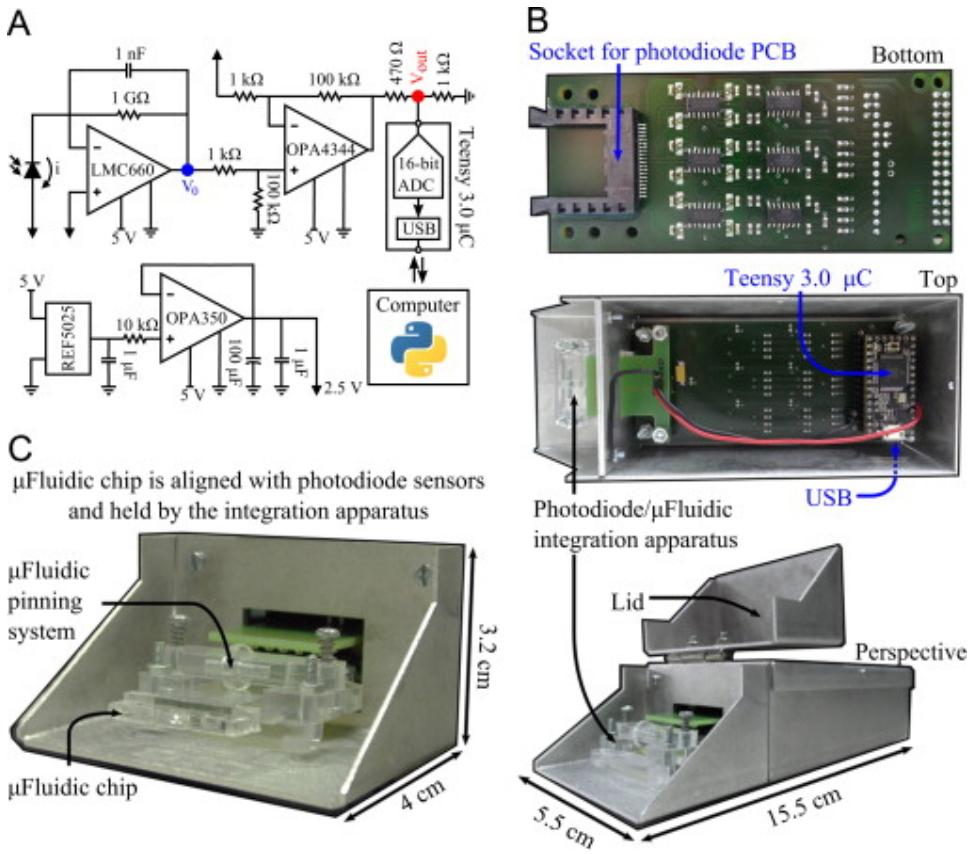

Fig. 1.2: PoC prototype device details. (A) Photodiode amplification circuit schematics, (B) a hand-held prototype box: (top) bottom view of the amplifier circuit board highlighting the socket where the PCB of Fig. 1-B is inserted; (middle) top view of the prototype box containing the amplifier circuit and the Teensy 3.0 microcontroller; (bottom) perspective view of the closed aluminum prototype box and (C) magnified perspective view of the microfluidics integration apparatus: the photodiode PCB and machined PMMA ensemble align and fix the microfluidic device to the photodiodes [41].

1.5 Fiber Optic Sensor

Due to the development of the laser in 1960, and the modern low-loss optical fibers in 1966, fiber optics was firstly used for sensor purposes at the early 1970s [110]. Since when the field of fiber optic sensor has continued to progress and developed enormously. Compared to other type of sensors, fiber optic sensors exhibit lots of advantages: compact and light weight, minimally invasive, immune to electromagnetic interference, no electrical currents flowing at sensing point, multiplexing capabilities, and chemical passivity [111, 112]. Later, a wide range of optical-fiber based sensors were developed for a variety of different sensing purpose, such as pressure, temperature, displacement, magnetic, and acceleration [110, 111, 113]. Those sensors could be broadly classified as extrinsic or intrinsic, based on modifying one or more properties of light passing through the fiber. Furthermore, they could be classified into to four main types, depending on the light property modified. The four types are intensity-modulated sensor, phase-modulated sensor, polarization-modulated sensor, and wavelength-modulated sensor [114]. Among these four types of sensors, the phase-modulated sensor is also known as interferometric sensor. The interferometric sensor works based on phase difference of coherent light traveling along two different paths, in the same fiber or different fibers. In general, it is considered as high-sensitivity sensors, due to its capability to respond to small changes of certain particular physical parameters. The use of interferometric measurement has been well established for many decades [115, 116-118]. Sensors based on fiber-based interferometers have been widely studied in the detection of pH [67], glucose [68] and bacteria [69] owing to its small size, in-line structures and high

sensitivity [70], [71]. In this report, the interferometric sensing was used to increase the sensitivity of our sensor.

1.6 Organization of this report

In this work, a biological/chemical sensing system based on degradable PAAm-based hydrogel with fiber optics or microfluidics was reported. The physical and chemical features of the PAAm-based degradable hydrogel were discussed, including the synthesis and cleavage reaction of the hydrogel. Two different hydrogels were described and the ways that these two hydrogels were used to detect two different agents were discussed, respectively. The introduction of the microfluidics to the sensing system to enhance the sensitivity and detecting speed was investigated. The introduction of fiber optics used to increase the sensitivity of the sensing system was also discussed.

The report is organized as follows:

Chapter 2 introduced two types of PAAm-based hydrogel, one could be used to detect DTT, while the other could be used to detect BoNT. The chapter also described how those two hydrogel used as Sensing Elements for Bio-/ chemical agent Detection.

Chapter 3 introduced a microfluidic detection of BoNT utilizing PAAm hydrogels with SNAP-25 peptide cross-linker, and described the instruction of microfluidics relative high sensitivity and fast detection speed.

Chapter 4 introduced a fiber optic biological/chemical sensing system which was based on degradable hydrogel, and described the introduction of the fiber optics enhance the sensitivity of the previous sensing system.

Chapter 5 combined the microfluidics and fiber optics together to further enhance the detecting speed and sensitivity.

Chapter 5 summarized the current work, and pointed out new directions for possible future work.

1.7 Reference

[1] A. K. F. Gerlach G, *Hydrogel Sensors and Biosensors*, Springer, Berlin 2010.

[2] N.A. Peppas, Hydrogels in Medicine and Pharmacy, vol. 1, CRC Press, 1986.

[3] H. Park, K. Park, Hydrogels in bioapplications, in: R.M. Ottenbrite, S.J. Huang, K. Park (Eds.), Hydrogels and Biodegradable Polymers for Bioapplications, American Chemical Society, Washington, DC, 1996, pp. 2–10.

[4] V. Kudela, Encyclopedia of Polymer Science and Engineering, Wiley, New York, 1987.

[5] T.R. Hoare, D.S. Kohane, Hydrogels in drug delivery: progress and challenges,Polymer 49 (8) (2008) 1993–2007.

[6] O. Wichterle, D. Lim, Hydrophilic gels in biological use, Nature 185 (1960) 117–118.

[7] Hoffman, A. S. Hydrogels for Biomedical Applications. Adv. Drug Delivery Rev. 2002, 54 (1), 3−12.

[8] Peppas, N. A.; Bures, P.; Leobandung, W.; Ichikawa, H. Hydrogels in Pharmaceutical Formulations. Eur. J. Pharm. Biopharm. 2000, 50, 27.46.

[9] Kopec.ek, J. Hydrogel Biomaterials: A Smart Future? Biomaterials 2007, 28 (34), 5185.5192.

[10] Haque, M. A.; Kurokawa, T.; Gong, J. P. Anisotropic Hydrogel Based On Bilayers: Color, Strength, Toughness, And Fatigue Resistance. Soft Matter 2012, 8 (31), 8008.8016.

[11] Huynh, C. T.; Nguyen, M. K.; Lee, D. S. Injectable Block Copolymer Hydrogels: Achievements and Future Challenges for Biomedical Applications. Macromolecules 2011, 44 (17), 6629.6636.

[12] Lee, W.; Cho, N.-J.; Xiong, A.; Glenn, J. S.; Frank, C. W. Hydrophobic Nanoparticles Improve Permeability Of Cell-Encapsulating Poly (Ethylene Glycol) Hydrogels While Maintaining Patternability. Proc. Natl. Acad. Sci. U. S. A. 2010, 107 (48), 20709.20714.

[13] P. Calvert, Adv. Mater. 2009, 21, 743.

[14] Lee, H., McKeon, R. J., and Bellamkonda, R. V. (2010), Sustained delivery of thermostabilized chABC enhances axonal sproutingand functional recovery after spinal cord injury. Proc. Natl. Acad. Sci.U.S.A. 107, 3340–3345.

[15] Chvatal, S. A., Kim, Y. T., Bratt-Leal, A. M., Lee, H. J., andBellamkonda, R. V. (2008), Spatial distribution and acute anti-inflammatoryeffects of Methylprednisolone after sustained local delivery tothe contused spinal cord. Biomaterials 29, 1967–1975.

[16] Jain, A., McKeon, R. J., Brady-Kalnay, S. M., and Bellamkonda,R. V. (2011), Sustained Delivery of Activated Rho GTPases and BDNFPromotes Axon Growth in CSPG-Rich Regions Following Spinal CordInjury. PloS One 6, 1–12.

[17] Wei, Y. T., He, Y., Xu, C. L., Wang, Y., Liu, B. F., Wang, X. M.,Sun, X. D., Cui, F. Z., and Xu, Q. Y. (2010), Hyaluronic acid hydrogelmodified with nogo-66 receptor antibody and poly-(L)-lysine to promoteaxon regrowth after spinal cord injury. J. Biomed. Mater. Res., Part B

95B, 110–117.

[18] Wei, Y. T., Tian, W. M., Yu, X., Cui, F. Z., Hou, S. P., Xu, Q. Y.,and Lee, I. S. (2007), Hyaluronic acid hydrogels with IKVAV peptides fortissue repair and axonal regeneration in an injured rat brain. Biomed.Mater.2, S142–S146.

[19] Tian, W. M., Zhang, C. L., Hou, S. P., Yu, X., Cui, F. Z., Xu,Q. Y., Sheng, S. L., Cui, H., and Li, H. D. (2005), Hyaluronic acidhydrogel as Nogo-66 receptor antibody delivery system for the repairingof injured rat brain: in vitro. J. Controlled Release 102, 13–22.

[20] Prang, P., Muller, R., Eljaouhari, A., Heckmann, K., Kunz, W.,Weber, T., Faber, C., Vroemen, M., Bogdahn, U., and Weidner, N.(2006),The promotion of oriented axonal regrowth in the injured spinalcord by alginate-based anisotropic capillary hydrogels. Biomaterials27, 3560–3569.

[21] Banerjee, A., Arha, M., Choudhary, S., Ashton, R. S., Bhatia,S. R., Schaffer, D. V., and Kane, R. S. (2009), The influence of hydrogelmodulus on the proliferation and differentiation of encapsulated neuralstem cells. Biomaterials 30, 4695–4699.

[22] Shanbhag, M. S., Lathia, J. D., Mughal, M. R., Francis, N. L.,Pashos, N., Mattson, M. P., and Wheatley, M. A. (2010) NeuralProgenitor Cells Grown on Hydrogel Surfaces Respond to the Productof the Transgene of Encapsulated Genetically Engineered Fibroblasts.Biomacromolecules 11, 2936–2943.

[23] Kubinova S, Horak D, Kozubenko N, Vanecek V, Proks V, Price J, Cocks G, Sykova E (2010), The use of superporous Ac-CGGASIKVAVS-OH-modified PHEMA scaffolds to promote celladhesion and the differentiation of human fetal neural precursors. Biomaterials 31:5966–5975

[24] Kubinova S, Horak D, Sykova E (2009), Cholesterol-modified superporous poly(2-hydroxyethyl methacrylate) scaffolds for tissue engineering. Biomaterials 30:4601–4609

[25] Kumar N, Ganapathy H, Kim J, Jeong YS, Jeong YT (2008), Preparation of poly2-hydroxyethyl methacrylate functionalized carbon nanotubes as novel biomaterialnanocomposites. Eur Polym J 44:579–586

[26] Gong C, Shi S, Dong P-W, Kan B, Gou M, Wang XH, Li X-Y, Luo F, Zhao X, Wei Y-Q,Qian ZY (2009), Synthesis and characterization of PEG-PCL-PEG thermosensitive hydrogel.Int J Pharmaceutics 365:89–99

[27] Lin C, Anseth K (2008), Cell–cell communication mimicry with poly(ethylene glycol)hydrogels for enhancing β-cell function. Pharmac Res 26:6380–6385

[28] Kim B, Peppas N (2003),Poly(ethylene glycol)-containing hydro-gels for oral protein deliveryapplications. Biomed Microdevices 5:333–341

[29] Lum L, Elisseeff J (2003), Ch. 4 In: Ashammakhi N, Ferretti P (eds) Topics in tissue

engineering. University of Oulu, Oulu

[30] Li J, Wang N, Wu X (1998) Poly(vinyl alcohol) nanoparticles prepared by freezing- thawingprocess for protein/peptide drug delivery. J Control Release 56:117–126

[31] Eagland, D. et al, 1994. Complexation between polyoxyethylene andpolymethacrylic acid-the importance of the molar mass ofpolyethylene. Eur. Polym. J. 30, 767–773.

[32] Mathur, A.M. et al, 1998. Equilibrium swelling of poly(methacrylicacid-g-ethylene glycol) hydrogels. J. Control. Rel. 54, 177–184.

[33] Yokoyama, F. et al, 1986. Morphology and structure of highly elasticpoly(vinyl alcohol) hydrogel prepared by repeated freezing-andmelting.Colloid Polym. Sci. 264, 595–601.

[34] Goosen, M.F.A. et al, 1985. Optimization of microencapsulationparameters: semipermeable microcapsules as a bioartificial pancreas.Biotechnol.Bioeng. 27, 146–150.

[35] Gombotz, W.R., Wee, S.F., 1998. Protein release from alginatematrices.Adv. Drug Deliv. Rev. 31, 267–285.

[36] Yoshikawa, E. et al, 1994. Genetically engineered fluoropolymers.Synthesis of repetitive polypeptides containing p-fluorophenylalanineesidues. Macromolecules 27, 5471–5475.

[37] Cappello, J. et al, 1998. In-situ self-assembling protein polymer gelsystems for administration, delivery, and release of drugs. J.Control. Rel. 53, 105–117.

[38] Tanaka, T. Collapse of gels and the critical endpoint. Phys. Rev. Lett. 1978, 40 (12), 820 - 823.

[39] A. Richter, G. Paschew, S. Klatt, J. Lienig, K. F. Arndt and H. J. P. Adler, Sensors, 2008, 8, 561.

[40] Lang HP, Hegner M, Gerber C. Cantilever array sensors. MaterialsToday 2005;8:30–6.

[41] Irie, M.; Misumi, Y.; Tanaka, T. Stimuli-responsive polymers: chemical induced reversible phase separation of an aqueous solution of poly(N-isopropylacrylamide) with pendent crown ether groups. Polymer 1993, 34 (21), 4531 – 4535.

[42] Li, W.; Zhao, H.; Teasdale, P.R.; John, R.; Zhang, S. Synthesis and characterisation of a polyacrylamide-polyacrylic acid copolymer hydrogel for environmental analysis of Cu and Cd. React. Funct.Polym. 2002, 52, 31 – 41.

[43] Alla, S.G.A. et al, 2012. Swelling and mechanical properties ofsuperabsorbent hydrogels based on Tara gum/acrylic acid synthesizedby gamma radiation. Carbohydr.Polym. 89, 478–485.

[44] Amin, M.C.I.M. et al, 2012. Synthesis and characterization of thermoandpH-responsive bacterial cellulose/acrylic acid hydrogels fordrug delivery.Carbohydr.Polym. 88, 465–473.

[45] Garner, B. W.; Cai, T.; Ghosh, S.; Hu, Z.; Neogi, A. RefractiveIndex Change Due to Volume-Phase Transition inPolyacrylamide Gel Nanospheres for Optoelectronics andBio-photonics. Appl. Phys. Express 2009, 2, 057001-4.

[46] M. F. Akhtar; M. Hanif; N. M. Ranjha.(2015) Methods of synthesis of hydrogels.Saudi Pharmaceutical Journal.

[47] Nadler, A., E. Perfect, and B. D. Kay. 1996. Effect of polyacrylamide application on the stability of dry and wet aggregates. Soil Sci. Soc. Am. J. 60: 555–561.

[48] Sojka, R. E., R. D. Lentz, C. W. Ross, T. J. Trout, D. L. Bjorneberg, and J. K. Aase. 1998. Polyacrylamide effects on infiltration in irrigated agriculture. J. Soil Water. Conserv. 53: 325–331.

[49] Jobin, P., J. Caron, P. Bernier, and B. Dansereau. 2004. Impact of two hydrophilic acrylic-based polymers on the physical properties of three substrates and the growth of Petuniahybrida ‘Brilliant Pink.’ J. Am. Soc. Hortic. Sci. 129: 449–457.

[50] El-Rehim, H. A. A., E. A. Hegazy, and H. L. A. El-Mohdy. 2004. Radiation synthesis of hydrogels to enhance sandy soils water retention and increase plant performance. J. Appl. Polym. Sci. 93: 1360–1371.

[51] Al-Humaid, A. I., and A. E. Moftah. 2007. Effects of hydrophilic polymer on the survival of buttonwood seedlings grown under drought stress. J. Plant Nutr. 30: 53–66.

[52] M. L. Frisk, W. H. Tepp, G. Lin, E. A. Johnson, and D. J. Beebe, "Substrate-Modified Hydrogels for Autonomous Sensing of Botulinum Neurotoxin Type A," Chem. Mater, vol. 44, no. 19, pp. 5842-5844, 2007.

[53] X. Wu, C. Li, G. Lin, X. Huang, W. H. Tepp, E. A. Johnson, and H. Jiang, "Microfluidic Detection of Botulinum Neurotoxin Type A Utilizing Polyacrylamide Hydrogels," IEEE SENSORS JOURNAL, vol. 15, pp. 1091-1097, Feb. 2015.

[54] X. Wu et al., "A microfluidic sensor of botulinum neurotoxin type A utilizing SNAP-25 incorporated responsive hydrogel," IEEE Sensors, Baltimore, MD, USA, Nov. 2013, pp. 629–632.

[55] Saraydin, D., D. Karadag, and O. Guven. 2001. Use of superswelling acrylamide-maleicacid hydrogels for monovalent cationic dye adsorption. J. Appl. Polym. Sci. 79: 1809–1815.

[56] Guilherme, M. R., R. D. Silva, A. F. Rubira, G. Geuskens, and E. C. Muniz. 2004. Thermo-sensitive hydrogels membranes from PAAm networks and entangled PNIPAAm: Effect of temperature, cross-linking and PNIPAAm contents on the water uptake and permeability. React. Funct.Polym. 61: 223–243.

[57] Panayiotou, M., and R. Freitag. 2005. Influence of the synthesis conditions and ionic additives on the swelling behaviour of thermo-responsive polyalkylacrylamide hydrogels. Polymer 46: 6777–6785.

[58] Kosmas Deligkaris, Tadele Shiferaw Tadele, Wouter Olthuis, Albert van den Berg. Hydrogel-based devices for biomedical applications. Sensors and Actuators B 147 (2010) 765–774

[59] S. S. Sridharamurthy, A. K. Agarwal, D. J. Beebe and H. Jiang, "Dissolvable membranes as sensing elements for microfluidics based biological/chemical sensors," Lab on a Chip, vol. 6, pp. 840-842, May 2006.

[60] M.A.Hamburg, "Bioterrorism: responding to an emerging threat," *Trends Biotechnol*, vol. 20, pp. 296–298, July 2002.

[61] R. C. Spencer, N. F. Lightfoot, "Preparedness and Response to Bioterrorism," *Journal of Infection*, vol. 43, pp. 104–110, Sep. 2001.

[62] P. Cunniff, "Official Methods of Analysis of AOAC International," 16th ed. AOAC Intern Inc, Washington, pp. 46–48.

[63] R. W. Phillips, D. Abbott, "High-throughput enzyme-linked immunoabsorbant assay (ELISA) electrochemiluminescent detection of botulinum toxins in foods for food safety and defence purposes," *Food Addit Contam Part A*, vol. 25, pp. 1084-1088, Sep. 2008.

[64] B. Klaubert, N. Vujtovic-Ockenga, R. Wermter, K. Schad, L. MeyerL, "Determination of botulinum toxins after peptic sample pre-treatment by multidimensional nanoscale liquid chromatography and nano-electrospray ion-trap mass spectrometry," *J Chromatogr B*, vol. 877, pp. 1084-1092, Apr. 2009.

[65] A. Woolfitt, H. Moura, S. Kalb, C. P. Quinn, J. R.Barr, "Quantitative mass spectrometry for bacterial protein toxins-a sensitive, specific, high-throughput tool for detection and diagnosis," *Molecules*, vol. 16, pp. 2391-2413, 2011.

[66] D. R. Franz, P. B. Jahrling, A. M. Friedlander, et al "Clinical recognition and management of patients exposed to biological warfare agents," *JMMA*, vol. 278, pp. 399.411, Aug. 1997.

[67] J. B. Tucker, “Toxic Terror: Assessing the Terrorist Use of Chemical and Biological Weapons,” Cambridge, Mass: MIT Press, 2000.

[68] S. WuDunn, J. Miller, W. J. Broad, “How Japan germ terror alerted world,” New York Times, May 26, 1998:A1, A10.

[69] S. S. Arnon, R. Schechter, T. V. Inglesby, et al, “Botulinum Toxin as a Biological WeaponMedical and Public Health Management” *JMMA*, vol. 8, pp. 1059-1070, Feb. 2001.

[70] E. Aranda, M/ M. Rodriguez, M. A. Asensio, J. J. Cordoba, “Detection of Clostridium botulinum types A, B, E and F in foods by PCR and DNA probe,” *Lett Appl Microbiol*, vol. 25, pp. 186-190, 1997.

[71] F. Anniballi, B. Auricchio, E. Delibato, M. Antonacci, D. Medici, L. Fenicia, “Multiplex real – time PCR SYBR Green for detection and typing of group III Clostridium botulinum,” *Vet Microbiol*, vol. 154, pp. 332-338, 2012.

[72] M. Lindstrom, H. Korkeala, “Laboratory diagnostics of botulism,” *Clin Microbiol Rev*, vol. 19, pp. 398-314, 2006.

[73] L. M. Wein and Y. Liu, “Analyzing a bioterror attack on the food supply: The case of botulinum toxin in milk,” *PNAC*, vol. 102, pp. 9984-9989, July 2005.

[74] G. Deng and G. Sanyal, “Applications of mass spectrometry in early stages of target based drug discovery,” *J. Pharm. Biomed. Anal.*, vol. 40, pp. 528-538, Feb. 2006.

[75] T. Grenda, E. Kukier, K. Kwiatek, “Methods and difficulties in detection of Clostridium botulinum and its toxins” *Polish Journal of Veterinary Sciences*, vol. 17, pp. 195-205, 2014.

[76] A. Boyer, H. Moura; A. Woolfitt, S. Kalb; L. McWilliams, A. Pavlopoulos, J. Schmidt; D. Ashley, and J. Barr, "From the mouse to the mass spectrometer: detection and differentiation of the endoproteinase activities of botulinum neurotoxins A-G by mass spectrometry," Anal. Chem. 2005, 77, 3916-3924.

[77] S. Cai, B. R. Singh, and S. Sharma, "Botulism diagnostics: from clinical symptoms to in vitro assays," Clin. Rev. Microbiol. 2007, 33, 109-125.

[78] W. S. Hong, E. W. K. Young, W. H. Tepp, E. A. Johnson, and D. J. Beebe, "A Microscale Neuron and Schwann Cell Coculture Model for Increasing Detection Sensitivity of Botulinum Neurotoxin Type A ," Toxicol Sci. doi: 10.1093/toxsci/kft082.

[79] A. K. Singh, L. H. Stanker, and S. K. Sharma, "Botulinum neurotoxin: where are we with detection technologies?" Critical Reviews in Microbiology, 2013, 39, 43-56.

[80] L. D. S. Smith, and H. Sugiyama, (1988). "Botulism. The Organism, its Toxin, the Disease," Springfield, IL: Charles C. Thomas.

[81] G. R. Smith, and C. J. Moryson, (1977)."A comparison of the distribution of Clostridium botulinum in soil and in lake mud," J Hyg (Lond) 78, 39-41.

[82] Biological and chemical terrorism: strategic plan for preparedness and response: recommendations of the CDC Strategic Planning Workgroup. MMWR Morb Mortal Wkly Rep2000;49(RR-4):1-14.

[83] H. M. Solomon, and T. J. Lilly, (2001) "Clostridium botulinum. In: Bacteriological analytical manual", 8th Ed. Silver Spring, MD, USA: US Food and Drug Administration.

[84] S. J. Eliasberg, J. L. Ferreira, “Detection of Preformed Type A Botulinal Toxin in Hash Brown Potatoes by Using the Mouse Bioassay and a Modified ELISA Test,” J. AOAC Int. 2001, 84, 1460-1464.

[85] M. C. Scotcher, L. W. Cheng, and L. H. Stanker, “Detection of Botulinum Neurotoxin Serotype B at Sub Mouse LD50 Levels by a Sandwich Immunoassay and its Application to Toxin Detection in Milk,” PLoS ONE, 2010, 5, e11047.

[86] H. Wu, Y. Huang, S. Lai, Y. Huang, and M. F. Shaio, “Detection of Clostridium botulinum neurotoxin type A using immuno-PCR,” Lett Appl Microbiol, 2001, 32, 321-325.

[87] M. Lindstrom, R. Keto, A. Markkula, M. Nevas, S. Hielm, and H. Korkeala, “Multiplex PCR assay for detection and identification of Clostridium botulinum types A, B, E, and F in food and fecal material,” Appl. Environ. Microbiol. 2001, 67, 5694-5699.

[88] J. R. Barr, H. Moura, A. E. Boyer, A. R. Woolfitt, S. R. Kalb, A. Pavlopoulos, L. G. McWilliams, J. G. Schmidt, R. A. Martinez, and D. L. Ashley, “Botulinum neurotoxin detection and differentiation by mass spectrometry,” Emerging Infect. Dis. 2005, 11, 1578-1583.

[89] S. Pellett, W. H. Tepp, S. I. Toth, and E. A. Johnson, “Comparison of the primary rat spinal cord cell (RSC) assay and the mouse bioassay for botulinum neurotoxin type A potency determination,” J. Pharmacol. Toxicol.Methods 2010, 61, 304-10.

[90] R. C. M. Whitemarsh, C. L. Pier, W. H. Tepp, S. Pellett, and E. A. Johnson, “Model for studying Clostridium botulinum neurotoxin using differentiated motor neuron-like NG108-15 cells,” Biochem. Biophys. Res. Commun. 2012, 427, 426-430.

[91] J. Schmidt, R. Stafford, and C. Millard. “High-throughput assays for botulinum neurotoxin proteolytic activity: serotypes A, B, D, and F,” Anal. Biochem. 2001, 296, 130-137.

[92] W. Liu, V. Montana, E. Chapman, U. Mohideen, and V. Parpura, “Botulinum toxin type B micromechanosensor,” Proc. Natl. Acad. Sci. U. S. A. 2003, 100, 13621-13625.

[93] F. Gessler, S. Pagel-Wieder, M. A. Avondet, and H. Bohnel, “Evaluation of lateral flow assays for the detection of botulinum neurotoxin type A and their application in laboratory diagnosis of botulism,” Diagn.Microbiol. Infect. Dis. 2007, 57, 243-249.

[94] J. E. Keller and E. A. Neale, “The role of the synaptic protein snap-25 in the potency of botulinum neurotoxin type A,” J. Biol. Chem. 2001, 276, 13476-13482.

[95] S. Bandyopadhyay, A. W. Clark, B. R. DasGupta, and V. Sathyamoorthy, “Role of the heavy and light chains of botulinum neurotoxin in neuromuscular paralysis,” J. Biol. Chem. 1987, 262, 2660-2663.

[96] Tirtn J, Tenea L, and Hok B, 1989, A batch-fabricatednon-reverse valve with cantilever beam manufacturedby micromachining of silicon, *Sensors Acluators*, 18389-96.

[97] J. Knight, A. Vishwanath, J. Brody, R. Austin. *Phys. Rev. Lett.,* 80, 3866 (1998).

[98] Smits J G, 1990, Piezoelectric Microoumo with three valves working peristaltically,*Sensors Actuators A,* 21-23, 203-6

[99] A. Manz, N. Graber, H. Widmer, *Sens. Actuators, B1*, 244 (1990).

[100] D. Harrison, K. Fluri, K. Seiler, Z. Fan, C. Effenhauser, *A. Manz. Science*, 261, 895 (1993).

[101] D. Harrison, A. Manz, P. Glavina, *Transducers*, 917, 92 (1991).

[102] B. Weigl, P. Yager, Science, 283, 346 (1998).

[103] P. Renaud, U. Seger, S. Gawad, *Proc. Nanotech2002*, Montreux, (2002)

[104] A. Kalmholz, B. Weighl, B. Finlayson, P. Yager, *Anal. Chem.*, 23, 71 (1999)

[105] Dittrich, P. S. & Manz, A. Lab-on-a-chip: microfluidics in drug discovery. *Nature Rev. DrugDiscov*. 5, 210–218 (2006).

[106] Sia, S. K. & Whitesides, G. M. Microfluidic devices fabricated in poly(dimethylsiloxane) forbiological studies. Electrophoresis 24, 3563–3576 (2003).

[107] Manz, A. et al. Planar chips technology for miniaturization and integration of separationtechniques into monitoring systems — capillary electrophoresis on a chip. J. Chromatog.593, 253–258 (1992).

[108] Novo, P.,Chu, V., Conde, J.P., 2014. Biosens. Bioelectron. 57, 284–291.

[109] E. Kumacheva1 andP. Garstecki, Introduction to Microfluidics, Oxford University Press, 2011

[110] Grattan, K.T.V. and Sun, T. (2000), “Fiber optic sensor technology: an overview”, Sensors and Actuators A: Physical, Vol. 82 Nos 1-3, pp. 40-61

[111] A.D. Kersey, A review of recent developments in fiber optic sensor technology, Opt. Fiber Technol. 2 1996. 291–317.

[112] E. Udd, Fiber Optic Sensors, Wiley, USA, 1992.

[113] K.T.V. Grattan, B.T. Meggitt, in: Optical Fiber Sensor Technology, Vols. 1–5 Kluwer Academic Publishing, London, 1998–2000.

[114] Y.N. Ning, K.T.V. Grattan, in: K.T.V. Grattan, B.T. Meggitt Eds.., Optical Fiber Sensor Technology: Devices and Technology Vol. 2 Chapman & Hall, London, 1998, 1.

[115] OFS CD, Collected papers of the International Conferences on Optical Fiber Sensors 1983–1997, SPIE, Washington, USA, 1999.

[116] B.T. Meggitt, Fiber optic white-light interferometric sensors, in: K.T.V. Grattan, B.T. Meggitt Eds.., Optical Fiber Sensor Technology, Chapman & Hall, London, 1995, pp. 269–312.

[117] Y.J. Rao, D.A. Jackson, Principles of fibre-optic interferometry, in: K.T.V. Grattan, B.T. Meggitt Eds.., Optical Fiber Sensor Technology: Fundamentals Vol. 1 Chapman & Hall, London, 2000.

[118] Y. Lu, R. Pechstedt, A study of effects of phase modulator characteristics on interferometer system performance,European Workshop on Optical Fibre Sensors, 8–10 July 1998, Peebles, Scotland, SPIE 3483, 1998. 146.

CHAPTER 2. DEGRADABLE PAAM-BASED HYDROGEL AS SENSING ELEMENTS FOR BIO-AGENT DETECTION

2.1 Introduction

Hydrogel could be regarded as one large molecule on macroscale with cross-linked 3-D hydrophilic polymer network containing significant amounts of water (70-99 wt %)[1-4]. Moreover, due to its physiochemical similarity with the native extracellular matrix both compositionally and mechanically, hydrogel has high biocompatibility [5]. Great efforts have been made in this area, in which the first research on hydrogels could be traced back as early as in 1960s to a poly (2-hydroxyethyl methacrylate) related paper by Wichterle et al [6]. To date, due to its intrinsic half-liquid and half-solid characteristic, hydrogel was used in a broad range of applications such as pharmaceutical and biomedical [7-12], soft electronics, soft robotics and machines [12, 13]. In order to satisfy the requirement used in various applications, many types of hydrogel had been developed. Among these hydrogels, polyacrylamide (PAAm) is one of great popular ones, and was used in great number of applications [14-21]. The PAAm hydrogel is made from acrylamide (AAm) monomers. The monomer consists of a $CONH_2$ group and a carbon double bond, which makes it really suitable to crosslink many other monomers. Therefore, the property of the hydrogel can be varied by adjusting the synthesis conditions, by copolymerization with other monomers and/or crosslinkers, or through chemical modification of the synthesized hydrogel [22-24]. Moreover, the PAAm hydrogel is a covalently crosslinked hydrogel which is termed as chemical hydrogel [25]. Chemical hydrogels have good mechanical strength, and can be made to be biodegradable or

chemical-degradable [25]. During the degradation of the hydrogel, the crosslinker is a key part. The crosslinker crosslinks the hydrogel monomers polymer chains from liquid to solid hydrogel network. When the crosslinker in the hydrogel matrix was cleaved by target agent, the network structure of the hydrogel broke down, and the hydrogel became pasty and later totally water-soluble. By taking a special agent as the crosslinker which could be cleaved by a related target chemical- or bio-agent, the hydrogel could be potentially used to detect the target agent, due to its dramatically morphology change of the hydrogel resulting from the degradation. Based on the feature, some sensors had been developed [19, 26]. In this chapter, we will focus on checking that the PAAm hydrogel based sensor could fundamentally work.In the following chapter, we will realize some real sensors. Specifically, two target agents were selected as examples to fundamentally to check our idea. The first selected target agent is dithiothreitol (DTT) which is a chemical agent.We took N, N' – bis(Acryloyl) crystamine as the crosslonker to detect DTT. This crosslinkerincludes a disulfide bond, which could be cleaved by a reducing agent, DTT. Therefore the PAAm-based disulfide-crosslinked hydrogel could be used to detect DTT (a chemical agent). The disulfide bond is really high chemical activity to cleave the crosslinker, N, N' – bis(Acryloyl) crystamine, and then the detection of DTT could be used to get quick result and archive the first experience for the detection of other agents. The second selected target agent is Clostridium botulinum neurotoxin (BoNT) which is a bio-agent, because BoNT is the most natural toxic substance. We took a peptide, SNAP25-mer, as crosslinker which could be cleaved by BoNT.

In this chapter, the preliminary study was introduced. To get a fundamental confirmation of our concept, The DTT-responsive and BoNT-responsive hydrogel

were used to detect the related target agents separately through observing the morphology change of the hydrogels by our naked eyes through a normal optical microscope. Becausethe DTT-responsive hydrogel is much more active in chemistrythan the BoNT-responsive hydrogel. Therefore, the DTT responsive hydrogel was tested firstly, and then the BoNT responsive hydrogel.

2.2 Detecting Mechanism

A crosslinker crosslinks water-soluble acrylamide chains to water insoluble network hydrogel. The crosslinker can be cleaved by a specific chemical or bio-agent, and the hydrogel could be water-souble after the cleavage, revealing the existence of the target agent (Fig. 2.1).

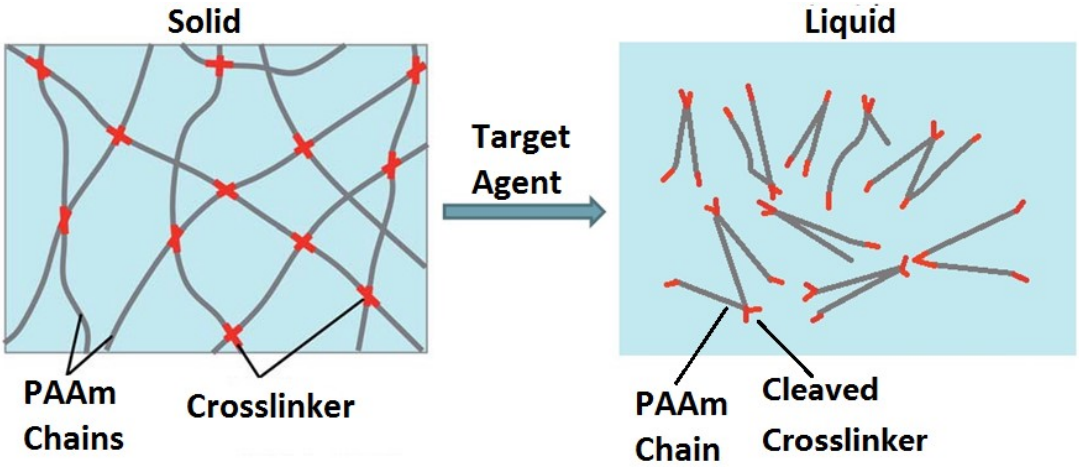

Fig. 2.1: Schematic diagram of the cleavage of the hydrogel. After cleavage, the status of hydrogel becomes liquid from solid.

Fig. 2.2 shows how we utilize the dramatically morphology change of the hydrogel resulted from the cleavage of the hydrogel to detect related chemical- or bio-agents. The hydrogel is patterned on a substrate firstly, and then tested by a liquid sample. If

the sample includes the related target agent, the hydrogel will be cleaved, and then the hydrogel pattern will disappear. If the sample does not include the related target agent, the hydrogel pattern will keep intact.

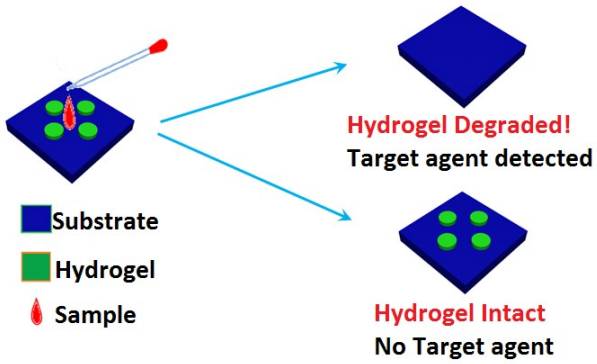

Fig. 2.2: Schematic diagram of the detection of the target agent. Tested by sample with target agent, the hydrogel would be degraded; while tested by sample without target agent, the hydrogel would keep intact.

2.3 Detecting DTT

2.3.1 Experimental

In our experiment, the PAAm based pre-hydrogel was photo-polymerized by UV light. The materials used for pre-hydrogel was acrylamine (AAm, Aldrich Chemicals), N, N' – bis(Acryloyl) crystamine (cross-linker, Aldrich Chemicals), 4-benzoy(benzyl) trimethyl-ammonium chloride (BP+, Aldrich Chemicals), N-methyl-diethanolamine (NMDA, Aldrich Chemicals), and DI water. Those five chemicals were mixed in the ratio by weight (0.15: 0.00375: 0.02: 0.02: 1) to get around 10 mL pre-hydrogel solution. 10 μL pre-hydrogel was put on a glass substrate and then exposed to UV light with intensity 18 mW/s, 180 s to be polymerized. In the pre-hydrogel, the

monomer, acrylamide (AAm), would combine to AAm long chains, which was soluble by water. Meanwhile, the crosslinker would link those AAm long chains to a network structure, which could not be dissolved by water. And the related chemical reaction equation was showed in Fig. 2.3. After the photo-polymerization, the hydrogel was flushed by ethanol (100%) for 5 mins to eliminate umpolymerized pre-hydrogel, and then the whole device was baked on a hotplate at 50 ℃ for 5 min to remove ethanol. After that, the hydrogel was flushed by DI water for 5 mins. And then it was ready for detection. One group of the hydrogel was tested by DTT solution, while the other group was tested by DI water as control.

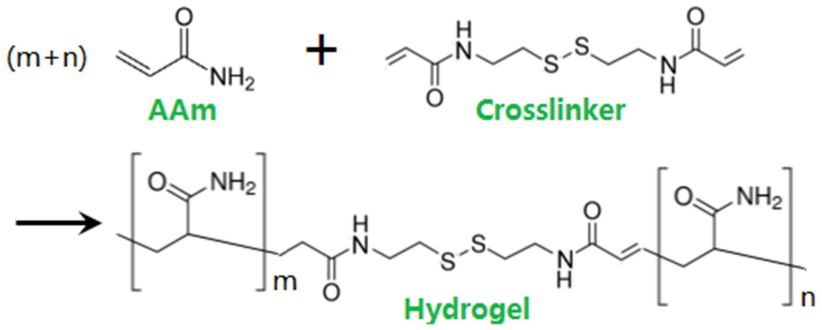

Fig. 2.3: The synthesis of the hydrogel.

2.3.2 Results and Discussion

Firstly, we used DTT solution to dissolve the cross-linker, and found the crosslinker was dissolved by DTT solution easily. Andwe observed that the original liquid pre-hydrogel become solid gel, after UV light exposure of the hydrogel without crosslinker. But when the solidified hydrogel was immersed by DTT solution, the solidified hydrogel (non-crosslinker) was dissolved by DTT solution very quickly in 1

min. Therefore, we got that both of PAAm chain and crosslinker could be dissolved by DTT solution. Meanwhile, we also tried DI water, and found both of PAAm chain and crosslinker could also be dissolved by DI water. According to this simple step above, we highly believed that the degraded hydrogel should be dissolved by DTT and DI water. Just based on the preliminary outcome above, we supposed that the hydrogel immersed by DTT solution should be totally dissolved and there was no any hydrogel left. And then we used this hypothesis to guide our first experiment on DTT responsive hydrogel. Specifically, we made a relative thick hydrogel film (about 300μm), since thick film was easy to be observed. Then we used DTT solution to test a photo-polymerized hydrogel, while we also used DI water to test another photo-polymerized hydrogel as control group. There was no obvious change under microscope for the DI water treated hydrogel after 3 days. However, for the DTT treated hydrogel, although we did observe some changes for the DTT treated hydrogel,like becoming pasted, the hydrogel was still here, not totally dispersed as expectation, and the change is not obvious, because the hydrogel is highly transparentespecially in aqueous solutionunder strong light of microscope. Hence it is hard to observe if there was any difference. In order to overcome it, we took a tweeter to pick up the two hydrogels out. Then the difference became very clear (see Fig. 2.4).

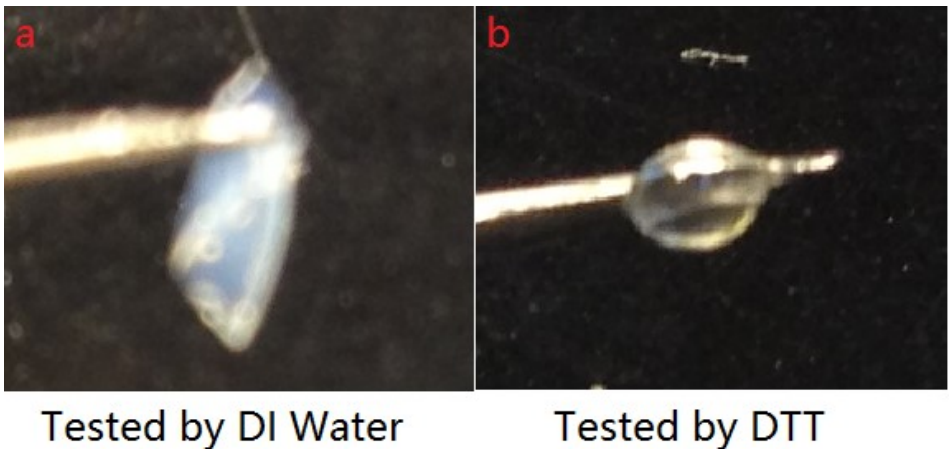

Fig. 2.4: The difference of the hydrogels tested by DI water and DTT solution separately. (a) the hydrogel tested by DI water; (b) the hydrogel tested by DTT solution.

According to Fig. 2.4, the hydrogel tested by DI water, still kept its original morphology, as a film, and no any obvious change could be foundfor the thickness of the film. The hydrogel tested by DTT became very viscous, and lost the film shape. Most of the hydrogel had already been dissolved by DTT solution because the volume of the hydrogel was much smaller than the initial hydrogel (at the very beginning, the two hydrogel tested by DI water or DTT were the same size and volume). However,when we took the DTT treated hydrogel back to the DTT solution, the hydrogel returned back to the film shape (see fig. 2.5).

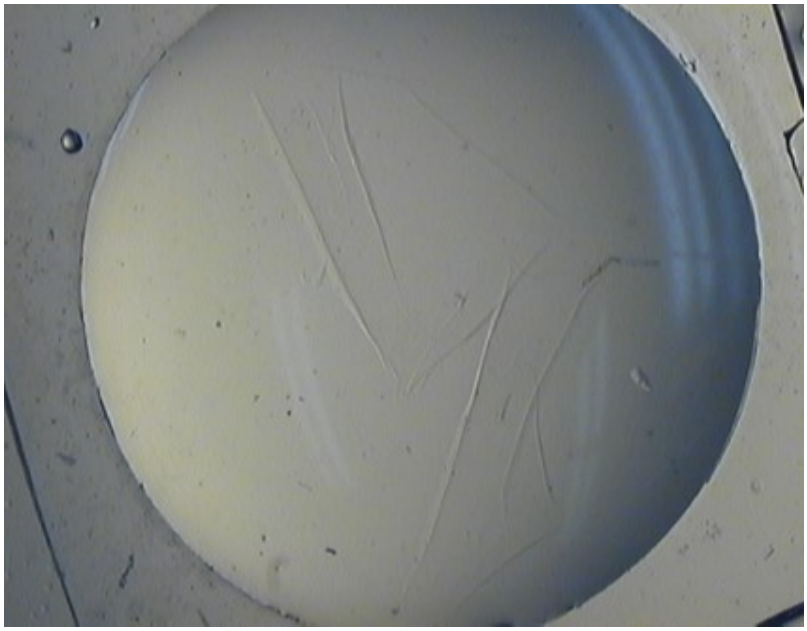

Fig. 2.5: DTT treated hydrogel

In addition, there is another difference between the two hydrogel films. The film tested by DTT is much more viscous and the hydrogel is much weaker than the hydrogel film tested by DI water. It is because that when we picked up the DTT treated hydrogel film, it is much easier to be broken down to two pieces, while for the DI water treated hydrogel film, it always kept intact and never rarely was broken down. Through the experiment above, we fundamentally confirmed that the DTT could cleaved the disulfide-crosslinked hydrogel, and got the first idea what changes we could observe after the degradation of the hydrogel.

2.4 Detecting BoNTs

2.4.1 Experimental

In this charter, we synthesized the cross-linker first, and prepared the pre-hydrogel, which would be used to be photo-patterned on a glass substrate later. Next, we spread10 μL pre-hydrogel on a glass substrate by pipet, which was exposed to UV light under a standard photolithograph process (UV light intensity: 25mW/cm^2, 180s). After the photo-polymerization, the hydrogel was flushed by ethanol (100%) for 5 mins to eliminate umpolymerized pre-hydrogel, and then the whole device was baked on a hotplate at 50 ℃ for 5 min to remove ethanol. After that, the hydrogel was flushed by DI water for 5 mins. And then it was ready for detection. Lastly, we tested photo- polymerized hydrogel with trypsin, Light Chain of BoNT (LC), Hepes buffer, and DTT solution respectively.

A. The synthesis of cross-linker

As a disulfide-linked dichain (heavy and light) 150 kDapolypeptide,BoNT operates exclusively via enzymatic cleavage of its target substrate, the SNAP-25 peptide. To make the hydrogel responsive to BoNT, we first synthesized SNAP-25-contained crosslinker to introduce enzymatic cleavage sites into hydrogel structures in the following polymerization process under UV luminescence. Once the cross-linker containing modified SNAP-25 peptide in the hydrogen matrix is cleaved by BoNT, the solid network structure of the hydrogel will break down, and the hydrogel will become pasty and later totally water-soluble. The synthesis process of crosslinker is shown below:

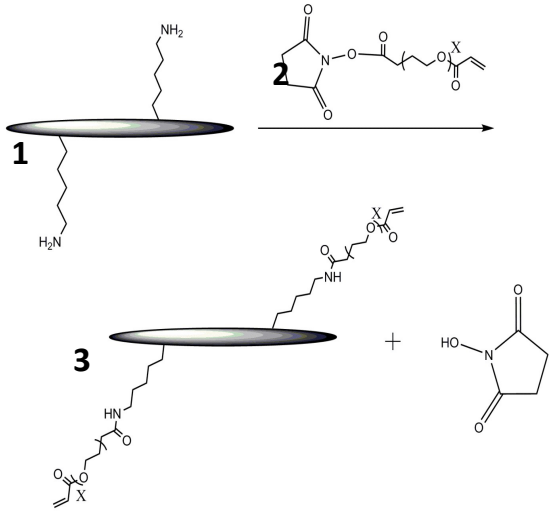

Fig. 2.6: Synthesized crosslinker for BoNT/A responsive hydrogel. The crosslinker is formed by reacting a SNAP peptide 25-mer peptide with APN. BoNT/A cleaves the 25-mer in the crosslinker between amino acids Q and R.

Solution (a):

25-mer (KGGGSNRTRIDEANQRATR{Nle}LGGGK) of 5 mg was dissolved at 1 mg/mL in 100 mM TEOA(triethanolamine), pH 8.0, to form 5ml solution.

Solution (b):

30mg APN (acryloyl-PEG-NHS, MW: 5000; 3× molar excess) was dissolved separately in 1 ml of 50 mM NaHCO3, pH 8.35**.**

The two solutions [(a) and (b)] were mixed together and shaken at room temperature overnight. Pipetide crosslinker was dialyzed against DI water using 8000-10000 MWCO Spectra/Por® regenerated cellulose dialysis membranes (Spectrum), lyophilized, and stored at 20ºC until use. The weight of the obtained product is about 15-16 mg.

The related chemical reaction is showed in Fig. 2.6. In this equation, reagent 1 is recombinant SNAP-25 peptide (KGGGSNRTRIDEANQRATR{Nle}LG-GGK); reagent 2 is Acryloyl-PEG-NHS (APN); the obtained product 3 is the cross-linker we need.

B. The preparation of pre-hydrogel

The solution contained 9-14% (w/v) pipetide crosslinker in an AAm (Acrylamide) prepolymer (62.5:25:12.5 AAm:NMDA (N-methylenediethanolamine):BP+(4-(benzoylbenzyl)trimethyl ammonium chloride), 1:9 ACN:pH 8.0 100 mM TEOA) with 2-4% (v/v) 300 mg/mL (2,2'-dimethoxy-2-phenylacetophenone)DMPA(2,2'-dimethoxy-2-phenylacetophenone) in N-vinyl-2-pyrolidinone (NVP).

C. The test of the hydrogel cleavage by BoNT/A

We treated those photo-polymerized hydrogels with trypsin, BoNT, Hepes buffer and DTT aqueous solution, respectively. First, we used trypsin to treat the hydrogel, because the trypsin has multiple cleavage sites and high cleaving efficiency for many types of protein, including SNAP-25. We would be able to observe cleavage and compromising of the hydrogel much sooner than by using BoNT. This step serves as confirmation of our approach and pre-screening. Next, we performed test using the light chain of BoNT (live toxin was not used due to safety issue). Hepes buffer aqueous solution was also applied to the hydrogel as control. In order to confirm that our design removes the false alarm due to DTT, we also treated those hydrogels with DTT aqueous solution. In order to accelerate the process of the cleavageduring the experiment, we refreshed those corresponding solutions every 4 hours.

2.4.2 Results and Discussion

We tested the hydrogel with trypsin firstly, and treated another hydrogel with Hepse buffer as control group, because of high cleaving efficiencyof the trypsin comparing to

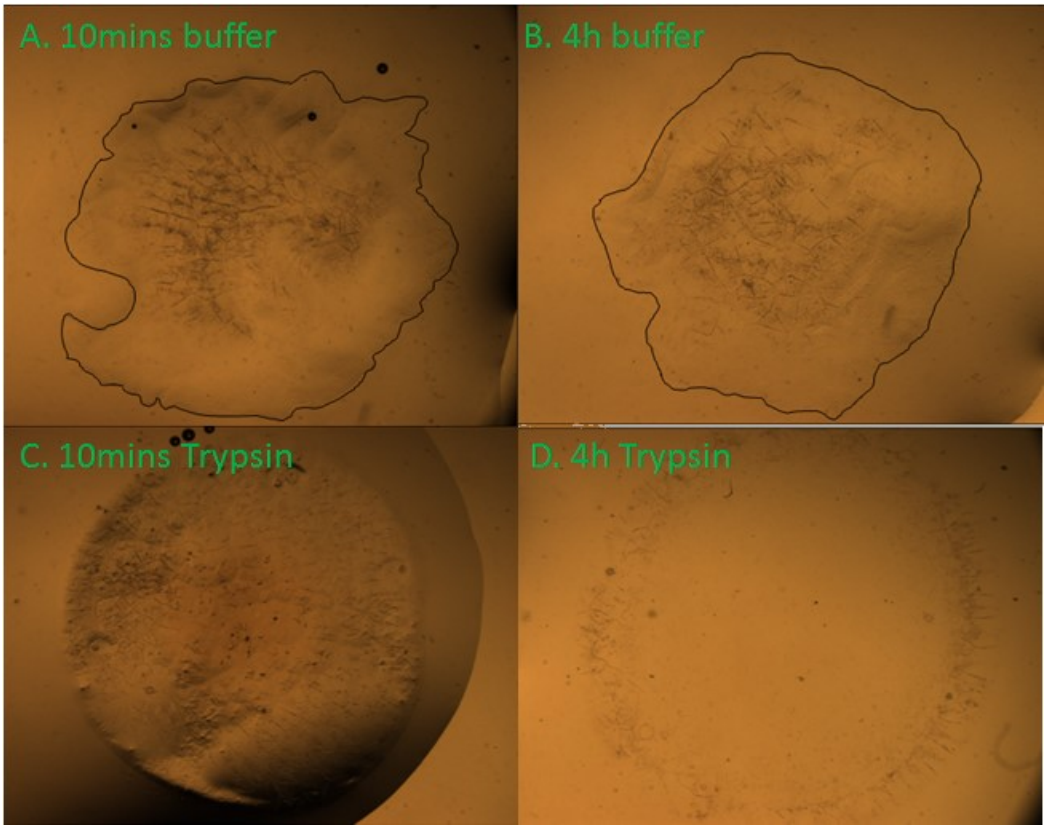

Fig. 2.7: (A, B) treated with just buffer, while (C, D) treated with 100mg/ml Trypsin. And (A, C) show the result 10 mins after corresponding treatment, while (B, D) show the results 4 hours later.

BoNT, and then we could get quick result from trypsin. Fig. 2.7 shows additional results for the hydrogel treated with trypsin. In Fig. 2.7, 4 hours later, the middle part

of the hydrogel treated with trypsin was degraded and dissolved, and just left a hydrogel rim. While for the hydrogel treated by buffer there is no distinct change.

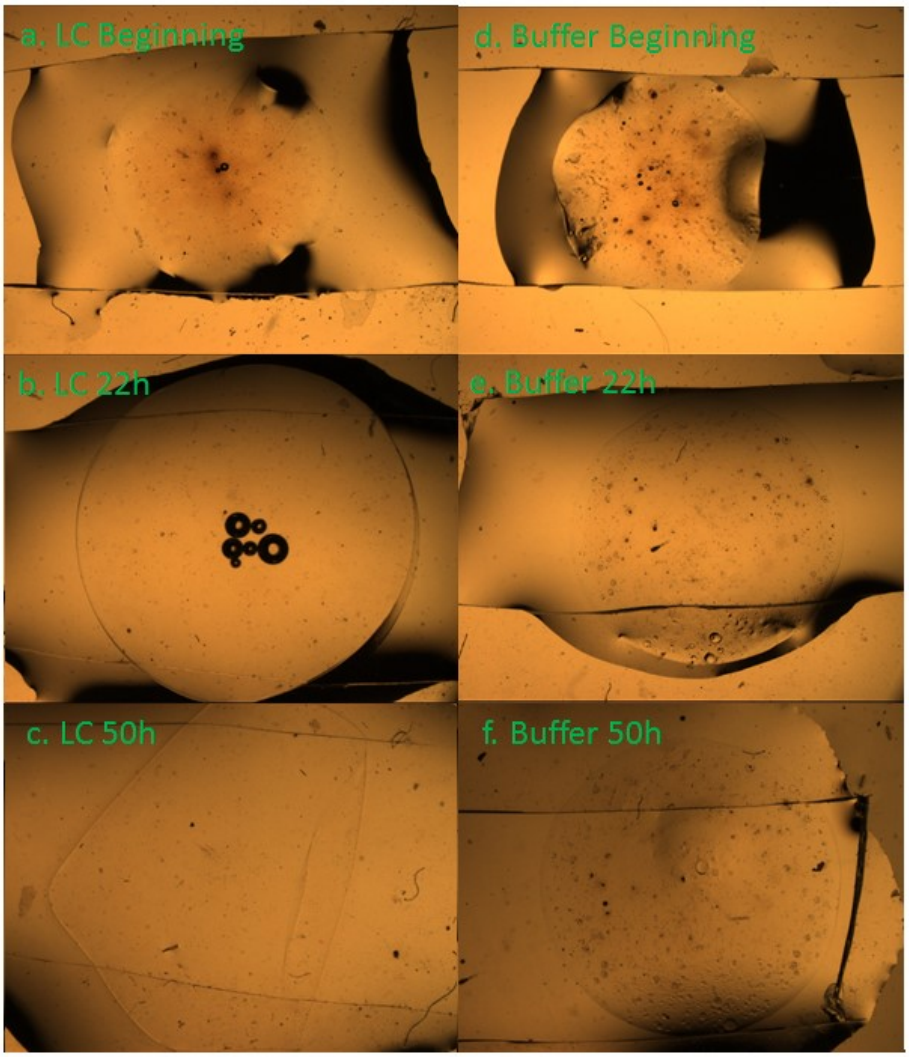

Fig. 2.8: (a-c) treated with LC (90 μg/ml), while (d-f) treated with Hepes buffer.

Next, a hydrogel was tested by LC, and another hydrogel was treated by Hepes buffer as control group. In Fig. 2.8, (a, b, c) show the results of the hydrogel treated with Light Chain (LC), while (d, e, f) show the results of the hydrogel only treated with buffer. The hydrogel treated by LC became viscous and curled, which is similar

to the DTT-responsive hydrogel treated with DTT (See Fig. 2.4). For this phenomenon, we thought the hydrogel films became pasted, justbecause the hydrogel film was cleaved by LC, and then the film became thinner and more viscous. Once the hydrogel became thin and viscous enough,the hydrogel film would be very fragile and then automatically curl, since an ultra-thin film could not support its original flat structure. Later, we will show more evident in this charter to confirm that the hydrogel film treated with LC really became thinner.

Finally, we used four hydrogel posts at one time, and treat those four with trypsin, BoNT/A (LC), Hepse buffer and DTT respectively. The related results are shown in Fig. 2.9. All of those four hydrogel posts with a diameter about 3mm after photo-polymerization. Fig. 2.9 (a-c) show the results treated with trypsin (100 μg/mL). After two hours, the middle parts of the hydrogel were cleaved by trypsin, and the remaining parts of hydrogel became wrinkled and pasty. After four hours, the hydrogel was almost completely cleaved. Fig. 2.9 (d-f) show the results of hydrogels treated with BoNT/A (45 μg/mL). After 24 hours, some outer parts of the hydrogel were cleaved by BoNT/A. After 38 hours, much larger portion of the hydrogel was cleaved and the edge area of the hydrogel became folded. We believe that this folding was attributed to the reduction of the thickness of the hydrogel. With the cleavage of BoNT/A, the hydrogel becomes thinner and thinner, which makes it much easier to fold. Fig. 2.9 (g-i) show the results of hydrogels treated with Hepes buffer (30 mM). After 38 hours and then 100 hours, the hydrogel posts remained intact. From the experiment results, the cleavage demonstrated in Fig. 2.9 (a-c) and Fig. 2.9 (d-f) caused by trypsin and BoNT/A confirmed the capability of our sensor to detect BoNT/A. In Fig. 2.9 (j-l), the hydrogel posts were treated with DTT (13 mM). After

38 hours, the hydrogel posts were intact, and no remarkable cleavage trace was observed, indicating that our design eliminated the false alarm successfully.

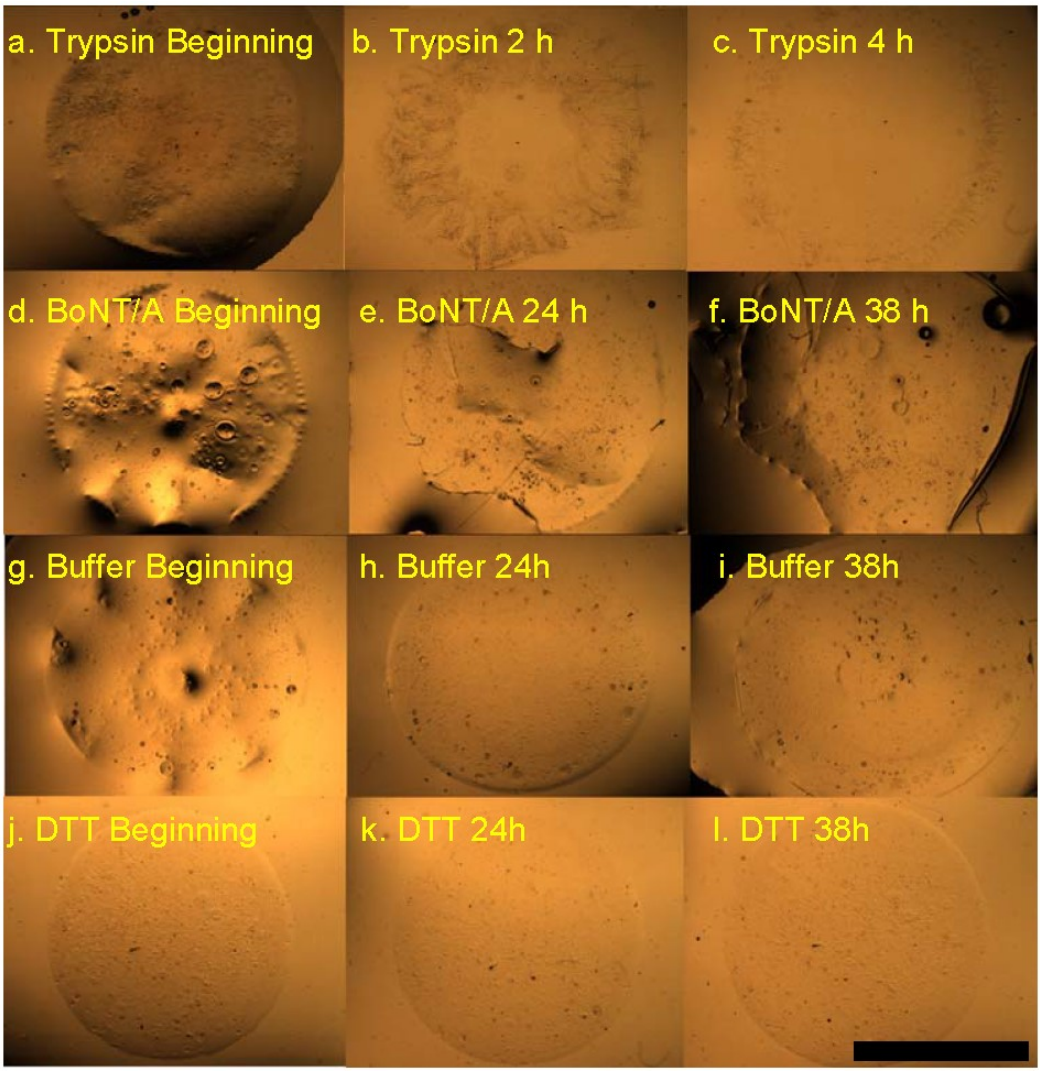

Fig. 2.9: Testing of the responsive hydrogel structures. (a-c), treatment with trypsin (100 μg/mL); (d-f), treatment with BoNT/A (45 μg/mL); (g-i), treatment with Hepes buffer (30mM) only as control; (j-l), treatment with DTT (13mM) as control. The hydrogel was cleaved by trypsin and BoNT/A but remained intact in Hepes and DTT. The scale bar is 2 mm.

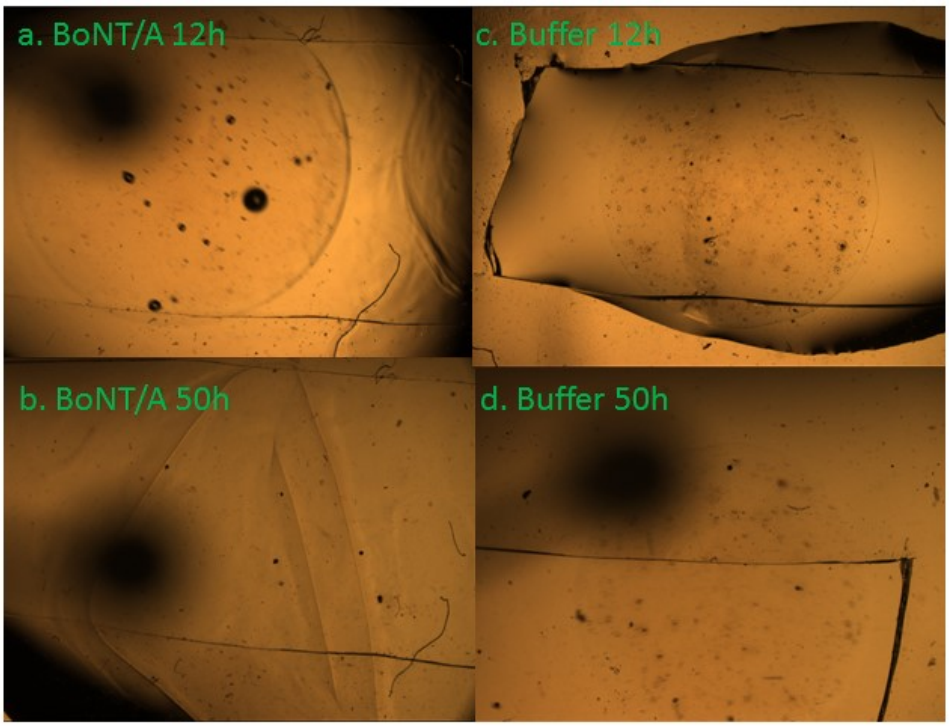

Fig. 2.10: (a, b) the hydrogel treated by BoNT/A, when flushed by DI water, some floccular materials came out. (c, d) the hydrogel was treated by Hepes buffer, when flushed by DI water, no any floccular materials came out.

During the process, we found an interesting phenomenon. Specifically, we used DI water to flush the hydrogel film every 4 hours. In fig. 2.10 (a, b), when we use DI water flush the hydrogel film, we found there were some floccularmaterials came out around the hydrogel film treated with LC, while in fig 2.10 (c, d) there was no floccularmaterials at allfor the hydrogel film treated with buffer. Therefore, we guessed that the hydrogel was cleaved by LC and then form the floccular materials. In order to double check our guess, we carefully repeated this experiment again and the related results were shown in Fig. 2.11.Fig. 2.11(a) shows the results for the hydrogel treated with BoNT/A (LC). When we executed the refreshing process using the

BoNT/A (LC), some pasty hydrogel was washed out (highlighted in the red circle) due to the cleavage by BoNT/A. However, the buffer treated hydrogel film remained and no floccular materials came out when flushing with Hepes buffer or DI water (Fig. 2.11(b)). Therefore, we highly confirmed that the BoNT cleaved the hydrogel and made the hydrogel became viscous. The floccular materialswere resulted from the cleaved hydrogel. We further assumed that the cleaved pasted hydrogel would block the contact between the BoNT and hydrogel, hence hinder the cleavage to continue. In order to check our idea, later we repeated the experiments for many times, and also increased the flushing time with DI water. We did findthat the flushing speeded up cleavage reaction of the hydrogel extremely; while there was no obviouschange for the hydrogel treated by Hepes buffer. One of the typical results shows in Fig. 2.12. Comparing with the results of the hydrogel treated by BoNT for 38 hours in Fig. 2.9, the hydrogel treated with BoNT for 46 hours in was cleaved more, and the cleavage

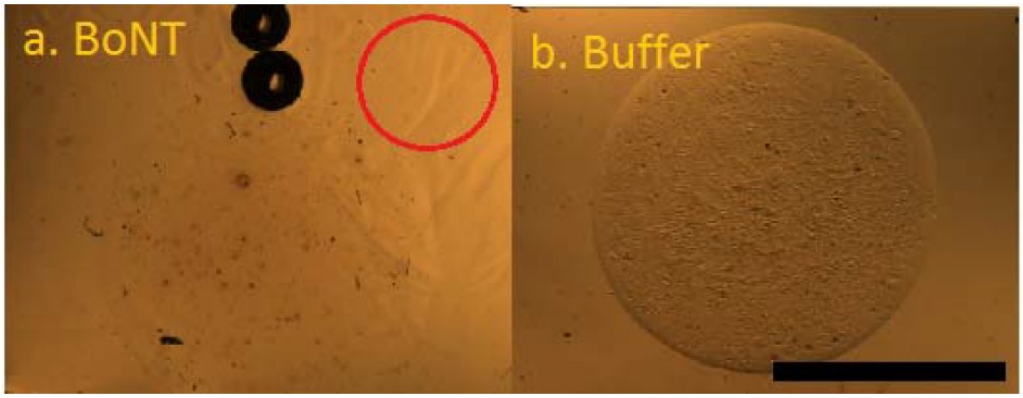

Fig. 2.11: (a) Cleavage of responsive hydrogel by BoNT/A LC (45 μg/mL). The hydrogel structure was collapsed, became pasty. It was washed out when being flushed by BoNT/A LC (the red circled area); (b) the hydrogel was intact in Hepes buffer. The scale bar is 2mm.

speed really was speeded up. Furthermore, most of BoNT-responsive hydrogel had been cleaved for the first time.Previously, we even thought that the BoNT-responsive hydrogel could not be totally cleaved. In addition, we also found too strong flushing would flow away or even break the hydrogel.

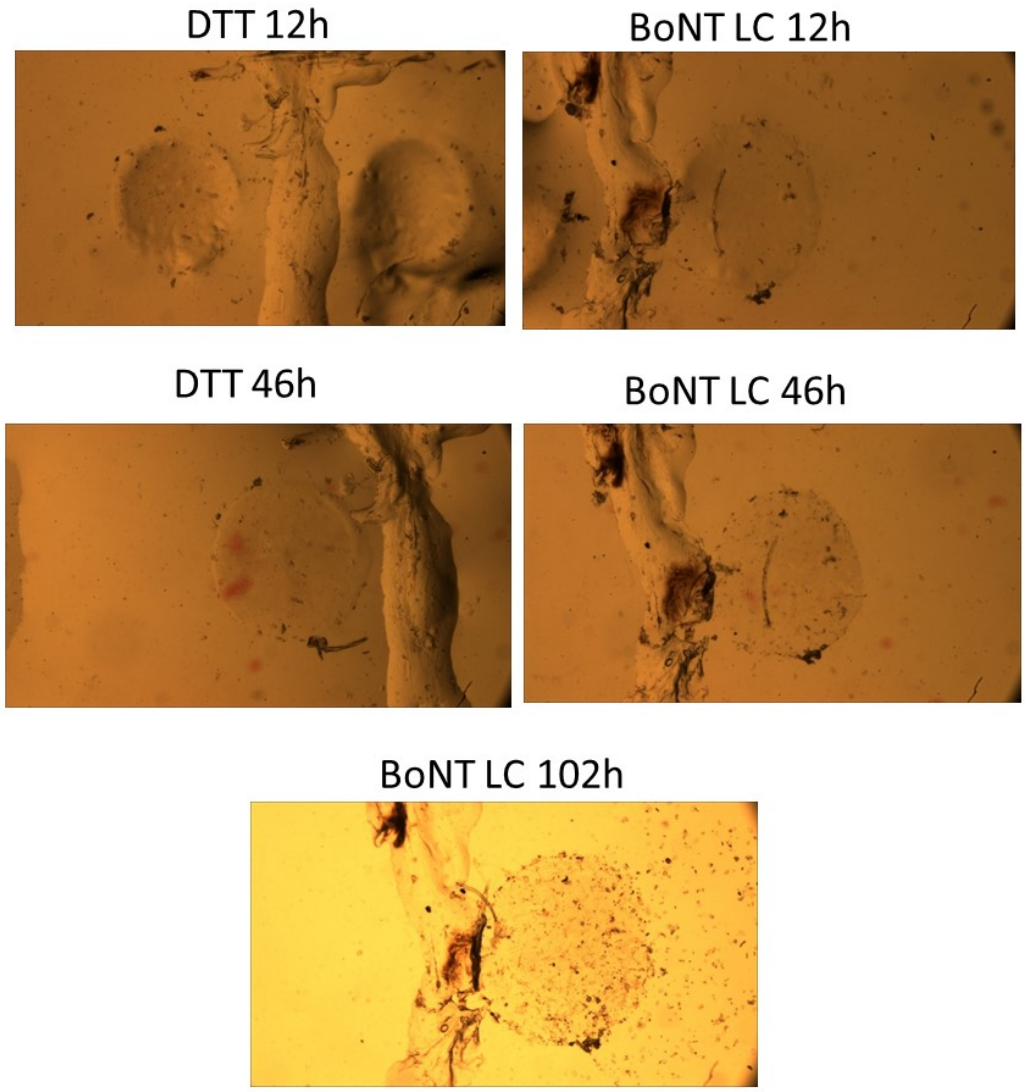

Fig. 2.12: The results of hydrogel with higher DI water flushing time.

2.5 Introducing carbon power and photonic crystal to improve the detection sensitivity

In order to get better visual result and improve the detecting sensitivity, we introduced carbon powder and photonic crystal to the hydrogel.

2.5.1 Introducing carbon power

A. Carbon powder add to DTT-responsive hydrogel

First, we put carbon powder to the pre-hydrogel solution directly. As a result, most of powder went to the edge area. In order to solve this problem, we found an easy method, which is to spread the carbon powder on the glass followed by dropping pre-hydrogel solution. Then the powder would stay at their original place and hardly movetogether or to the edge area. Based on this modification, the related experimental process flow is shown in Fig. 2.13. Firstly, we spread carbon powder on the glass substrate. Secondly, 100 μL pre-hydrogelwas dropped off on the glass substrate followed with another same size glass substrate cover it very quickly. Flood exposure (UV light intensity: 25 mW/s, 180s) was used to photo-polymerize the hydrogel. Then the hydrogel was treated with testing samples. If there was DTT in this ample, the hydrogel layer would be cleaved, and the carbon powder would be released. Finally, the carbon powder would gather together, or at least the pattern of the carbon powder would change.

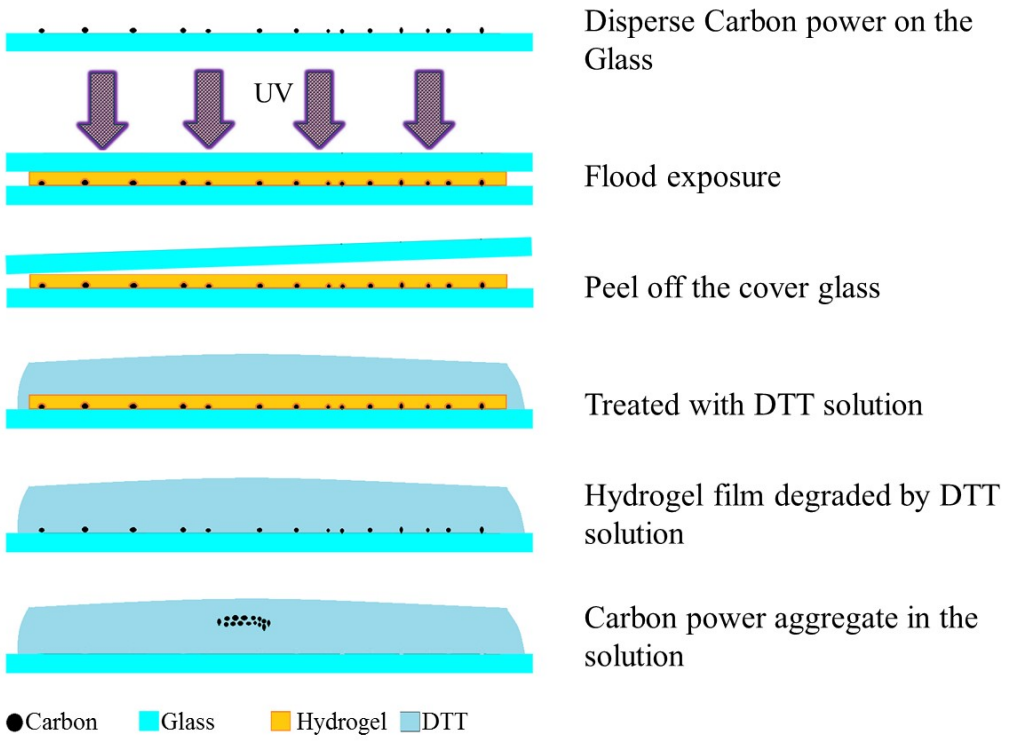

Fig. 2.13: The experimental process flow

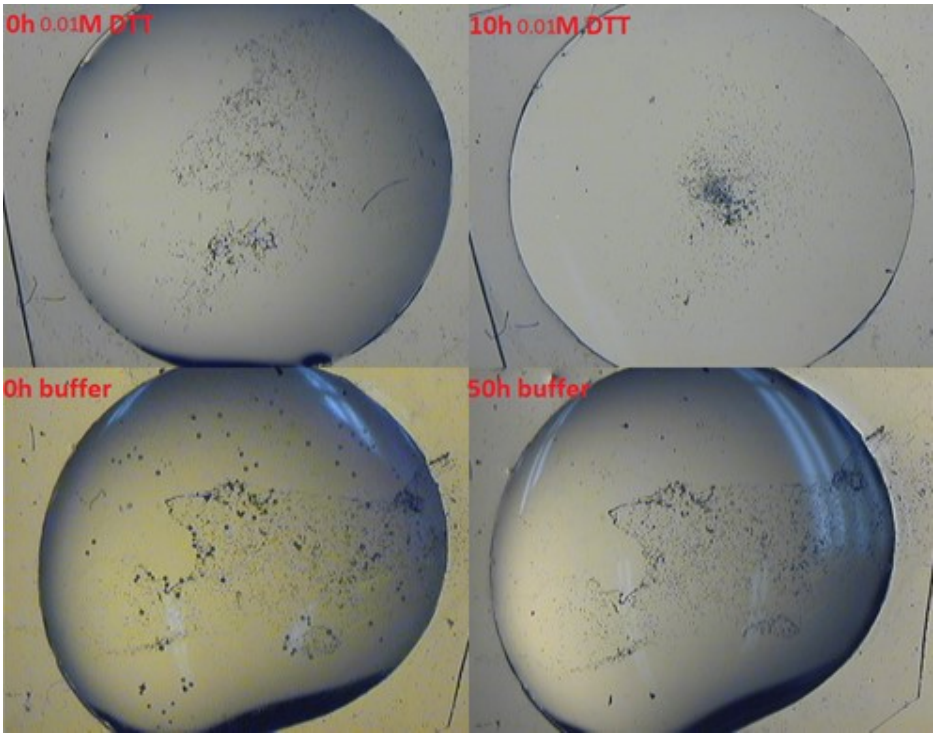

Fig. 2.14: The first set of sample with carbon powder treated by DTT

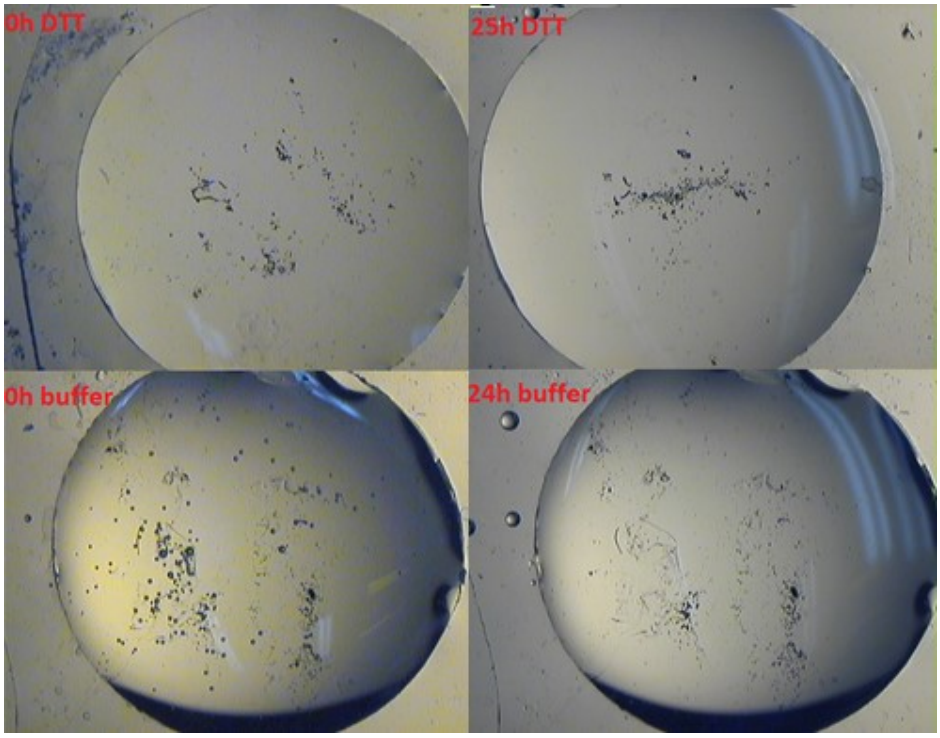

Fig. 2.15: The Second set of sample with carbon powder treated by DTT

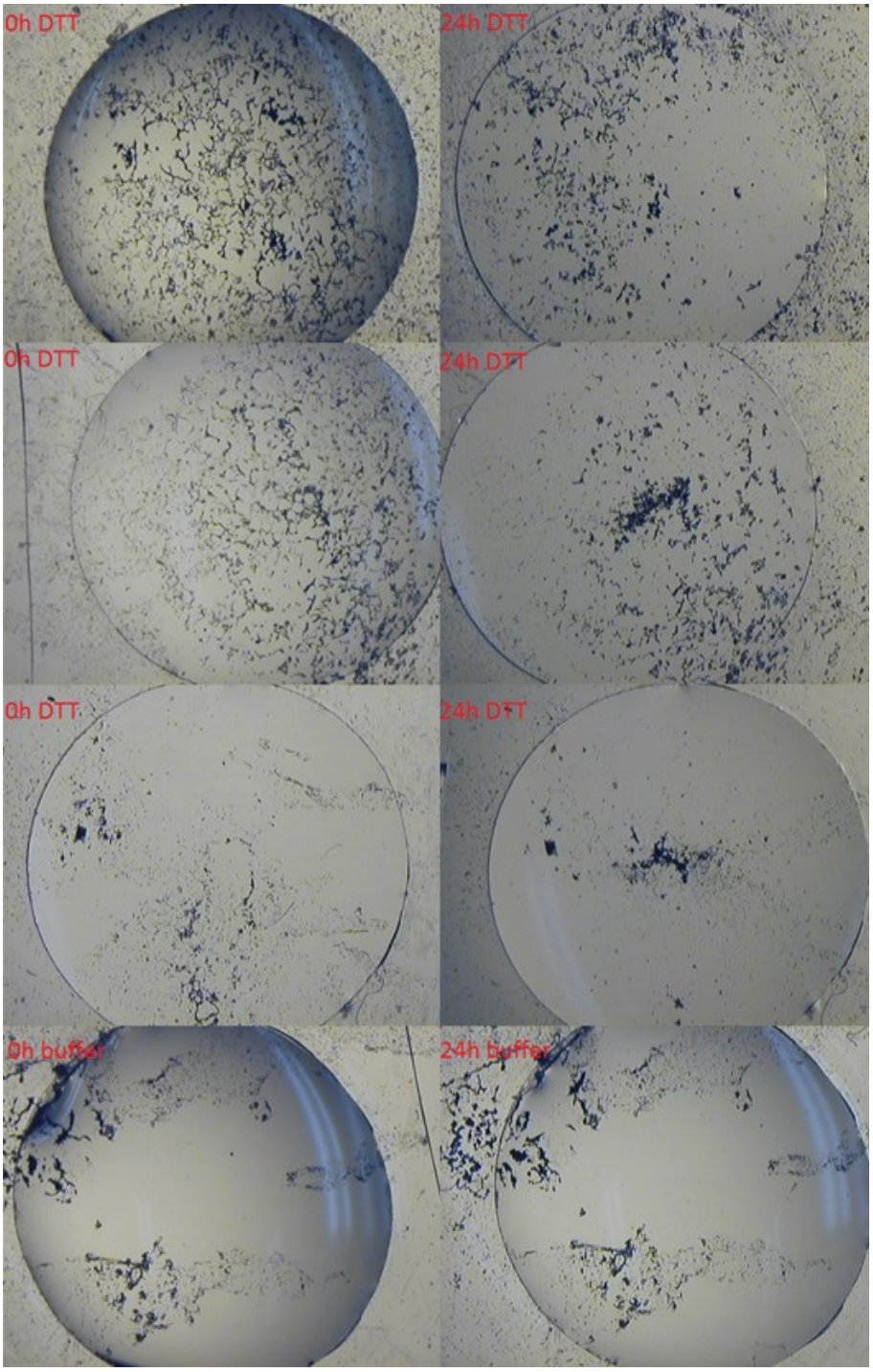

Fig. 2.16: The first set of sample with carbon powder treated by DTT

From the 3 samples above (Fig. 2.14, 2.15, 2.16), all the hydrogel films tested by DTT (0.01M) were really degraded because the pattern of the carbon power changed, some of them gathered together, while there was no change for the hydrogel film tested by buffer.

Finally, we got significant clear result showed in the Fig. 2.17 and especially in Fig. 2.18. In Fig. 2.17, there are two samples: one ((a) and (b)) was treated by 0.01M DTT solution, and the pattern of the carbon power changed dramatically after 10 hours; the other (for the (c) and (d)) was only treated by Hepes buffer, where there was no any change for the pattern after 10 hours. The reason for the great difference between the two samples is that the thin hydrogel film of the first sample was degraded by DTT solution, and the carbon power was released to solution. Then the power would move in the solution and converged together as Fig. 2.17 (b) shows, since carbon power in an aqueous solution has a trend to converge. While for the second sample,only buffer had nothing to do with the hydrogel film, hence the film kept intactand theoriginal pattern of the carbon powder.

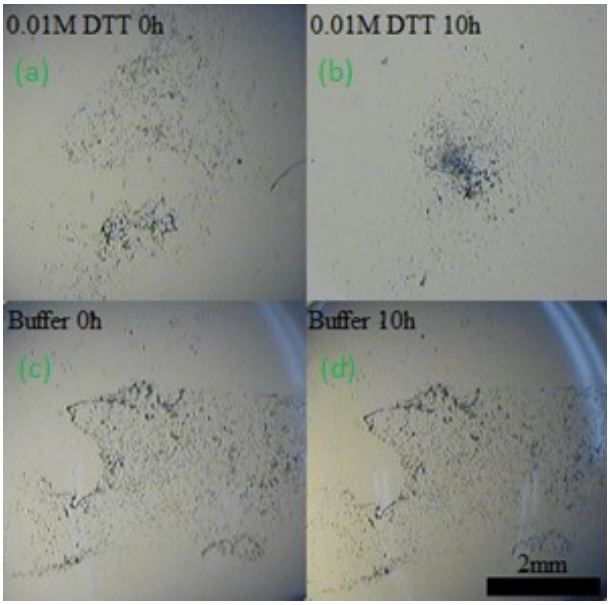

Fig. 2.17: The samples treated by DTT and buffer respectively

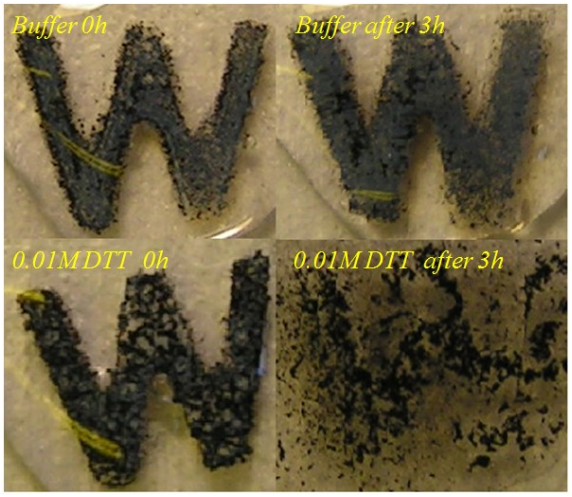

Fig. 2.18: Testing of the DTT-responsive hydrogel structures.

According to Fig. 2.18, the hydrogel treated with DTT (0.01 M) was cleaved and then the pattern collapsedafter 3 hours, while the hydrogel treated by Hepes buffer (30 mM) was kept intact. It definitely confirmed that adding carbon powder could make

the morphology change of the hydrogel significantly more clearly and easier to be observed.

B. Carbon powder add to BoNT-responsive hydrogel

When we got really good result for DTT-responsive hydrogel by introducing carbon powder, and we planned to introduce carbon powder into the BoNT-responsive hydrogel, which could make the hydrogel network structure weak, hence to reduce the degrading time. But once we mixed the pre-hydrogel with carbon powder, the carbon powder could not be photo-polymerized. In order to solve this problem, we modified the initial process. The modified process of the fabrication is showed in Fig. 2.19. First, some carbon powder was loaded on the surface of glass slide (Fig. 2.19 (a)). Then liquid pre-hydrogel was dropped onto the carbon powder and treated with UV light to be polymerized subsequently. Finally, the hydrogel was immersed with a liquid testing solution. Most part of the carbon power would flow away, leaving only the rim part, which looked like a carbon powder ring in the central area of the hydrogel (see fig. 2.20 (a, e)). Fig. 2.20 shows the testing result, the carbon powder was introduced to the hydrogel, and the thickness of the hydrogel is 80μm. The hydrogel film was treated with the low concentrated LC of BoNT/A (concentration: 4.5 μg/mL; amount: 10 μL; refreshed every 8 hours). Figs. 2.20 (b-d) shows that the carbon powder ring was broken in 10 hours, while Fig. 2.20 (e-f) shows that another identical hydrogel filmwas treated with the Hepes buffer and DTT solution together as control group. The hydrogel film remained intact in both Hepes buffer and DTT solutions. In comparison with the result of the hydrogel treated by 10 times higher concentration (45 μg/mL) for 38 hour in Fig. 2.9, the degradation of the

hydrogelin Fig. 2.20 could be observed more clearly. The advantage of carbon powder hydrogel ring seemed to the availability to offer significant potential to realize much higher sensitivity to test BoNT/A. However, there are much more challenges need be solved. It waschallenged to repeat the carbon powder ring in the same shape and same quality. Sometimes, we could get good result like what was shown in Fig. 2.20. However, most of other cases, it washard to say that the difference resulted from the BoNT or just the difference of the carbon powder rings themselves. Later we also tried carbon nanotube, graphene and some other micro-particles, and we found the carbon powder was the best materials out of them.

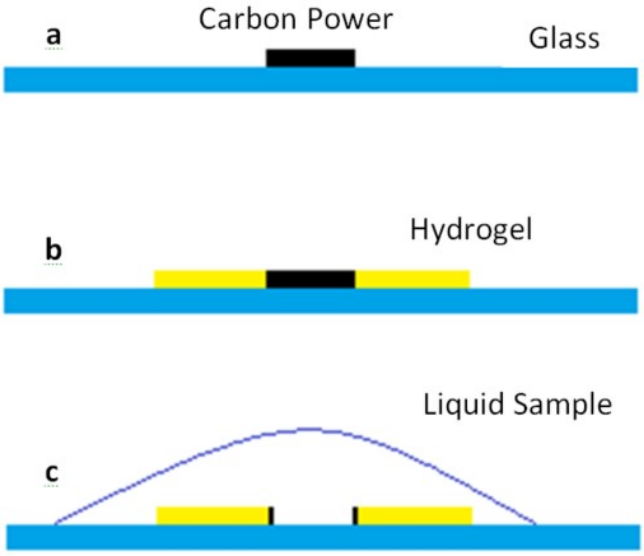

Fig. 2.19: Schematic of the formation of hydrogel with a carbon powder ring.

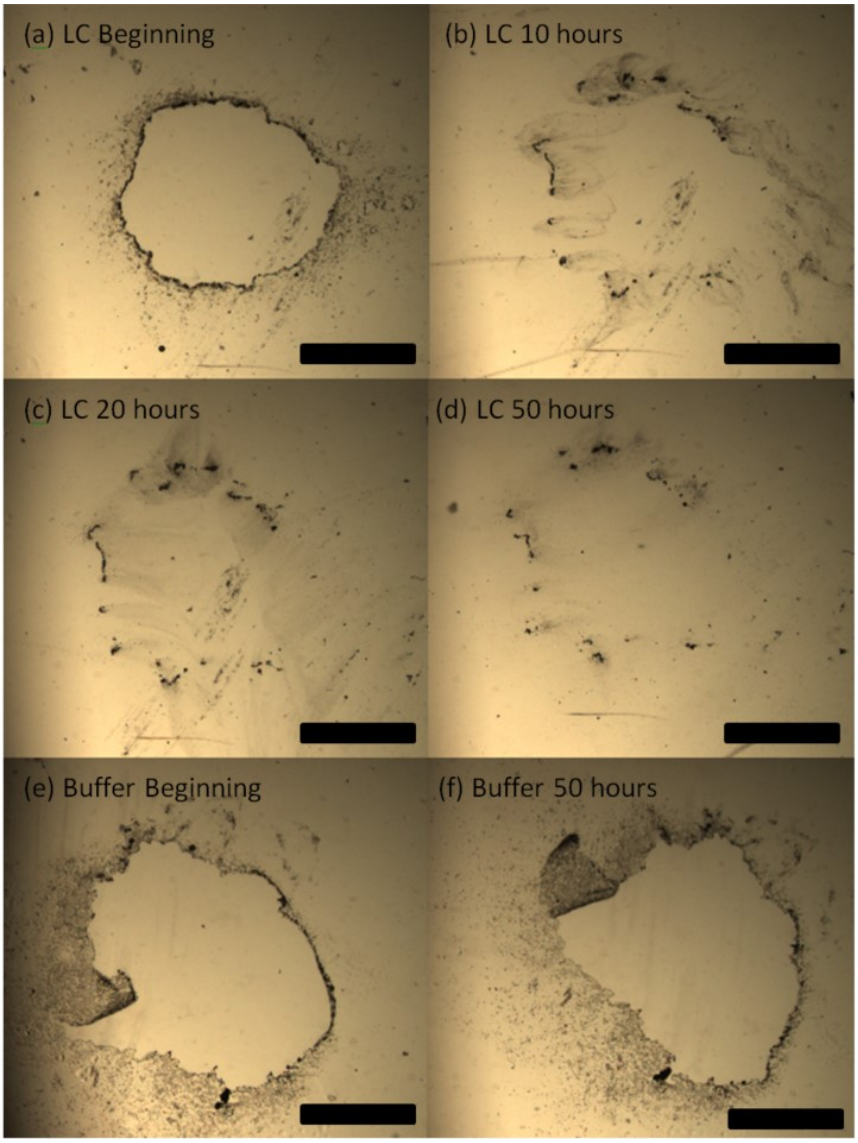

Fig. 2.20: Images of BoNT/A-responsive hydrogel post patterned with carbon powder and treated with: (a-d) low concentration of LC of BoNT/A (4.5 µg/mL); (e,f) buffer solution. Reagents and reaction time are indicated in individual panels. Just 10 hours later, the carbon powder ring was broken. The hydrogel treated with buffer remained intact throughout the process. All scale bars are 1 mm.

2.5.2 Introducing photonic crystal (PC)

We would like to introduce the PC to make the morphology change of the hydrogel easier to be observed, and then increased the detecting sensitivity. Fig. 2.21 shows the mechanism of this idea. The hydrogel layer could block or partially block the color of the PC layer. In Fig. 2.21 (a), if the sample includes target agent (DTT), the hydrogel layer would be cleaved and solved by water, and then the color of the PC layer would show up; In fig. 2.21 (b), if no target agent (DTT) in the sample, there will beno change for the hydrogel, and the color would not change.

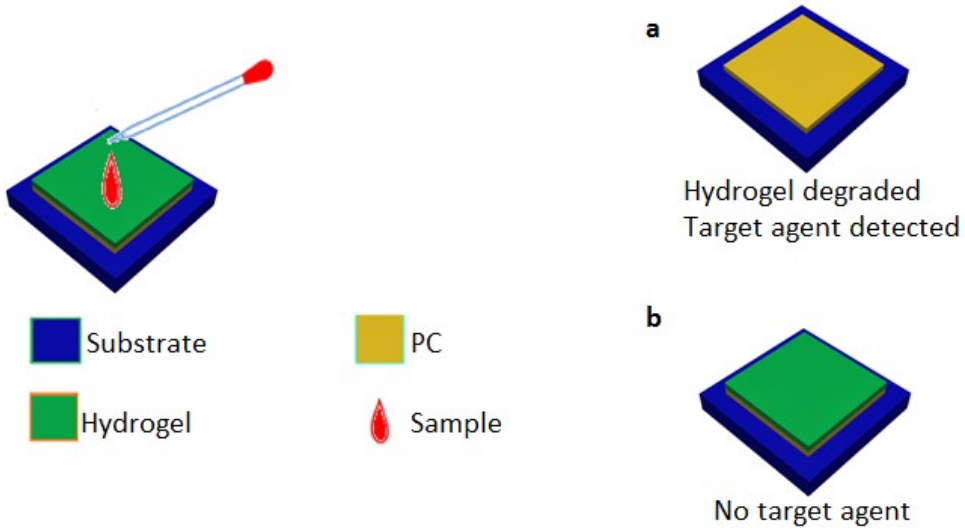

Fig. 2.21: The detecting mechanism. (a) if the sample includes target agent (DTT), the hydrogel is degraded; (b) if no target agent (DTT) in the sample, no change for the hydrogel.

Based on the mechanism above, the related experimental process flow is shown in Fig. 2.22. Firstly, we grew one layer of PC on a glass substrate. Secondly, we spined the pre-hydrogel to cover the PC layer, followed by a UV light exposure to photo-polymerize the hydrogel. When the color of the PC layer would be blocked or

partially blocked, then the device was treated by samples. If the sample included target agent, the hydrogel layer would be cleaved, and the color of the PC layer would show up again. While if there was no target agent in the sample, there was no any change in color.

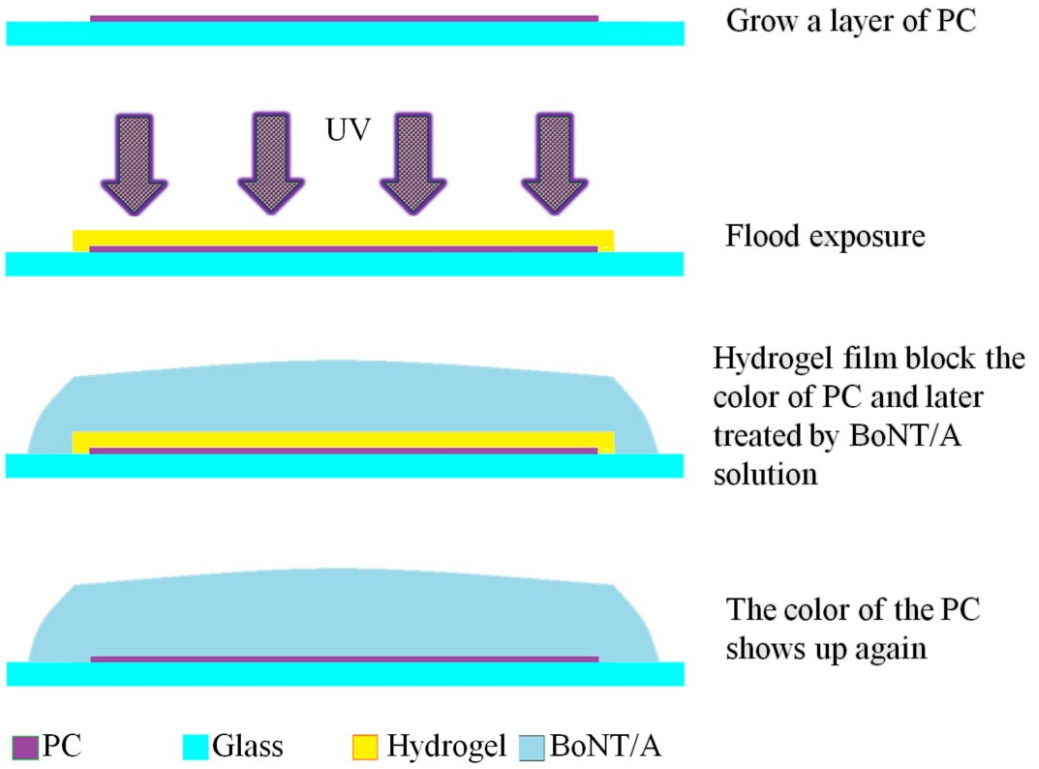

Fig. 2.22: The experimental process flow.

In our experiment, we fabricated two PC. The first one is based on ZnO colloid spheres, the second is based on Poly(methylmethacrylate) (PMMA) spheres.

A. ZnO colloid spheres and photonic crystals

Monodisperse ZnO colloidal spheres were produced by a two-stage reaction process. First, ZnO was formed by hydrolysis of zinc acetate dihydrate (ZnAc). In a typical reaction, 0.03 mol ZnAc was added to 300 ml diethylene glycol (DEG). This reaction solution was heated under reflux to 160 °C. Shortly after reaching the working temperature, precipitation of ZnO occurred. The product was placed in a centrifuge. The supernatant (DEG, dissolved reaction products, and unreacted ZnAc and water) was decanted off and saved, and the white powder was discarded. The secondary reaction began in the same way as a primary reaction: 0.03 mol ZnAc was added to 300 ml DEG and the reaction solution was heated under reflux. Prior to reaching the working temperature, however, typically at 150 °C, some volume of the primary reaction supernatant was added to the solution. Following this addition, there was a temperature drop, and precipitation would typically occur at a lower temperature than without such an addition. After reaching 160 ºC, the reaction was stirred for one hour, after which the heat source was removed, and the flask was cooled down to room temperature. A scanning electron micrograph (SEM) and a photo of the ZnO-particles formed photonic crystal structure are shown in Fig. 2.23. Our planned next step for this section would be to control the ZnO nanoparticles with better size distribution and the uniformity in thickness of the resulting photonic crystal thin film, and to incorporate them with the responsive hydrogel.

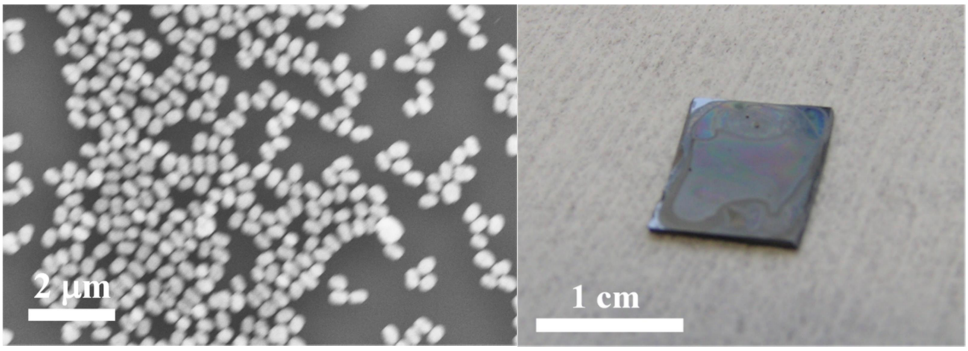

Fig. 2.23: (Left) SEM image of ZnO colloidal spheres. (Right) A photonic crystal structure formed by the ZnO nanoparticles. The colorful fringes indicate nonuniform thickness of the photonic crystal thin film.

B. PMMA spheres and photonic crystals

Batches of monodisperse PMMA spheres were prepared by the method of Schroden et al [27]. The size of the PMMA spheres produced using this method is highly dependent on the composition of the synthesis mixture and the reaction temperature. Syntheses were carried out in a 1-necked round-bottomed flask (25 mL), fitted with a mechanical stirrer (glass shaft with Teflon stirrer blade), thermometer, water-cooled reflux condenser, nitrogen bubbler and a glass quickfit stopper. The procedure used is outlined below. Deionized water (16 mL) and methyl methacrylate (MMA, 3 mL) were added to the 1-necked round-bottomed flask.

Nitrogen gas was then slowly bubbled through the resulting two-phase system and vigorous mechanical stirring of the mixture commenced. The mixture was then heated to either 70^{o}C, whereupon 2,2”-azobis(2-methylpropionamidine) dihydrochloride (0.02 g) was added as an azo initiator and polymerisation of the MMA commenced.

The temperature of the reaction mixture increased initially on introduction of the initiator, but then stabilized after approximately 30 min. After stabilization, the reaction mixture was maintained at the initial temperature of either 70^{o}C for 40 mins. Heating was then discontinued, and the reaction mixture allowed to be cooled to room temperature. The resulting colloidal suspensions of PMMA spheres were then centrifuged at 4000 rpm for 20 mins. The supernatant was discarded and the precipitates were collected for later use.

Dilute 50 mL of previously prepared PMMA nanospheres in 20 mL distilled water. Clean the glass silde by soaking in iso-propanol for 10 minutes followed by soaking in pure water for 5 minutes. Suspend the glass slide into the diluted PMMA nanosphere suspension you prepared earlier. To promote the growth of high quality close packed layers on the glass slide, evaporate the solution in a controlled temperature environment on a hot plate. At 50 ^{o}C, the solution will evaporate in about 36 hours. After the solution has evaporated, a dry film of the close-packed PMMA nanospheres remains on the glass slide. A scanning electron micrograph (SEM) and a photo of the PMMA nanospheres formed photonic crystal structure are shown in Fig. 2.24. The average diameter of each nanosphere is about 200nm, and the entire area coverage of the thin-film is approximately 1 cm^{2}.

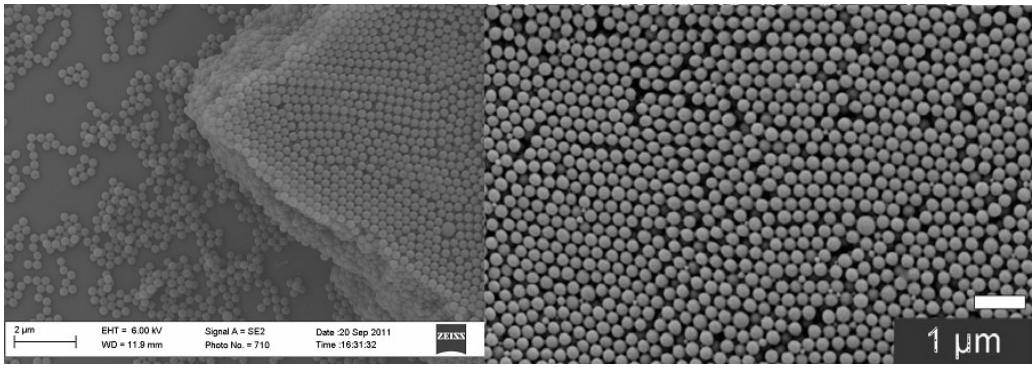

Fig. 2.24: SEM image of the fabricated PCs. The PMMA nanospheres show good periodicity.

Although we got the PCs with high quality, there were still other challenges needed be solved. The most challengewas that the hydrogel was really clear, and then it could not to block the color of the PC layer. Later, we added some dye to the hydrogel, but it brought about more challenge, because he hydrogel layer was too thin and polymerization would be affected by the dye. Specifically, if we just addedtiny amount of dye, the hydrogel would not show any color under the strong light of the microscope. If we addedenough dye to let the hydrogel with color, the hydrogel could not photo-polymerization.

2.6 Conclusion

In this chapter, we fundamentally confirmed that the PAAm-based hydrogel could be used to detect chemical- and bio-agents. Firstly, by taking cystaminebisacrylamide as crosslinker, we confirmed that the PAAm-based hydrogel could be used to detect chemical agent,like DTT. Secondly, by taking SNAP-25mer as crosslinker, the hydrogel could be used for detecting bio-agent, like BoNT. At the beginning, the result was not clear as we expected: the hydrogel could not totally removed.

Especially, sometimes, there was no great change for the morphology of the hydrogel in aqueous solution. In order to speed up the cleavage reaction and make the morphology change resulting from cleavage clearer, we took two methods to try to figure out this issue. The first one is to introducing the carbon powder to the hydrogel. It really worked for the DTT-responsive hydrogel, but there were some challenges for the BoNT-responsive hydrogel. The second one is to combine the PC to the hydrogel system, and it still faced some challenges, due to the transparency of the hydrogel and un-polymerization when adding dye. However, during the whole process of our experiment, we gradually focused on a very important phenomenon: when flushing the BoNT-responsive hydrogel treated by BoNT, some floccular materials came out from the hydrogel; while the BoNT-responsive hydrogel treated with Hepes buffer, no any such floccular materials came out. We also repeated the experiment, and got the same result. Moreover, after several times of repeating the experiment, we found that more flushing could increase the cleavage of the hydrogel by BoNT; while in the hydrogel treated by Hepes buffer, there was no such change, or at least no such obvious change. Therefore, the floccular materials should result from the cleavage of the hydrogel by target agent. The floccular materials would affect the contact between the BoNT solution and the hydrogel, thus hinder the cleavage process. By increasing the flushing time with more DI water, we found it did increase cleavage speed of the hydrogel extremely. However,too strong flushing would flow away or brokethe hydrogel even just treated with buffer. In order to solve this problem, we introduced microfluidics.By photo-polymerized the hydrogel in micro-channel, the top and bottom surface of the hydrogel could be attached to the micro-channel, and then the polymerized hydrogel would be much more stable than before. The detail would be

discussed in next charter. Moreover, microfluidics is a great tool to control the liquid flow.

2.7 Reference

[1] A. K. F. Gerlach G, *Hydrogel Sensors and Biosensors*, Springer, Berlin **2010**.

[2] N.A. Peppas, Hydrogels in Medicine and Pharmacy, vol. 1, CRC Press, 1986.

[3] H. Park, K. Park, Hydrogels in bioapplications, in: R.M. Ottenbrite, S.J. Huang, K. Park (Eds.), Hydrogels and Biodegradable Polymers for Bioapplications, American Chemical Society, Washington, DC, 1996, pp. 2–10.

[4] V. Kudela, Encyclopedia of Polymer Science and Engineering, Wiley, New York, 1987.

[5] T.R. Hoare, D.S. Kohane, Hydrogels in drug delivery: progress and challenges,Polymer 49 (8) (2008) 1993–2007.

[6] O. Wichterle, D. Lim, Hydrophilic gels in biological use, Nature 185 (1960) 117–118.

[7] Hoffman, A. S. Hydrogels for Biomedical Applications. Adv. Drug Delivery Rev. 2002, 54 (1), 3−12.

[8] Peppas, N. A.; Bures, P.; Leobandung, W.; Ichikawa, H. Hydrogels in Pharmaceutical Formulations. Eur. J. Pharm. Biopharm. 2000, 50, 27.46.

[9] Kopec.ek, J. Hydrogel Biomaterials: A Smart Future? Biomaterials 2007, 28 (34), 5185.5192.

[10] Haque, M. A.; Kurokawa, T.; Gong, J. P. Anisotropic Hydrogel Based On Bilayers: Color, Strength, Toughness, And Fatigue Resistance. Soft Matter 2012, 8 (31), 8008.8016.

[11] Huynh, C. T.; Nguyen, M. K.; Lee, D. S. Injectable Block Copolymer Hydrogels: Achievements and Future Challenges for Biomedical Applications. Macromolecules 2011, 44 (17), 6629.6636.

[12] Lee, W.; Cho, N.-J.; Xiong, A.; Glenn, J. S.; Frank, C. W. Hydrophobic Nanoparticles Improve Permeability Of Cell-Encapsulating Poly (Ethylene Glycol) Hydrogels While Maintaining Patternability. Proc. Natl. Acad. Sci. U. S. A. 2010, 107 (48), 20709.20714.

[13] P. Calvert, Adv. Mater. 2009, 21, 743.

[14] Nadler, A., E. Perfect, and B. D. Kay. 1996. Effect of polyacrylamide application on the stability of dry and wet aggregates. Soil Sci. Soc. Am. J. 60: 555–561.

[15] Sojka, R. E., R. D. Lentz, C. W. Ross, T. J. Trout, D. L. Bjorneberg, and J. K. Aase. 1998. Polyacrylamide effects on infiltration in irrigated agriculture. J. Soil Water. Conserv. 53: 325–331.

[16] Jobin, P., J. Caron, P. Bernier, and B. Dansereau. 2004. Impact of two hydrophilic acrylic-based polymers on the physical properties of three substrates and the growth of Petuniahybrida ‘Brilliant Pink.’ J. Am. Soc. Hortic. Sci. 129: 449–457.

[17] El-Rehim, H. A. A., E. A. Hegazy, and H. L. A. El-Mohdy. 2004. Radiation synthesis of hydrogels to enhance sandy soils water retention and increase plant performance. J. Appl. Polym. Sci. 93: 1360–1371.

[18] Al-Humaid, A. I., and A. E. Moftah. 2007. Effects of hydrophilic polymer on the survival of buttonwood seedlings grown under drought stress. J. Plant Nutr. 30: 53–66.

[19] M. L. Frisk, W. H. Tepp, G. Lin, E. A. Johnson, and D. J. Beebe, "Substrate-Modified Hydrogels for Autonomous Sensing of Botulinum Neurotoxin Type A," Chem. Mater, vol. 44, no. 19, pp. 5842-5844, 2007.

[20] X. Wu, C. Li, G. Lin, X. Huang, W. H. Tepp, E. A. Johnson, and H. Jiang, "Microfluidic Detection of Botulinum Neurotoxin Type A Utilizing Polyacrylamide Hydrogels," IEEE SENSORS JOURNAL, vol. 15, pp. 1091-1097, Feb. 2015.

[21] X. Wu et al., "A microfluidic sensor of botulinum neurotoxin type A utilizing SNAP-25 incorporated responsive hydrogel," IEEE Sensors, Baltimore, MD, USA, Nov. 2013, pp. 629–632.

[22] Saraydin, D., D. Karadag, and O. Guven. 2001. Use of superswelling acrylamide-maleicacid hydrogels for monovalent cationic dye adsorption. J. Appl. Polym. Sci. 79: 1809–1815.

[23] Guilherme, M. R., R. D. Silva, A. F. Rubira, G. Geuskens, and E. C. Muniz. 2004. Thermo-sensitive hydrogels membranes from PAAm networks and entangled PNIPAAm: Effect of temperature, cross-linking and PNIPAAm contents on the water uptake and permeability. React. Funct.Polym. 61: 223–243.

[24] Panayiotou, M., and R. Freitag. 2005. Influence of the synthesis conditions and ionic additives on the swelling behaviour of thermo-responsive polyalkylacrylamide hydrogels. Polymer 46: 6777–6785.

[25] Kosmas Deligkaris, Tadele Shiferaw Tadele, Wouter Olthuis, Albert van den Berg. Hydrogel-based devices for biomedical applications. Sensors and Actuators B 147 (2010) 765–774

[26] S. S. Sridharamurthy, A. K. Agarwal, D. J. Beebe and H. Jiang, "Dissolvable membranes as sensing elements for microfluidics based biological/chemical sensors," Lab on a Chip, vol. 6, pp. 840-842, May 2006.

[27] R.C. Schroden, M. Al-Daous, C.F. Blanford, A. Stein, Chem. Mater. 14 (2002) 3305.

CHAPTER 3. MICROFLUIDIC DETECTION OF BOTULINUM NEUROTOXIN TYPE A UTILIZING POLYACRYLAMIDE HYDROGELS WITH SNAP-25 PEPTIDE CROSS-LINKER

3.1 Introduction

CLOSTRIDIUM botulinum Neurotoxins (BoNTs), the most toxic substance known to humans with a median lethal dose (LD50) of approximately 1 ng/kg body weight, have attracted much attention in the last few decades due to their potential use as a bioterrorism agent [1-5]. BoNTs have traditionally been immunologically distinguished into seven serotypes (BoNT/A–G), among which BoNTs A, B, E and F are known to cause human botulism [6,7]. An accidental or deliberate release of BoNTs in civilian population, especially in food supply, would seriously threaten human health and may cause panic resulting in large economic losses. Therefore, highly sensitive and facile assays in the early stage are essential to harness outbreak or controlled distribution of BoNTs. The current gold standard for detection of the seven serotypes of Clostridium botulinum neurotoxin (BoNT/A-G) is the mouse bioassay [8,9]. Due to the high cost, low throughput and the need for highly trained personnel and large number of animal sacrifices, a practical alternative to the mouse bioassay is needed.

To date, much efforts have been made to improve technologies to sense the presence of BoNTs either in vivo (testing in animals) or in vitro, such as enzyme-linked immunosorbent assay (ELISA) [10-12], immune/real-time-polymerase chain reaction (PCR) [13,14], mass spectrometry [15], cell culture assays [16,17], as well as

others [18-20]. These tools generally require complex instrumentation and are not

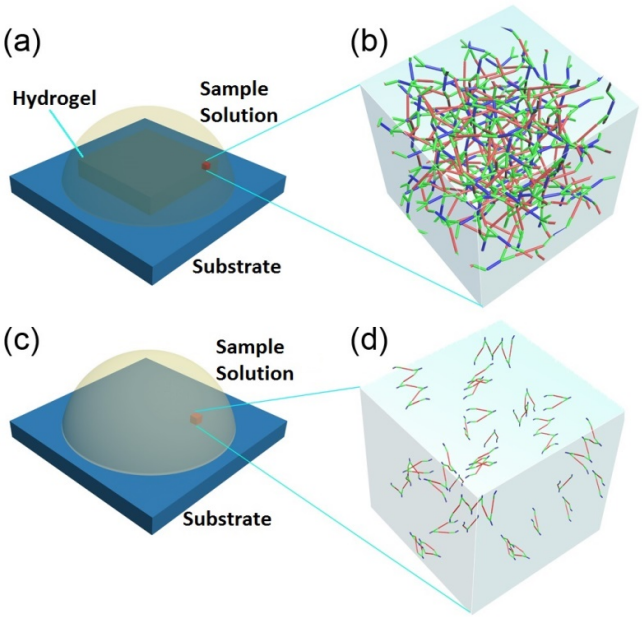

Fig. 3.1: Schematic of the cleavage of hydrogel by BoNT/A toxin. (a, b) The original network structure of the hydrogel. (c, d) The degraded hydrogel network in the sample solution after cleavage.

suitable for in-field testing. Furthermore, some of these assays are not able to distinguish between active and inactive BoNTs. An alternative highly efficient toxin-screening approach developed by M. Frisk et al. [5] was to use a synthetic synaptosomal-associated protein of 25-kDa (SNAP-25) substrate peptide cleavage assay in a microfluidic channel to detect BoNT/A. Peptide integrated hydrogels have been used as sacrificial structures in tissue engineering by decomposition in the presence of a stimulus, such as an enzyme. SNAP-25 is one of three synaptic proteins recognized by the 50-kDa light chain (LC) of BoNT/A in the proteolytic activity leading to paralysis [21,22]. Thus the decomposition of a hydrogel combined with

SNAP-25 modified crosslinker in the presence of BoNTs provides a rapid and accurate detection for the active BoNTs [5].

Although the polyacrylamide (PAAm) hydrogel with SNAP 25-mer (sequence: CGGGSNRTRIDEANQRATR{Nle}LGG- GC) containing a crosslinker developed in the previous work [5] showed sensing capabilities with both LC and BoNT/A, the disulfide bonds in the hydrogel were not stable under reducing conditions and could cause a false positive alert, which limits its application as an on-site sensor for BoNT/A. This is particularly problematic *in vitro* since BoNT/A requires reduction for full activity in substrate cleavage assays. In addition, PAAm SNAP peptide hydrogels without disulfide bonds were investigated to detect BoNT/A. The poor degradation of gels observed was associated with the conjugation points that seemed to prevent the crosslinked portion from being cleaved by BoNT/A [5]. To develop an on-site BoNT hydrogel sensor with higher accuracy, it is important to develop a new SNAP-25 peptide hydrogel without disulfide bonds, where the SNAP-25 has optimized conjugation sites for the crosslinker such as acryloyl-PEG-NHS (APN) to anchor. We previously reported preliminary work in the synthesis of such hydrogel in [23]. Here, we present a more comprehensive study on this approach.In this work, we synthesized a modified 25-mer peptide containing PAAm hydrogel that can be specifically cleaved by BoNT/A. The hydrogel was patterned in a microchannel by an ultraviolet (UV) assisted polymerization process. The hydrogel patterns undergoing cleavage by BoNT/A displayed clear visual changes and could thus serve as a toxin readout as shown in Fig. 3.1. The novel 25-mer (KGGGSNRTRIDEANQRATR{Nle}LG- GGK) with three maximum conjugation sites for APN was used to improve the sensitivity and visual observation in BoNT/A

detection by lowering the degree of crosslinking as shown in Fig. 3.2. Using this new 25-mer removes any disulfide bonds in the ultimate crosslinker, thus avoiding potential false positives due to the needed reduction by dithiothreitol (DTT) of the BoNT/A. All three conjugation sites on the new 25-mer come from the two lysines including two branch primary amino groups and one N-terminus, fewer than the 4 sites on the 25-mer used in the previous work [5]. Using the newly synthesized and photo-patterned hydrogel, we built microfluidics-based devices for sensing BoNT/A by observing the morphology change of the hydrogels located in the polydimethylsiloxane (PDMS) microchannel. As a result, the hydrogels in the microchannel were compromised and cleaved in 500 μg/ml of trypsin in 15 minutes, and in a solution containing the LC of BoNT/A (concentration: 45 μg/mL) in 38 h. Such a device could be a promising candidate for a simple, low-cost, portable, and real-time sensor of bio-active BoNTs, such as in food packages and for on-site detection.

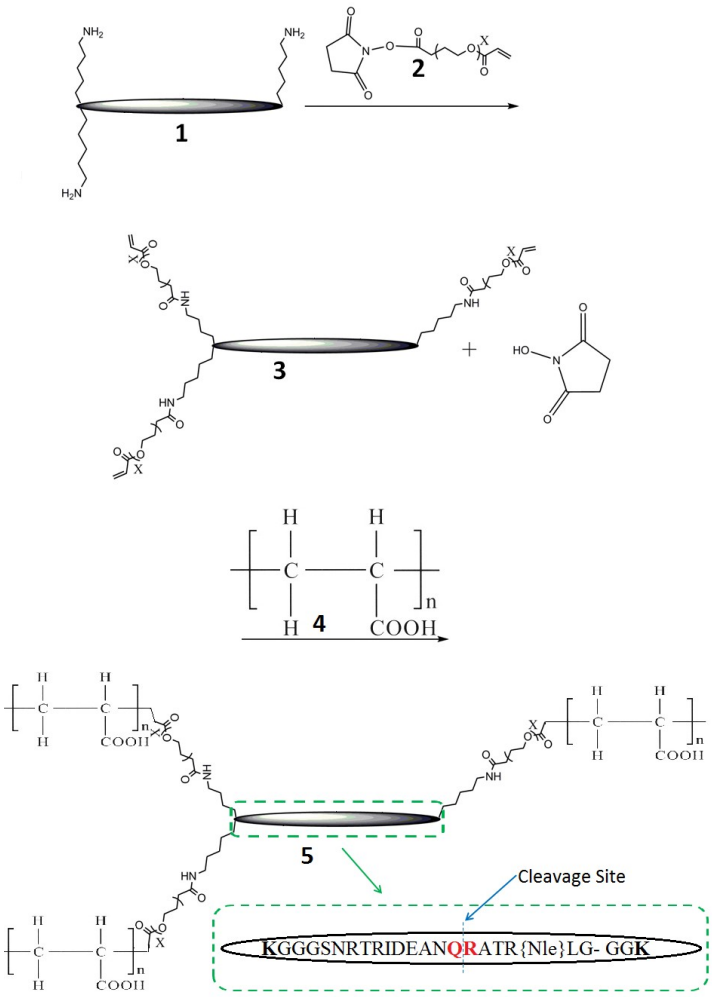

Fig. 3.2: Schematic of synthesis of SNAP-25 containing crosslinker for BoNT/A responsive hydrogel. The callout shows the modification of the 25-mer with lysine（K）replacing cysteine (C) at both ends. The cleavage site between glutamine (Q) and arginine (R) is also shown.

3.2 Experimental

3.2.1 Materials and Equipment

Acrylamide (AAm), 4-(benzoylbenzyl)trimethyl ammonium chloride (BP+), 2,2'-

dimethoxy-2-phenylacetophenone (DMPA), triethanolamine (TEOA), Sodium bicarbonate (NaHCO3), and N-methylenediethanolamine (NMDA) were purchased from Aldrich Chemicals. N-vinyl-2-pyrolidinone (NVP) was obtained from Acros Organics (Fair Lawn, NJ). 25-mer of SNAP-25 peptide and APN were bought from Peptide 2.0 Inc. (Chantilly, VA) and Nektar Therapeutics (Huntsville, AL), respectively. BoNT/A LC (concentration: 729 μg/mL) was provided by the Johnson laboratory at the University of Wisconsin-Madison, and was further diluted to 45 and 4.5 μg/mL, respectively, with Hepes buffer. Deionized (DI) water was used for all solutions. Lithography was operated on Omnicure series 2000. Hydrogel diameters were measured on an Olympus BX60 microscope. Figs 3.3 to 3.6 were taken on an Olympus SZX12 stereoscope using a Leica DFC 300 camera.

3.2.2 Synthesis of the Modified Crosslinker

To synthesize the crosslinker, 5 mg 25-mer peptide was dissolved in 5 ml 100 mM TEOA aqueous solution at pH 8.0. 3× molar excess (30 mg) APN was dissolved in 1 ml 50 mM NaHCO3 aqueous solution at pH 8.4. The two solutions were then mixed together and shaken at room temperatureovernight. Acryloyl-PEG-SNAP peptide crosslinker was dialyzed against DI water using 8000-12000 MWCO Spectra/Por® regenerated cellulose dialysis membranes (Spectrum), lyophilized, and stored at -20ºC until use.

3.2.3 Hydrogel Post Photopolymerization and Photo Patterning

DMPA was dissolved in NVP at a concentration of 300mg/mL (solution a); 5 M HCL was added dropwise to 100 mM TEOA aqueous solution to adjust pH value to 8.0 (solution b); 20 μL solution a was mixed with 180 μL solution b to produce solution c; 30 mg AAm, 12 mg NMDA and 6 mg BP+ were mixed together to get

solution d; 200 µL solution c and 48 mg solution d were mixed together to make solution e; 4 mg acryloyl-PEG-SNAP peptide crosslinker, 20 µL solution e and 0.8 µL solution a were mixed to make BoNT/A-responsive pre-hydrogel. The pre-hydrogel was photo-patterned to form posts on glass substrates using standard lithography (exposure intensity 25 mW/cm^2, 180 s).

3.2.4 Fabrication

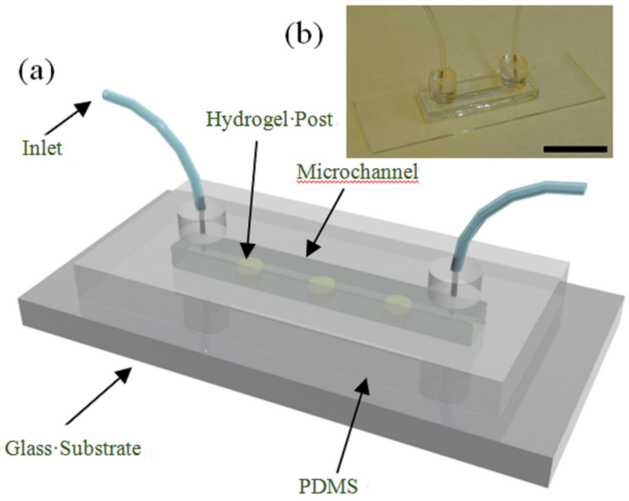

Fig. 3.3: Schematic of the BoNT/A sensor structure. (a) The microfluidic channel is formed between a glass substrate and a PDMS cover. Hydrogel micro-posts are photo-patterned in the microchannel. (b) The photo of the device. The scale bar is 2.5 mm.

The schematic and the photo of the sensor structure are shown in Fig. 3.3(a, b), respectively. Hydrogel posts were photo-patterned in a PDMS microchannel with typical parameters of 30 mm × 100 µm × 100 µm. Specifically (Fig. 3.4(a)), an SU-8 structure (SU-8 2100, UV light intensity: 10 mW/cm^2, 35s) was first photo-patterned to form a line on a glass substrate. Prepared PDMS was subsequently applied to cover the SU-8 line, followed by baking on a hotplate at 70 ºC for 3 hours for curing

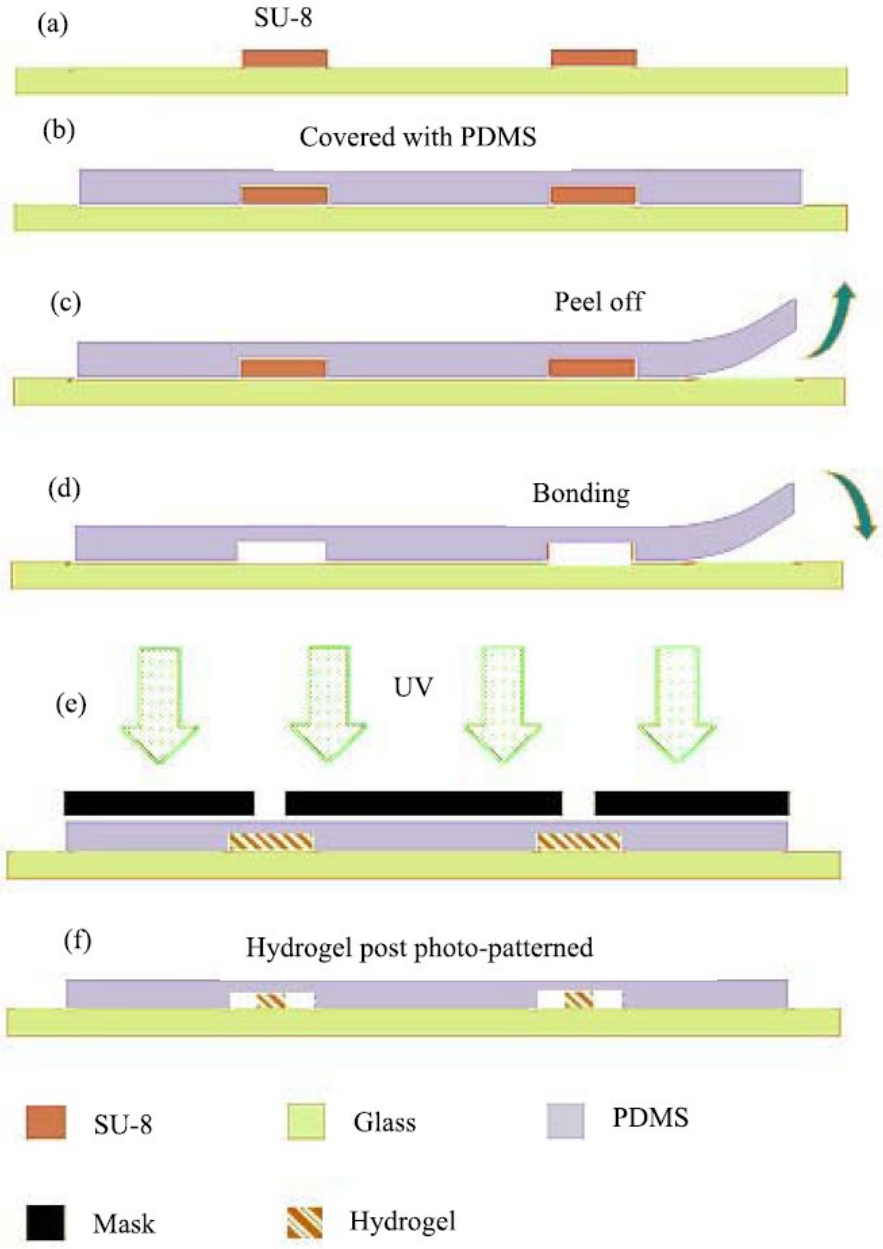

Fig. 3.4: The fabrication process of the device.

(solidification, Fig. 3.4(b)). After solidification, the PDMS layer was peeled off and then bonded with a glass slide on a hotplate at 90 ºC for 3 hours (Fig. 3.4(c, d)). The glass slide was pre-treated with oxygen plasma to enhance the bonding. Finally, liquid

pre-hydrogel was injected into the microchannel and underwent a standard photolithography process (Fig. 3.4(e); UV light intensity of 25mW/cm^2 for 180s). As a result, hydrogel microposts were defined in the microchannel (Fig. 3.4(f)).

3.3 Detection Mechanism

Enzymatic cleavage sites contained in acryloyl-PEG-SNAP peptide crosslinker were introduced into the solid hydrogel matrix by a polymerization process with AAm under ultraviolet light (UV) illumination. When the crosslinker in the hydrogel matrix was cleaved by BoNT/A, the network structure of the hydrogel broke down, and the hydrogel became pasty and later totally water-soluble. The modified substrate contained residues 187 to 203 of SNAP-25 (SNKTRIDEANQRATKML) with the BoNT type A cleavage site between Q197 and R198. M202 was replaced with norleucine (Nle) to eliminate the risk of thioether oxidation, and K189 and K201 were replaced with arginines (R) for increasing peptide hydrolysis [24,25].

Glycine spacers (GGG) were added at the termini to alleviate stress at crosslinking junctions and facilitate the recognition of BoNT/A. In this work, we added lysine (K) at the termini of the new 25-mer rather than cysteine (C) as reported in ref. 5. This modification brought about two significant advantages. First, it helped to eliminate a potential false alarm stemming from the formation of disulfide bonds in thioglycolic groups of cysteines, which can be cleaved by chemical reagents such as DTT, a necessary reducing agent required for the full activation of BoNT/A during in vitro tests. Second, the modification contained one fewer conjugating sites for APN to anchor to the modified SNAP 25-mer. Since APN was used to crosslink the modified SNAP 25-mer and AAm chains, one fewer anchor site on the modified 25-mer for

APN means slightly weaker crosslinking between the crosslinker and AAm chains, which is conducive to the degradation of the hydrogel and allows it to be more easily cleaved, thus enhancing its sensitivity to BoNT/A.

3.4 Result and Discussion

After the PAAm hydrogel posts were defined in the microchannel via photo-patterning, their sensing functions of BoNT/A was tested by injecting liquid samples into the microchannels.

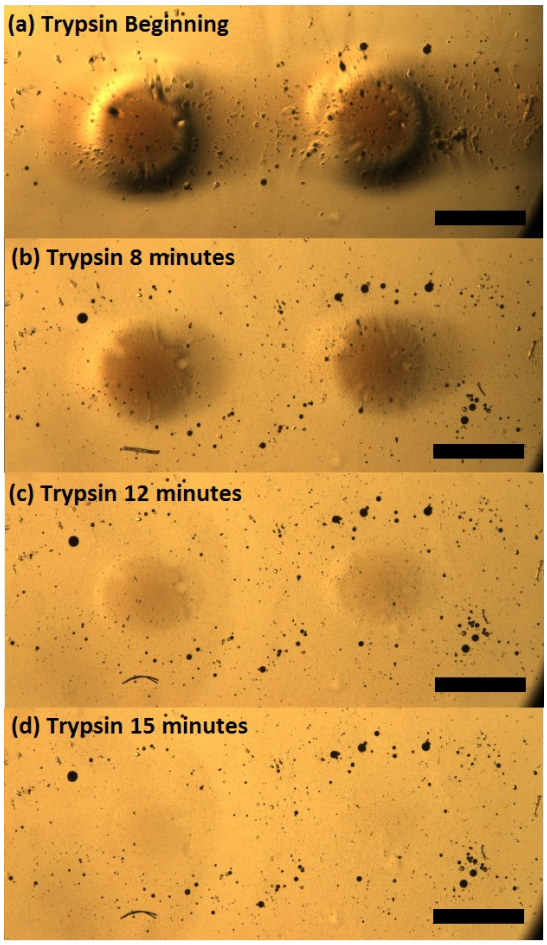

Fig. 3.5: Time course of testing of BoNT/A-responsive hydrogel with 500 µg/mL of trypsin. (a) Initial state. (b-c) After 8 and 12 minutes of treatment of trypsin, respectively. (d) Complete decomposition of hydrogel after 15 minutes. All scale bars represent 500 µm.

3.4.1 Testing with Trypsin

The PAAm hydrogel containing the modified SNAP 25-mer was first tested using trypsin as a control to ensure that the 25-mer was crosslinked into the hydrogel and was accessible in the crosslinked hydrogel matrix. Because trypsin can cleave peptides on the C-terminal side of lysines or arginines, there are 5 potential cleavage sites in the new peptide substrate [26]. In Fig. 3.5, two hydrogel posts with 1 mm in diameter and 240 μm in thickness was treated by trypsin (500 μg/mL; reaction temperature: 37°C). The results show that the hydrogel posts became smaller and thinner gradually and then disappeared completely in 15 minutes (Fig. 3.5(b-d)).

3.4.2 Testing with LC

In this work, we used the proteolytically active LC of BoNT/A to decompose the hydrogel, instead of the entire BoNT/A to avoid safety and regulatory issues. LC is the catalytic part of BoNT/A and can be used to represent the toxic activity of BoNT/A. Fig. 3.6 shows a hydrogel post with a diameter of 5 mm and thickness of 500 μm that was treated with LC (concentration: 45 μg/mL; amount: 10 μL; refreshed every 8 hours). We observed that the hydrogel became soft, and part of the rim was cleaved by LC incubated at 37°C in 40 h (Fig. 3.6(b)). An identical hydrogel post exposed to a buffer control (30 mM Hepes pH 7.4; reaction temperature: 37°C) was used as a negative control to exclude the impact of Hepes buffer solution that was used to dilute the LC. Fig. 3.6(c, d) showed that there was no change in the morphology of hydrogel. The result indicated that the new modified SNAP 25-mer containing hydrogel was indeed responsive to LC of BoNT/A. We also tested the hydrogel using the DTT solution to show the addition of a reducing agent would not cause a false alarm as previously discussed. Another identical hydrogel

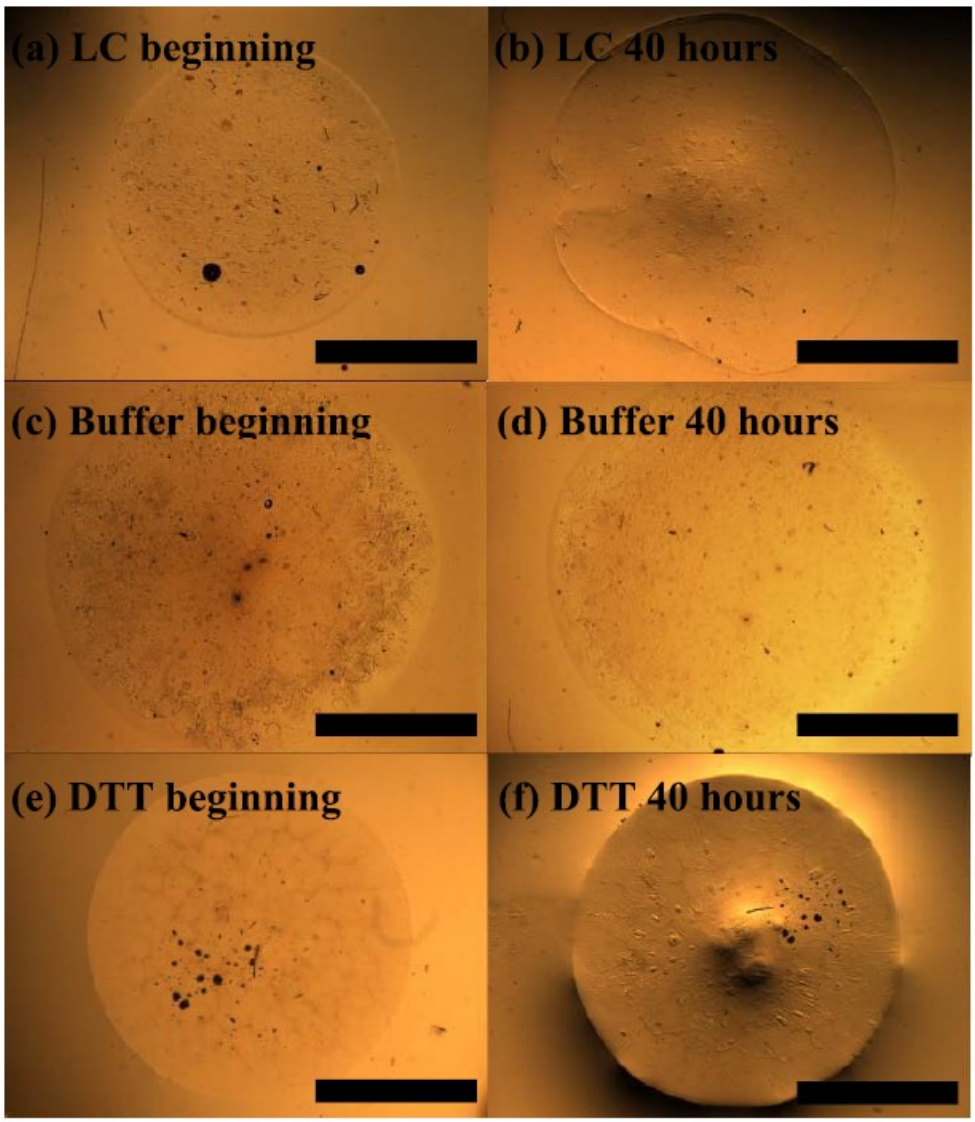

Fig. 3.6: Images showing the results of large-sized hydrogel posts exposed to LC of BoNT/A, DTT and Hepes buffer. Reagents and reaction times are indicated in the individual panels. (a-b) Results of the BoNT/A-responsive hydrogel treated with LC (45 μg/mL); (c-d) Results of responsive hydrogel treated with Hepes buffer (30 mM); and (e-f) Results of responsive hydrogel treated with DTT (13 mM in Hepes buffer). The hydrogel was able to be cleaved by LC of BoNT/A at 40 h post exposure, but remained intact in buffer and DTT. All scale bars are 2.5 mm.

post remained intact after being treated with DTT (13 mM in Hepes buffer solution; reaction temperature: 37°C) for 40 h as shown in Fig. 3.6(e-f), confirming that the newly designed acryloyl-PEG-SNAP peptide crosslinker was stable in DTT containing buffer.

3.4.3 Reduction of hydrogel size to improve the detection sensitivity

To enhance the sensitivity and shorten the response time of the BoNT/A-responsive hydrogel, as well as to reduce the cost associated with these hydrogels, we further improved the lithography and polymerization process to reduce the size of the photo-patterned hydrogel posts. Large-sized responsive hydrogel requires much longer reaction time to be cleaved. It also increases the cost of raw materials and requires longer UV exposure time to ensure complete crosslinking of the pre-hydrogel. It was observed that increasing the UV exposure could induce over-polymerization on the surface of hydrogels, which made them harder to be cleaved by LC of BoNT/A or even trypsin. In addition, the residue produced during the degradation of large gels formed a thicker blocking layer hindering further cleavage of the rest of the gel by inhibiting the diffusion of LC on the gel surface, thus lowering the sensitivity.

Fig. 3.7 shows the testing result of a hydrogel post with much reduced size of 200 μm in diameter and 50 μm in thickness, the smallest size achievable with our photo-patterning system. The hydrogel post was treated with the same concentration of LC of BoNT/A (concentration: 45 μg/mL; amount: 10 μL; refreshed every 8 hours) as in Fig. 3.6. Compared to the result in Fig. 3.6, the response time of this smaller sized hydrogel was dramatically shortened. Fig. 3.7(b-d) show that the smaller sized hydrogel post was degraded within 22 h. Identical hydrogel posts were also treated with the same Hepes buffer and DTT solutions as before as negative controls. These

hydrogel posts remained stable in both Hepes buffer and DTT solutions, similar to those shown in Fig. 3.6(c-f).

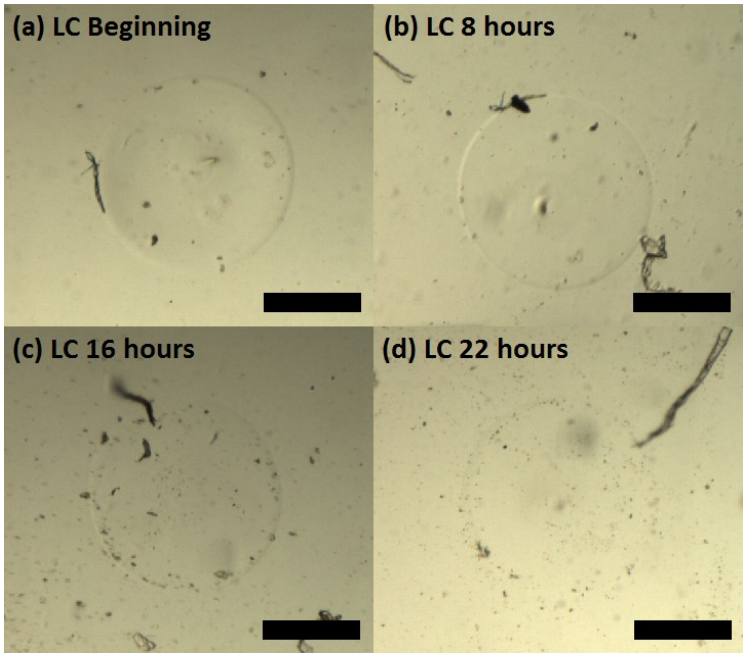

Fig. 3.7: Images showing the results of optimized BoNT/A-responsive hydrogel posts exposed to LC of BoNT/A (45 μg/mL). As exposure time proceeded, the hydrogel post became thinner and was nearly completely decomposed in 22 h. All scale bars represent 100 μm. Reaction time is indicted in individual panels.

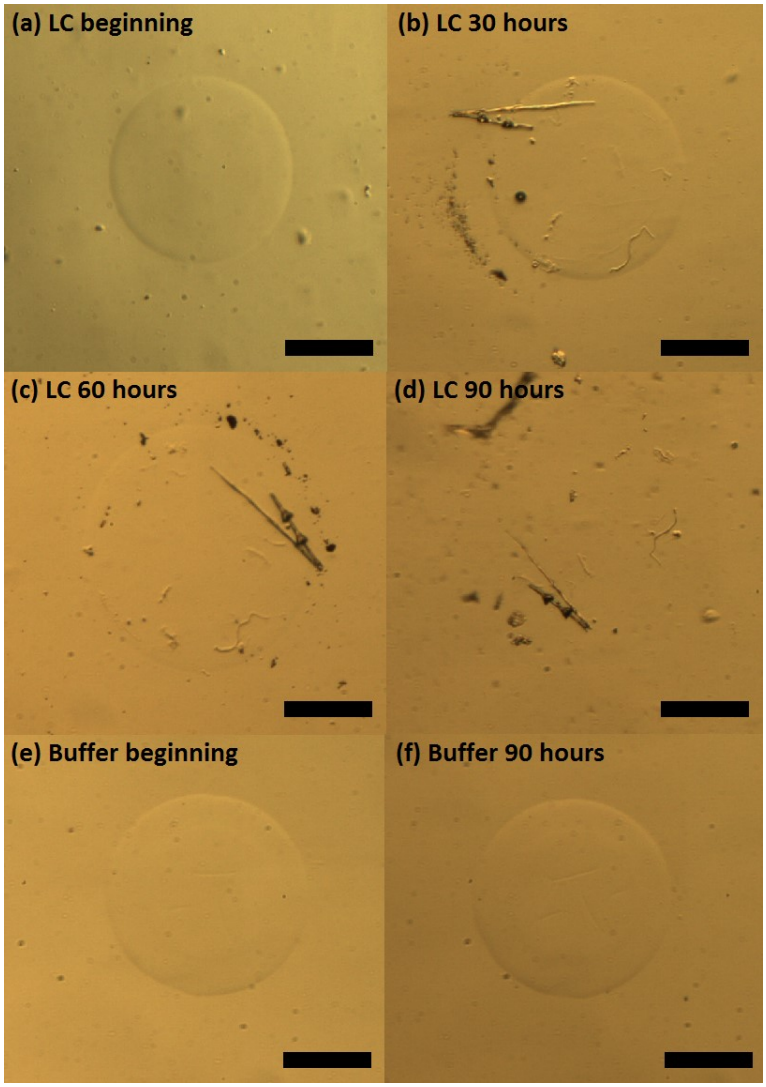

Fig. 3.8: Images of BoNT/A-responsive hydrogel post patterend in small size and treated with: (a-d) low concentration of LC of BoNT/A (4.5 μg/mL); (e,f) buffer solution. Reagents and reaction time are indicated in individual panels. As the reaction proceeded, the hydrogel in LC was cleaved and became thinner, and ultimately decomposed completely in 90 h. The hydrogel treated with buffer remain intact throughout the process. All scale bars are 100 μm.

With the reduced size of hydrogel structures, we studied the impact of LC concentration on gel cleavage. Fig. 3.8 shows that the rim area of the hydrogel post

200 μm in diameter and 50 μm in thickness collapsed in the presence of low concentration of LC of BoNT/A (concentration: 4.5 μg/mL; amount: 10 μL; refreshed every 8 hours) and was dissolved by water rapidly in 60 h. The whole structure was degraded in 90 h (Fig. 3.8(d)). Fig. 3.8(e-f) indicated that the post was stable in buffer solution without shape change. As comparison, we also used this low concentration of LC (concentration: 4.5 μg/mL; amount: 10 μL; refreshed every 8 hours) to treat a slightly larger sized hydrogel post (diameter 300 μm, thickness 80 μm). The collapse of gels first took place in the thin peripheral areas within 80 h. The whole posts was degraded and dissolved into water in 160 h, 1.7 times as slow as the case in Fig. 3.8. This confirms our concept that smaller hydrogel structure would have shorter response time to BoNT/A.

In order to double check our concept, we increased the size to600 μm in diameter and 50 μm in thickness, and tested the hydrogel with 4.5 4.5 μg/mL LC of BoNT/A. In Fig. 3.9, the hydrogel was first cleaved and became pasty, and subsequently expanded in size. After it reached the largest size as showing in the Fig. 3.9 (b), the rim of the hydrogel became so pasty and thin that it was easily cleaved and flushed away with the introduction of the refreshening BoNT/A solution. The same process went on and the hydrogel structure was reduced in size and ultimately completely cleaved after 160 hours. The hydrogel posts treated with Hepes buffer were in intact (Fig. 3.9 (g-h)). Comparing to the hydrogel with smaller size in the fig. 3.8, it took 160 hours to be totally cleaved. It took much longer time than the smaller size at the same concentration of LC.

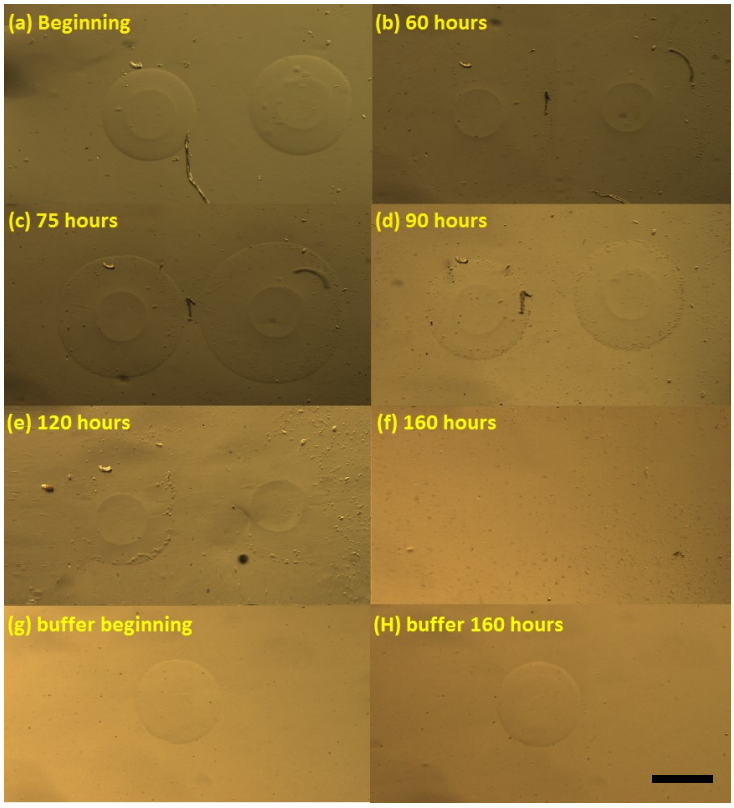

Fig. 3.9: (a-f)Cleavage of responsive hydrogel by BoNT/A (4.5 µg/mL). The hydrogel structure expended at the beginning, then collapsed, and became pasty. (g-h) The same hydrogel was intact in Hepes buffer. The scale bar is 0.5mm.

3.5 Conclusion

In this chapter, a new microfluidics-based PAAm hydrogel sensor incorporating a modified SNAP-25 peptide for the detection of BoNT/A was developed. The new modified SNAP 25 peptide used in the hydrogels possesses an optimized sequence and conjugation sites for the APN crosslinker to anchor. These gels could be degraded in trypsin, indicating that the modified SNAP 25 peptide was crosslinked into the hydrogel and was accessible to the enzyme. The degradation of the gels when exposed to the LC of BoNT/A depends on the concentration of LC, gel size and reaction time.

The BoNT/A can be detected by direct observation of the morphology change of the hydrogel. The best response of the BoNT/A sensing hydrogel we achieved was within 22 h at 45 μg/mL of LC, and the lowest LC concentration of 4.5 μg/ in 90 h, with hydrogel post 200 μm in diameter and 50 μm in thickness. The hydrogels remained intact in both control buffer and DTT solutions. The non-response to DTT because of the removal of the disulfide bonds in the crosslinker is an improvement compared with prior art, as it eliminates potential false alarms due to cleavage of the disulfide bonds linking the peptide to the APN by DTT, a necessary reducing agent used to fully activate the BoNT/A in in vitro tests. The newly designed SNAP-25 25-mer contributed to the high sensitivity, specificity and accuracy of sensing. The result shows the promise for this hydrogel to be used to detect bio-active BoNT/A. The detecting mechanism in this charter is just based on naked human eyes, and the hydrogel need be nearly totally cleaved by target agent, and then obvious changed could be observed by human naked eyes. Actually, once the target agent contacted the hydrogel, the change of the hydrogel started. Therefore, we try to get another way to observe the change of the hydrogel based on the cleavage by target agent, and this is motivation for the next chapter we introduce the fiber-optics to further improve the sensitivity of our device.

3.6 References

[1] A. Boyer, H. Moura; A. Woolfitt, S. Kalb; L. McWilliams, A. Pavlopoulos, J. Schmidt; D. Ashley, and J. Barr, “From the mouse to the mass spectrometer: detection and differentiation of the endoproteinase activities of botulinum neurotoxins A-G by mass spectrometry,” Anal. Chem. 2005, 77, 3916-3924.

[2] S. Cai, B. R. Singh, and S. Sharma, "Botulism diagnostics: from clinical symptoms to in vitro assays," Clin. Rev. Microbiol. 2007, 33, 109-125.

[3] W. S. Hong, E. W. K. Young, W. H. Tepp, E. A. Johnson, and D. J. Beebe, "A Microscale Neuron and Schwann Cell Coculture Model for Increasing Detection Sensitivity of Botulinum Neurotoxin Type A ," Toxicol Sci. doi: 10.1093/toxsci/kft082.

[4] A. K. Singh, L. H. Stanker, and S. K. Sharma, "Botulinum neurotoxin: where are we with detection technologies?" Critical Reviews in Microbiology, 2013, 39, 43-56.

[5] M. L. Frisk, W. H. Tepp, G. Y. Lin, E. A. Johnson, and D. J. Beebe, "Substrate-modified hydrogels for autonomous sensing of botulinum neurotoxin type A," Chem. Mater. 2007, 19, 5842-5844.

[6] L. D. S. Smith, and H. Sugiyama, (1988). "Botulism. The Organism, its Toxin, the Disease," Springfield, IL: Charles C. Thomas.

[7] G. R. Smith, and C. J. Moryson, (1977). "A comparison of the distribution of Clostridium botulinum in soil and in lake mud," J Hyg (Lond) 78, 39-41.

[8] H. M. Solomon, and T. J. Lilly, (2001) "Clostridium botulinum. In: Bacteriological analytical manual", 8th Ed. Silver Spring, MD, USA: US Food and Drug Administration.

[9] S. J. Eliasberg, J. L. Ferreira, "Detection of Preformed Type A Botulinal Toxin in Hash Brown Potatoes by Using the Mouse Bioassay and a Modified ELISA Test," J. AOAC Int. 2001, 84, 1460-1464.

[10] R. W. Phillips, and D. Abbott, "High-throughput enzyme-linked immunoabsorbant assay (ELISA) electrochemiluminescent detection of botulinum

toxins in foods for food safety and defence purposes," Food Addit. Contam. Part A, Chem. Anal. Control. Expo. Risk Assess. 2008, 25, 1084-1088.

[11] S. S. Arnon, "Botulinum toxin as a biological weapon: medical and public health management," J. Am. Med. Assoc. 2001, 285, 1059-1070.

[12] M. C. Scotcher, L. W. Cheng, and L. H. Stanker, "Detection of Botulinum Neurotoxin Serotype B at Sub Mouse LD50 Levels by a Sandwich Immunoassay and its Application to Toxin Detection in Milk," PLoS ONE, 2010, 5, e11047.

[13] H. Wu, Y. Huang, S. Lai, Y. Huang, and M. F. Shaio, "Detection of Clostridium botulinum neurotoxin type A using immuno-PCR," Lett Appl Microbiol, 2001, 32, 321-325.

[14] M. Lindstrom, R. Keto, A. Markkula, M. Nevas, S. Hielm, and H. Korkeala, "Multiplex PCR assay for detection and identification of Clostridium botulinum types A, B, E, and F in food and fecal material," Appl. Environ. Microbiol. 2001, 67, 5694-5699.

[15] J. R. Barr, H. Moura, A. E. Boyer, A. R. Woolfitt, S. R. Kalb, A. Pavlopoulos, L. G. McWilliams, J. G. Schmidt, R. A. Martinez, and D. L. Ashley, "Botulinum neurotoxin detection and differentiation by mass spectrometry," Emerging Infect. Dis. 2005, 11, 1578-1583.

[16] S. Pellett, W. H. Tepp, S. I. Toth, and E. A. Johnson, "Comparison of the primary rat spinal cord cell (RSC) assay and the mouse bioassay for botulinum neurotoxin type A potency determination," J. Pharmacol. Toxicol. Methods 2010, 61, 304-10.

[17] R. C. M. Whitemarsh, C. L. Pier, W. H. Tepp, S. Pellett, and E. A. Johnson, "Model for studying Clostridium botulinum neurotoxin using differentiated motor

neuron-like NG108-15 cells," Biochem. Biophys. Res. Commun. 2012, 427, 426-430.

[18] J. Schmidt, R. Stafford, and C. Millard. "High-throughput assays for botulinum neurotoxin proteolytic activity: serotypes A, B, D, and F," Anal. Biochem. 2001, 296, 130-137.

[19] W. Liu, V. Montana, E. Chapman, U. Mohideen, and V. Parpura, "Botulinum toxin type B micromechanosensor," Proc. Natl. Acad. Sci. U. S. A. 2003, 100, 13621-13625.

[20] F. Gessler, S. Pagel-Wieder, M. A. Avondet, and H. Bohnel, "Evaluation of lateral flow assays for the detection of botulinum neurotoxin type A and their application in laboratory diagnosis of botulism," Diagn. Microbiol. Infect. Dis. 2007, 57, 243-249.

[21] J. E. Keller and E. A. Neale, "The role of the synaptic protein snap-25 in the potency of botulinum neurotoxin type A," J. Biol. Chem. 2001, 276, 13476-13482.

[22] S. Bandyopadhyay, A. W. Clark, B. R. DasGupta, and V. Sathyamoorthy, "Role of the heavy and light chains of botulinum neurotoxin in neuromuscular paralysis," J. Biol. Chem. 1987, 262, 2660-2663.

[23] Xiudong Wu, Chensha Li, Guangyun Lin, Xuezhen Huang, William Tepp, Eric A. Johnson and Hongrui Jiang "A Microfluidic Sensor of Botulinum Neurotoxin Type A Utilizing SNAP-25 Incorporated Responsive Hydrogel," Technical Digest of the IEEE Conference on Sensors 2013, Baltimore, MD, Nov. 4-6, 2013, pp. 629 – 632.

[24] J. J.Schmidt, and K. A. Bostian, "Botulinum toxin: From poison to remedy," J. Protein Chem. 1997, 16, 19-26.

[25] J. J. Schmidt, and R. G. Stafford, “Fluorigenic substrates for the protease activities of botulinum neurotoxins, serotypes A, B, and F,” Appl. EnViron. Microbiol. 2003, 69, 297-303.

[26] B.R. DasGupta, and M.L. Dekleva, “Botulinum neurotoxin type A: sequence of amino acids at the N-terminus and around the nicking site,” Biochimie 1990, 72, 661-664.

CHAPTER 4. FIBER OPTIC BIOLOGICAL/CHEMICAL SENSING SYSTEM BASED ON DEGRADABLE HYDROGEL

4.1 Introduction

The detection of biological agents, especially biotoxins, plays a crucial role in a broad range of applications related to biodenfense, environmental monitoring, food safety and public health [1], [2]. A large variety of detection schemes based on different principles have been developed, such as mouse lethality assay [3], enzyme-linked chemiluminescence assay [4]-[8], electrochemiluminescence [9], immune/real-time-polymerase chain reaction (PCR) [10], [11], cell culture assay [12], [13], surface plasmon resonance (SPR) [3], [14], and mass-spectrometry [15]. Despite their high sensitivity, these methods generally require time-consuming sample preparation or long incubation time, need high-cost, complicated instrument and skilled personnel, and are generally not suitable for in-field detecting [14]. In addition, some of these methods, such as mass-spectrometry, cannot distinguish between active and inactive biotoxins [15]. However, swift in-field testing is often of utmost importance in biodefense [16]. Therefore, there is enormous demand for a low-cost, easy-to-use, fast screening tool that allows for rapid in-field detection of active biotoxins with high sensitivity and specificity.

Sridharamurthy *et al.* [17] previously reported on an autonomous sensing mechanism based on a polyacrylamide (PAAm) hydrogel. In this method, a crosslinker crosslinks water-soluble acrylamide chains to water insoluble network hydrogel (Fig. 4.1(a, b)). The crosslinker can be cleaved by a specific agent, and the hydrogel thus degrades and becomes water-soluble after the cleavage, revealing the

presence of the toxin in the sample (Fig. 4.1(c, d)). Various biological agents could be detected utilizing different crosslinkers. This approach exploits the intrinsic protease activityof the corresponding enzyme and thereby leverages the inherent amplification function associated with the targetenzyme. Therefore, the potential sensitivity and specificity of this method could be extremely high. In addition, it is well suited for detecting biotoxins, because many of them are proteases. For example, active botulinum neurotoxins could be detected with this method using a synaptosomal-associated protein (SNAP) 25-mer peptide as the crosslinker [18]-[20]. Although these works show the potential of low-cost, easy-to-use and in-field detection capability, a relatively large amount of toxin and long degradation process are needed to cause visible physical changes of the hydrogel. Consequently, the sensitivity and speed of detection is still much inferior to what this mechanism could offer.

To significantly improve the sensitivity and the speed of detection, we have adopted a fiber-optic method to detect the degradation of the hydrogel during the cleavage process. Sensors based on fiber optics, such as various fiber-based interferometers, have been widely studied in the detection of pH [21], glucose [22] and bacteria [23] owing to its small size, in-line structures and high sensitivity [24], [25]. Nevertheless, measurement of changes in the optical properties of hydrogels for toxin detection has yet been reported. In this work, we present a high-sensitivity, high-detection-speed PAAm hydrogel sensor based on an optic fiber Fabry Perot interferometer (FPI). As a demonstration, we applied dithiothreitol (DTT) solution to cleave the disulfide-crosslinked PAAm hydrogel, and monitored in real time in the optic fiber FPI the unique spectral changes of the interference induced by the degradation of the PAAm hydrogel due to the DTT solution.

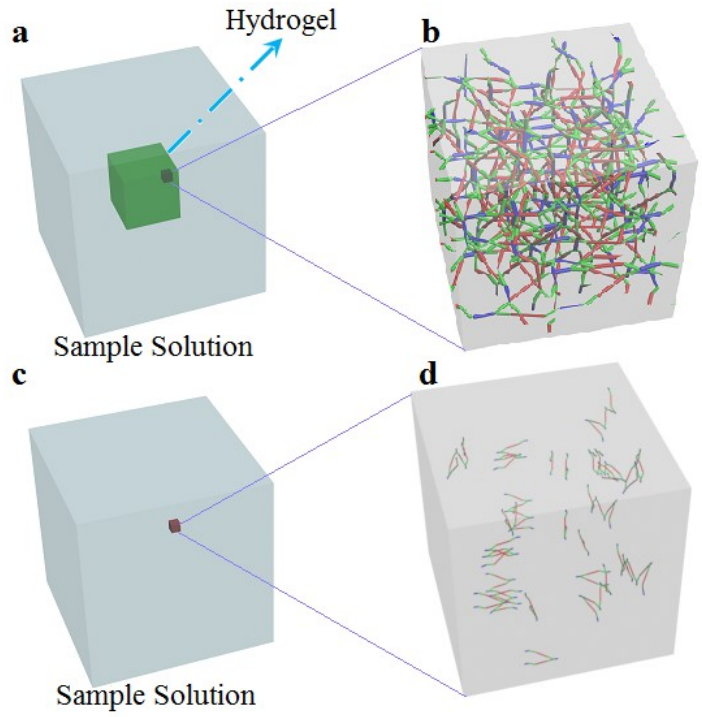

Fig. 4.1: Schematic diagram of the cleavage of the hydrogel. (a, b) The initial structure of the hydrogel before cleavage. (c, d) The structure of the hydrogel after cleavage.

4.2 Detection Mechanism

In previous works utilizing the mechanism discussed above, the presence of the target agent could only be confirmed after the hydrogel was completely degraded, showing a clear and visible morphology change. The degradation process in fact induces a continuous change of optical properties of the hydrogel, such as the refractive index (RI) [26]. Hence, monitoring such change in the RI throughout the degradation process could confirm the cleavage of the hydrogel at a very early stage, even at the onset, when there is still no distinguishable morphological change in the hydrogel. To demonstrate this concept, we used N, N' – bis(Acryloyl) crystamine as the crosslinker to closslink the PAAm hydrogel inside the cavity of the optic fiber FPI.

DTT solutions were utilized to cleave the disulfide bond in the closslinker (see section II A), and thus change the optical property such as the RI of the hydrogel. As a result,

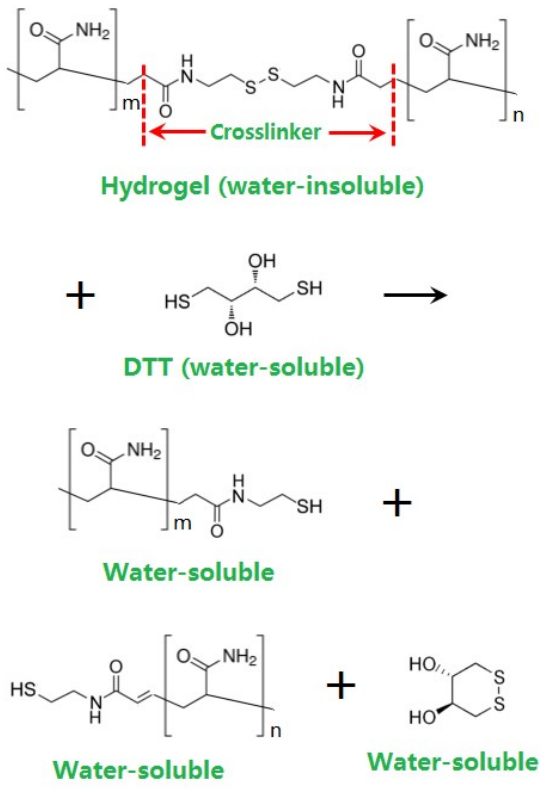

Fig. 4.2: The cleavage of the hydrogel. The disulfide bond in the hydrogel can be cleaved by the DTT. The hydrogel is initially water-insoluble, but all of the products after cleavage become water-soluble.

the interference of light in the optic fiber FPI varied, showing shifts in the reflected spectrum obtained from an optical spectrum analyzer (OSA), which in turn was used to determine the degradation of the hydrogel (see section II B).

4.2.1 Degradation of Hydrogel by DTT solution

Fig. 4.2 shows the chemical reaction of the cleavage of the hydrogel by DTT.

Before degradation, the hydrogel is water-insoluble. DTT is a reducing agent that can break the disulfide bond, hence the crosslinker. All products of the reaction then become water-soluble. Therefore,the hydrogel can now be dissolved by water. Fig. 4.1 shows the schematic of the cleavage of the hydrogel by a target agent. Fig. 4.1(a, b) shows the status of the hydrogel before degradation, which is a gel, while Fig. 4.1(c, d) shows the status afterwards. In prior works [18]-[20], clearly visible morphology change before and after the degradation must be present to conform the detection of the target agent, meaning that the cleavage reaction had to be almost finished. However, once the cleavage reaction starts, the RI of the hydrogel would change continuously until the end of the cleavage process, since the RIs of the reactants and the products are all different. Therefore, the target agent could be detected by monitoring the RI change of the hydrogel at the very beginning of the cleavage reaction. This would significantly improve the sensitivity and detection speed compared with observing the morphology change of the hydrogel.

4.2.2 Detection of RI Change by optic fiber FPI

The structure of our device is schematically illustrated in Fig. 4.3 (a). A single-mode optic fiber is mounted in a chamber with one polished end facing a vertical glass slide, forming two end faces of the FPI cavity. A gap of around 150 μm between the fiber end and the glass slide is filled with closslinked hydrogel. The reflected white light, I_1 and I_2, at the two end faces would interfere inside the core, as shown in Fig. 4.3 (b). Because the reflectivity at the end faces is low, multiple reflections in the cavity is negligible, and the interference of I_1 and I_2 can thus be modeled by the following equation [27]:

$$I = I_1 + I_2 + 2\sqrt{I_1 I_2}\cos(\frac{4\pi n \times L}{\lambda} + \phi_0), \quad (1)$$

where*I* is the intensity of the interference, *n* the RI of the medium filling the cavity, *L* the length of the cavity, ϕ_0 the initial phase of the interference, and λ the optical wavelength in vacuum.

When the phase of the cosine term turns to an odd number of π, that is,

$$\frac{4\pi nL}{\lambda_v} + \phi_0 = (2m+1)\pi, \ldots\ldots(2)$$

the interference intensity, *I*, reaches its minimum, which is the interference valley. Here, λ_v is the center wavelength of the interference valley. In our experiment, *L* remained constant, and only the RI of hydrogel, *n*, induced the shifts in the interference valleys and peaks. After being exposed to the DTT solution, the network structure of hydrogel starts to be broken down and dissolved by water, causing a time dependent change of RI, *n*. According to Eq. (2), taking the derivative of *n* with respect to λ_v and assuming a constant *L*, we obtain:

$$\Delta\lambda_v = \lambda_v \times \frac{\Delta n}{n}, \ldots\ldots(3)$$

which shows that the relative RI change of the hydrogel, Δ*n*, is proportional to the interference valley shift, $\Delta\lambda_v$.

4.3 Experimental

4.3.1 Fabrication of optic fiber FPI

The FPI device was fabricated based on a fiber optics connector (FOC; PLC-1X2, Fibertronics, Inc., FL, USA). The fabrication of the optic fiber FPI is shown in Fig.

4.4. First, four glass slides were glued together by ultra-violet (UV) glue after being exposed to UV light with an intensity of 25 mW/cm^2 for 1 min (Fig. 4.3(a)). Second, the end-section of the output fiber of the FOC was cut with an optic fiber cutter, followed by polishing using 5 different polishing films successively to smoothen its surface. Third, the prepared FOC was fixed on a glass slide by six rectangular solid

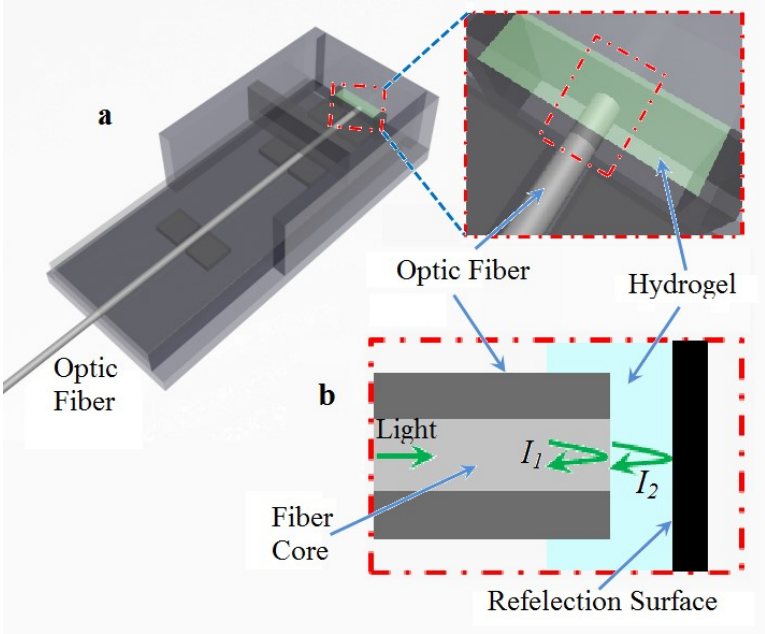

Fig. 4.3: (a) Schematic of an FPI device and the enlarged view of the FPI cavity. DTT cleaves the hydrogel (the green area)in the FPI cavity. As a result, the RI of the hydrogel would change. (b) The mechanism of the FPI. The RI change brings about the spectral shift for the FPI.

polydimethylsiloxane (PDMS) blocks with the end face of the FOC positioned out of the side face by 2 mm. The sides of the six PDMS blocks were parallel to the long side of the glass slide, which is also the direction of the fiber. The structure was then applied liquid PDMS and placed on a hotplate at 90°C for 60 min to cure (Fig. 4.4(b)).

Fourth, the components from step 1 and step 3 were combined using PDMS as adhesive (Fig. 4.4(c)). The process of combining the two was carefully performed under a microscope. The end of the fiber should be parallel to the opposite glass surface. It is important that the distance be around 100 μm between the end-section of the fiber and the corresponding opposite glass surface. If the distance is too large, the measured signal would be too weak; if the distance is too short, there would not be enough hydrogel between the two surfaces. Finally, the three glass slides (the green ones in Fig. 4.4(d)) were adhered to the device using PDMS (Fig. 4.4(d)). The end section surface and the glass surface thus formed an FPI cavity (the green area in Fig. 4.3(a)). The liquid pre-hydrogel would be injected into the cavity, and the four surrounding glass slides above the hydrogel (Fig. 4.3(a)) were to hold the liquid samples.

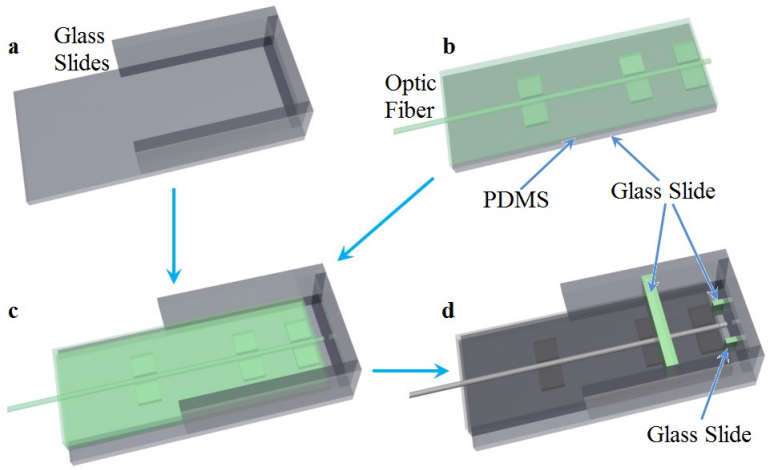

Fig. 4.4: The fabrication process of the FPI device. (a) Four glass slides are glued together. (b) The optic fiber is fixed on a glass slide with PDMS (in green). (c) The parts in (a) and (b) are combined using PDMS. (d) Three glass slides (in green) are glued to the device with PDMS.

4.3.2 Synthesis of hydrogel

In our experiment, the PAAm based pre-hydrogel was photo-polymerized by UV light. The materials used for the pre-hydrogel were acrylamine (AAm, Aldrich Chemicals), N, N' – bis(Acryloyl) crystamine (cross-linker, Aldrich Chemicals), 4-benzoy(benzyl) trimethyl-ammonium chloride (BP+, Aldrich Chemicals), N-methyl-diethanolamine (NMDA, Aldrich Chemicals), and DI water. These five materials were mixed in a ratio by weight (0.15: 0.00375: 0.02: 0.02: 1) to obtain 10 mL of pre-hydrogel solution.

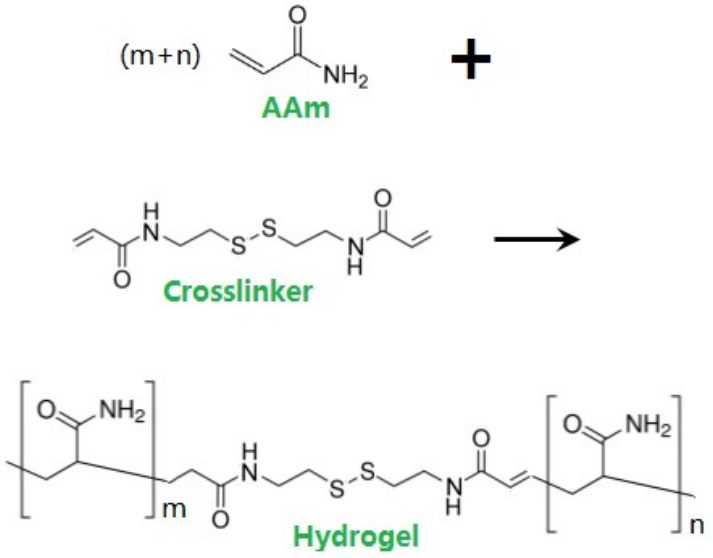

Fig. 4.5: The synthesis of the hydrogel.

The 10 mL pre-hydrogel was injected into the cavity (the green area in Fig. 4.3(a)), and then exposed to UV light with a dose of 18 mW/s for 180 s to be polymerized. In the pre-hydrogel, the monomer, acrylamide (AAm), would combine into AAm long chains, which was soluble by water. At the same time, the crosslinker would link those AAm long chains to a networked structure, which then became insoluble to

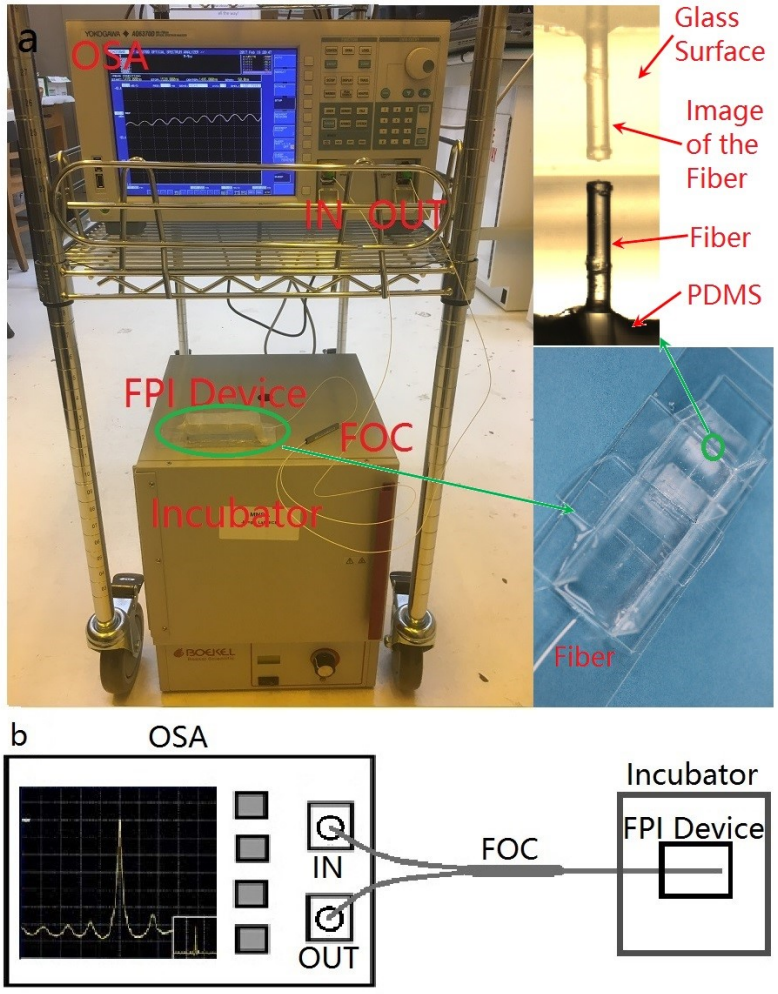

Fig. 4.6: Experimental setup of the FPI sensing system. (a) Photo of the experimental set up. (b) Schematic diagram of the experimental setup. The OSA serves as both the light source and the measurement apparatus. Two terminals of the FOC are connected to the light output and input of the OSA

water. The related chemical reaction is showed in Fig. 4.5. After the photo-polymerization, the hydrogel was flushed by ethanol (100%) for 5 min to eliminate unpolymerized pre-hydrogel, and the whole device was subsequently baked on a hotplate at 50 ℃ for 5 min to remove the ethanol. Afterward, 1 mL of DI water was

injected to soak and prep the hydrogel for 5 hrs before the water was removed. At this point, the interference spectrum stabilized and the device was ready for testing.

4.3.3 Experimental Setup

Fig. 4.6 shows a photo and the schematic diagram of the FPI sensing system. In our experiment, we used an OSA (AQ6370d, Yokogawa, Japan) to detect the interference spectrum of the reflected light. The light source (PLC-1X2, Fibertronics, Inc., FL, USA) was built into the OSA, which delivered wide-spectrum near-infrared light with the wavelength of between 1475 and 1485 nm. The resolution of the OSA was set at 0.5 nm, and each data was the result of averaging 5 measurements. One output of the FOC was connected to the built-in light source in the OSA. The other output of the FOC was connected to the input of the OSA for measurement. The input of the FOC was integrated into the FPI device during the fabrication, as shown in Fig. 4.6 (c). Throughout the testing, the FPI device was wrapped by a wet parafilm (Bemis Company Inc, WI, USA) to prevent the evaporation of the liquid in the FPI. The whole device was kept in an incubator at a temperature of 37±0.3 ℃. To avoid vibration of the device, which would induce inaccurate measurement of the highly-sensitive FPI, the incubator was placed on solid ground.

4.4 Results and discussion

In a test, liquid samples were injected into the optic fiber FPI device via a microfluidic channel. The diffusion of the DTT from the liquid to the hydrogel and the resultant degradation of the hydrogel would disturb and shift the output spectrum of OSA. Before we tested with the DTT solutions, spectral shifts induced by the

injection of DI water was first obtained as a reference data, representing the disturbances and the level of systematic errors in our testing system.

4.4.1 Spectral shift induced by DI Water

The hydrogel in the FPI cavity was previously immersed in DI water; therefore, adding new DI water would not change the RI and the texture of the hydrogel. Any variations in the spectrum obtained by the OSA were caused by the disturbances and systematic errors, which were recorded as reference data for the purpose of calibration. We injected 1 ml of DI water (37±0.3 ℃, identical to the temperature of the hydrogel) into the optic fiber FPI cavity, and measured the spectra from the very beginning (0 min) to 240 min after the injection. During the whole process, the FPI device was kept in the incubator with a temperature of 37±0.3 ℃. The spectra obtained at 0 min, 120 min and 240 min are shown in Fig. 4.7. It shows an initial slight red shift of about 0.4

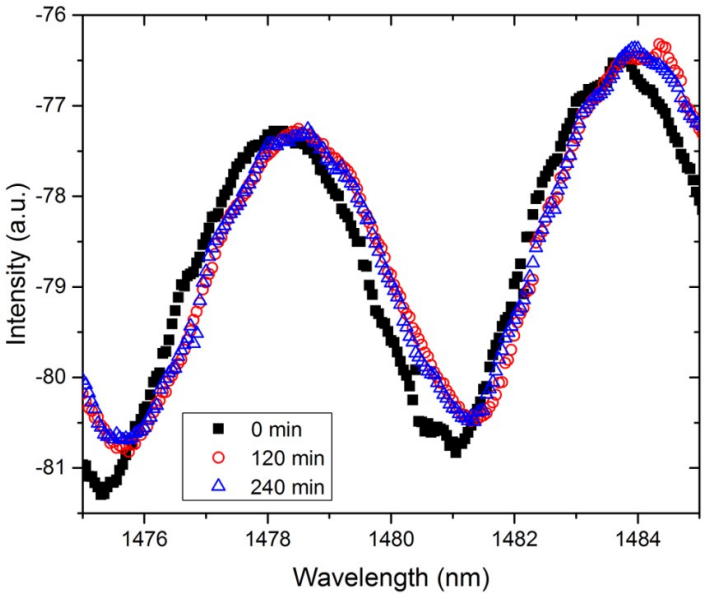

Fig. 4.7: The interfering spectrums acquired at 0 min, 120 min and 240 min after injection of DI water into the optic fiber FPI device.

nm after the DI water injection, and stabilized after 120 min. The red shift of the interfering spectrum with a rate of about 3 pm/min was mainly caused by the disturbance of liquid flow during the injection process of the DI water and the systematic errors of the testing device. During this process, the maximum blue spectral shift rate was much less than 1 pm/min. If we keep the environment of and within the testing device identical, any spectral shifts beyond the shifting rate of 3 pm/min would indicate the change of optical properties of the hydrogel in the FPI cavity.

4.4.2 Spectral shifts induced by DTT aqueous solutions

1 ml samples of the DTT aqueous solutions with concentrations of 1 mM, 100 μM and 50 μM were utilized to demonstrate the capability of our optic fiber FPI sensor. The DI water were kept in the incubator (37±0.3 ℃) for 2 hours, and then it was taken out to prepare the different concentrations of DTT solution for the testing immediately, minimizing the temperature difference between the target agents and the hydrogel in the FPI cavity. At the beginning, the temperature of the liquid sample would be little lower than the temperature in the incubator. The whole testing process was conducted in the incubator. The interfering spectra were acquired every 10 min.

Fig. 8 shows the test results with the 1 mM DTT solution. To show them clearly, the spectra are depicted in three charts, in Fig. 8 (a) to (c), respectively. From 0 min to 40 min after the injection of the DTT solution, the spectrum shows a clear red shift of about 4 nm, as demonstrated in Fig. 8 (a). In the first 10 min, the shifting rate was much higher than the rest of time, which was about 150 pm/min, 50 times higher than the shifting rate of DI water. Because the temperature of the liquid sample was little lower than the temperature in the incubator, the temperature of the liquid sample

would increase little bit, leading to such spectral red shift. The diffusion of the DTT increased the concentration of the DTT in the hydrogel gradually, and then increased the cleavage reaction rate. Therefore, the interfering spectrum started to shift towards the short wavelength region (blue shift). From 40 min to 80 min, the spectrum shifted about 1.75 nm with a rate of about 44 pm/min, as shown in Fig. 8 (b). The blue spectral shift lasted for a much longer time than the red spectral shift, indicating a long and slow degradation process of the hydrogel. From 80 min to 130 min, the spectrum continuously shifted to the short wavelength side with a decreased rate of about 20 pm/min, as shown in Fig. 8 (c). Because the rate of the blue spectral shift was still several times higher than the reference data obtained with DI water, it was mainly caused by the continuous change of the optical property of the hydrogel rather than disturbance or system errors. After 130 min, the blue spectral shift did not stop, but the shifting rate was slowing down. Such long-time and continuous spectral shift with decreasing shifting rate was consistent with the chemical cleavage reaction process of the hydrogel. The concentration of the DTT decreased as the cleavage process proceeded, resulting in a slowing reaction.

Similar phenomena in spectral shift induced by the DTT solution were also observed in samples with DTT concentrations of 100 μM and 50 μM. The difference was the onset time of the blue spectral shifts. During this onset period, there is a competence between red-shift caused by initial temperature increase and blue-shift caused by the cleavage reaction. Fig. 9 shows the result obtained with the 100 μM DTT solution. The red spectral shift lasted about 100 min, as shown in Fig. 9 (a), much longer than the results from the 1 mM DTT solution (40 min). The lower concentration of DTT led to a much slower cleavage reaction rate, which in turns prolonged the stabilization

process of the liquid system. We could observe clearly the blue spectral shift after 100

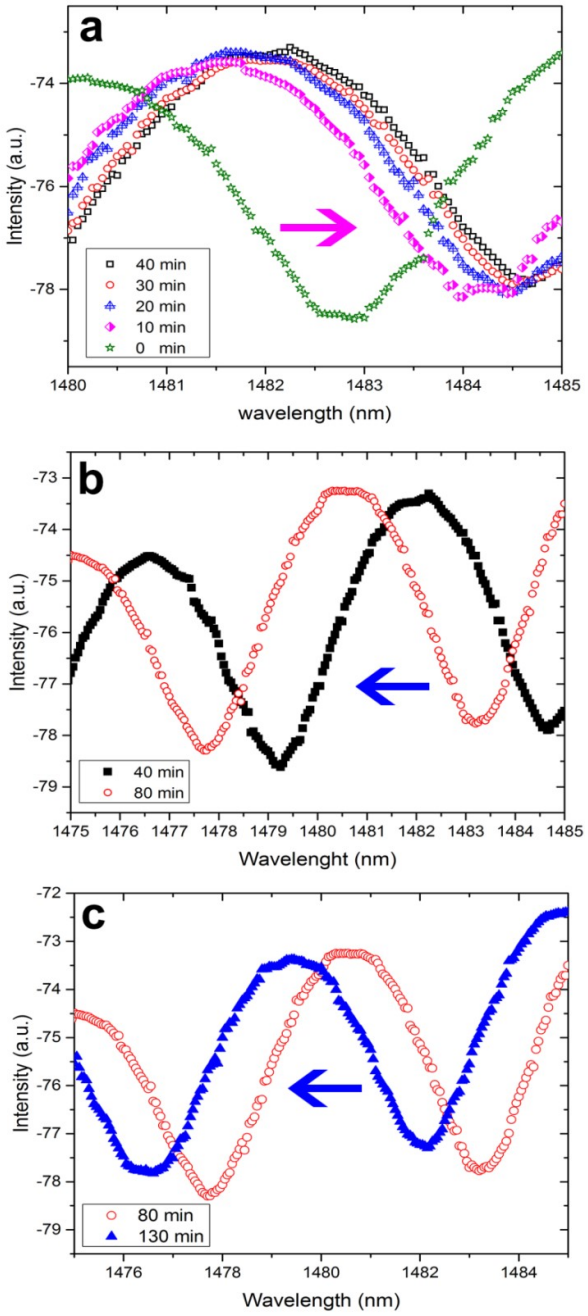

Fig. 4.8: The FPI device tested with 1 mM DTT. The red and blue arrows show the shift directions. Before 40 mins, it is red shift, and the red shift rate decreases with time. After 40 mins, it is blue shift.

min, as demonstrated in Fig. 9 (b), with an average shifting rate of about 16 pm/min. Compared to the results from the 1 mM DTT solution (44 pm/min), the cleavage process was also much slower because of the lower concentration of the DTT .

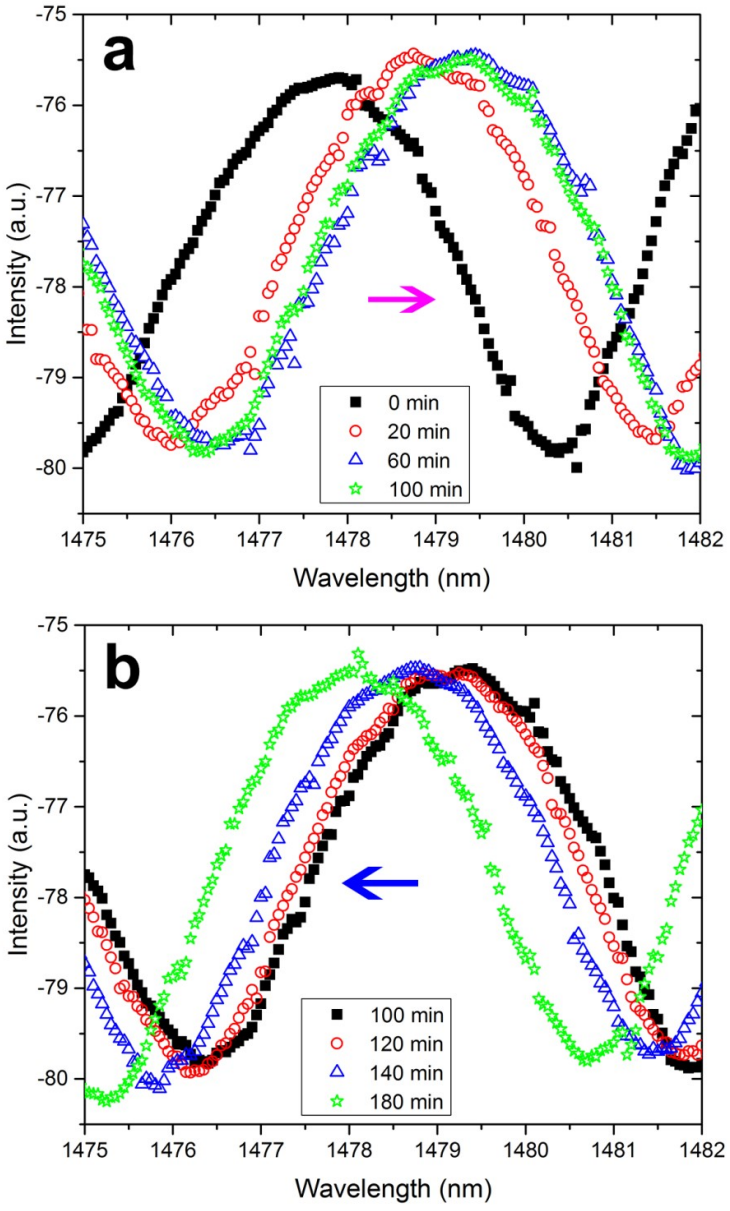

Fig. 4.9: The FPI device tested with 100 μM DTT. The arrows show the shift directions. Before 60 mins, it is red shift, and the shift rate decreases with time. After 60 mins, it starts to be a blue shift.

In the experiments shown above, the DTT solutions were pre-treated in the incubator for two hours so that their temperature was the same as that of the hydrogel in the FPI cavity. The reason for this pre-treatment was to eliminate the disturbance induced by the temperature changes. In real-world applications, temperature control of the samples might not practical. In order to investigate the disturbance induced by the temperature change during the sample injection process, we used a DTT solution with a concentration of 50 μM at the temperature of 20℃. The temperature of the target agent was much lower than that of the hydrogel. Once injected, it dramatically decreased the temperature of the overall cavity. The spectral shifting results are shown in Fig. 10. From 0 min to 60 min, the red spectral shift induced by initial temperature increase of the DTT solution was observed with a shift rate of 33 pm/min, as demonstrated in Fig. 10 (a). Fig. 10 (b) shows the red spectral shift from 60 min to 120 min. The rate of red spectral shift decreased during this period of time, and stopped around 100 min (the spectra at 80 min and 120 min are overlapped with each other, as shown in Fig. 10 (b)). The blue spectral shift started from 120 min, and the average blue shift rate was 10 pm/mins (from 120 mins to 240 mins), which was much higher than blue shift rate of the control group, as shown in Fig. 10 (c). The cleavage reaction rate by the DTT with lower concentration was much slower than that of high concentration ones, which took longer before the blue spectral shift started. Nevertheless, even when the concentration of DTT was reduced from 100 μM to 50 μM, the starting time of the blue spectral shift was almost the same. It seemed that the diffusion process of the DTT solution into the hydrogel was accelerated due to the larger temperature difference between the DTT solution and the hydrogel. This phenomenon could be helpful to shorten the stabilization period of the device and

improve the testing speed.

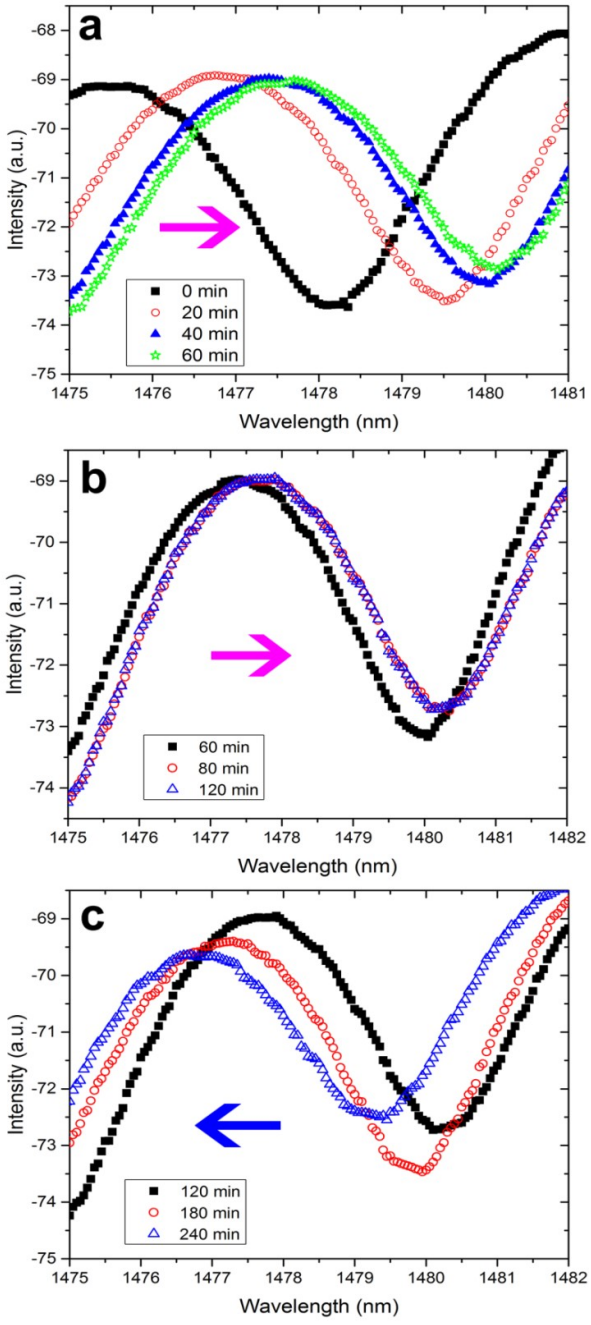

Fig. 4.10: The hydrogel tested with 50 μM DTT. The arrows show the shift directions. Before 120 mins, it is red shift, and the red shift rate decreases with time. After 120 mins, it becomes blue shift.

4.4.3 Discussion

The shifts of the interfering spectra indicate the change in the RI of the hydrogel in the FPI cavity. Fig. 11 is a demonstration which was conducted by an RSoft simulation on a FPI cavity with a length of 100 μm. The RI in the cavity was set to 1.4. When the RI in the cavity increased and decreased by 0.1%, the valley of the spectrum shifted to longer and shorter wavelength region by about 1.2 nm, respectively. The simulation result matches the experimental results shown above. Once DTT solution is injected, the initial temperature increase brings about red-shift. Concurrently, DTT starts to degrade the hydrogel and turns it back into the liquid phase with lower RI.

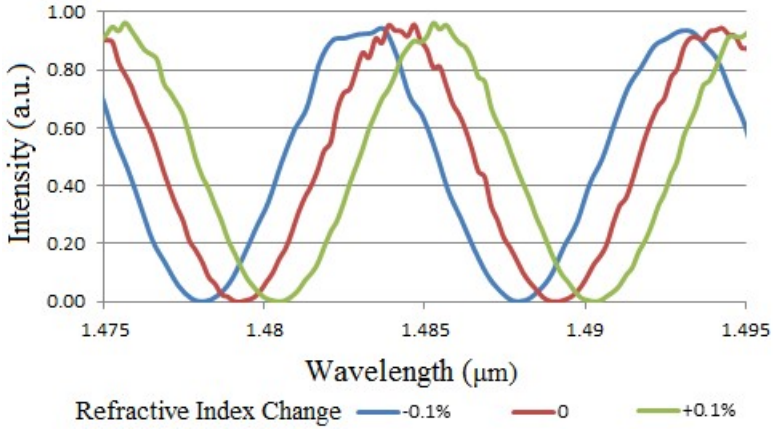

Fig. 4.11: Simulation result.When the RI of the target agent increases by 0.1%, the interfering spectrum red-shifts around 1.2 nm.When the RI of the target agent decreases by 0.1%, interfering spectrum blue-shifts around 1.2 nm.

Therefore, the interfering spectra shift to the longer wavelength region with the initial temperature increase, but the rate of the red spectral shift gradually declines until the temperature gradient between DTT solution and the hydrogel disappears.

After that, degradation of the hydrogel becomes the dominant reason of the blue spectral shift. The process of the blue spectral shift lasts longer because the cleavage of the hydrogel is a relatively slow process.

We investigated the spectral shifting process by measuring the amount of the spectral shift at different times, and the results are shown in Fig. 12. The initial position of the valley of the spectrum is defined as zero, and then red spectral shift direction was defined as positive direction. It demonstrates the complexity and uniqueness of the spectral shifting behavior during the testing process. For the DTT solution with different concentrations, the spectral shifting processes are similar, indicating the initial temperature of the DTT solution (red spectral shift) followed by a long period of decreasing RI (blue spectral shift) in the hydrogel cleavage process. For DTT solutions with low concentrations, blue spectral shifting rate should be lower than those of higher concentration samples; yet, the temperature of the target agent is also a factor that influences the shifting rate. As demonstrated in Fig. 12, because the temperature of the 50 μM DTT solution was much lower than that of the hydrogel, the diffusion rate was improved, which shortened the red spectral shifting period. We should emphasize that the blue spectral shifting processes can only be obtained when the hydrogel is cleaved. Any other chemicals which do not cleave the hydrogel, even if they may change the RI of the hydrogel in the FPI cavity, would not induce such complex spectral shifting curve shown in Fig. 12. Hence the high specificity of our sensing system. For example, a liquid with an RI or temperature higher or lower than that of the hydrogel would induce an initial red or blue spectral shift, but the shift would stop after the liquid diffusion is completed or the temperature gradient disappeared. Through this unique spectral changing pattern, our optic fiber FPI

sensor, when filled with a hydrogel with a specifically responsive crosslinker, can test the presence of a specific target agent, e.g. a biotoxin. In addition, we can estimate the concentration of the target agent in the liquid sample by analyzing the shifting rate and the starting time of the blue spectral shift process.

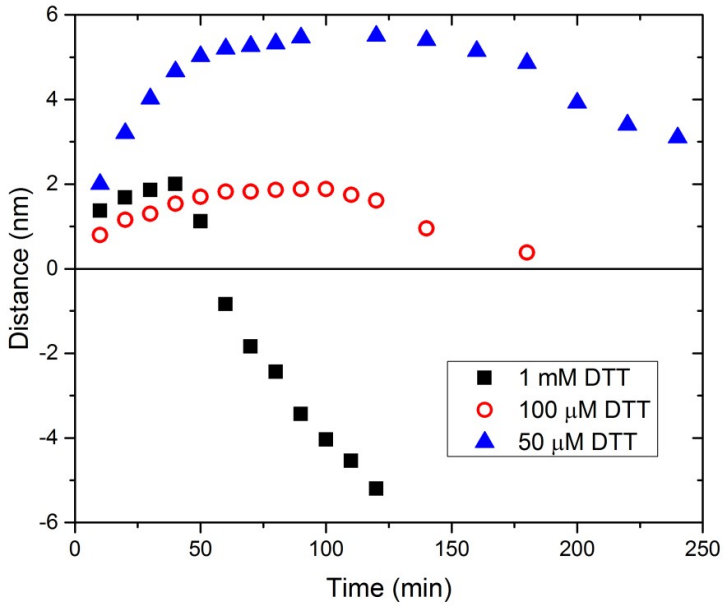

Fig. 4.12: Shift rates measured using three different concentrations of DTT. The shift direction towards longer wavelength is defined as positive.

More importantly, our FPI device can significantly improve the sensitivity and efficiency of the detection. In a previous work [17], the concentration of the target agent needed to be at least 100 mM for the reaction to induce visually observable degradation of the hydrogel, which usually took several hours. Here, the lowest concentration of the DTT solution was 50 μM, 2000 times lower than in the previous work. Furthermore, the testing time was much shortened. The presence of the target agent could be called when the blue spectral shift began rather than after hydrogel was

completely degraded into liquid phase. Fig. 4.13 (a) shows a photo of the hydrogel in the FPI cavity after the injection of 1 ml of DTT solution with a concentration of 50 μM. 4 hours later, no morphology change of the hydrogel could be observed as can be seen in Fig. 4.13 (b). However, the interfering spectrum had already shifted by several nm (note that the resolution of the OSA was 0.02 nm). Benefiting from the highly-sensitive interference optics, the detection of the degradation of the hydrogel, thus the presence of the cleaving agent, was accomplished within an hour. These results still have potential to be improved. For example, the thickness of the hydrogel applied in this experiment was 2 mm, which drastically extended the diffusion and reaction time. If the hydrogel was be patterned at the micro-scale, which could be achieved with well-established micro-lithography technologies, the detection speed as well as sensitivity of the device could be enhanced by several times.

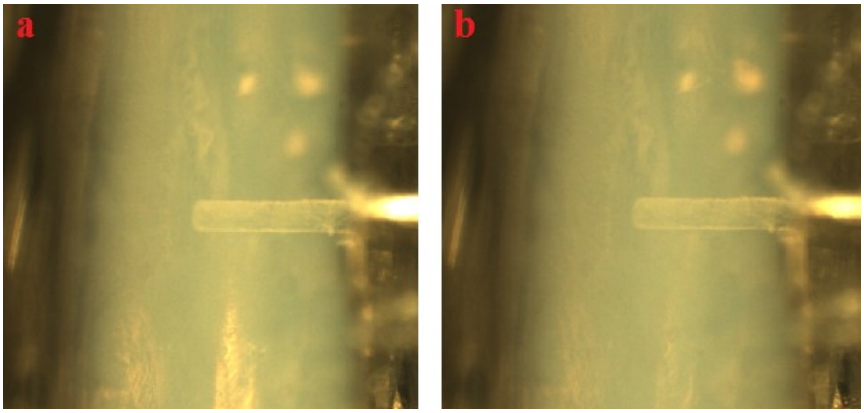

Fig. 4.13: Photos of the hydrogel at the beginning (a) and 4 hrs later (b) tested with 50 μM DTT. The light shadow is the hydrogel, and the small tube is the optic fiber.

4.5 Conclusion

We demonstrated an optic fiber FPI device that significantly improved the detection

sensitivity and efficiency of biological and chemical sensors based on degradation of hydrogels. THe hydrogels that we used in this work was PAAm hydrogel. The disulfide bond in the crosslinker of the PAAm hydrogel can be cleaved by a solution containing DTT, resulting in optical property changes in the hydrogel, even though they are not visually observable. By introducing the interfering optics shown in this work, such changes can be detected as the evidence of hydrogel cleavage. Our FPI device increased the detection sensitivity of DTT by 2000 times, and much shortened the detection time by several times, compared with prior work. We tested our device with DTT solutions with different concentrations. Spectral shift in the interference spectra that combines both red and blue shifts were observed. Such unique spectral shifting process is related to the DTT diffusion and hydrogel cleavage processes, which provides high specificity as well as the capability to determine the concentration of the target agent. We demonstrated a low concentration of detection of 50 μM of DTT and a detection time of 36 min. In the future, we will explore to further improve the sensitivity and the detection speed by reducing the thickness of the hydrogel to quicken the liquid diffusion and hydrogel reaction process. The centimeter-sized FPI sensors are promising for high-precision, ultra-sensitive and fast in-field detection of biological and chemical agents.

4.6 References

[1] M.A.Hamburg, “Bioterrorism: responding to an emerging threat,” *Trends Biotechnol*, vol. 20, pp. 296–298, July 2002.

[2] R. C. Spencer, N. F. Lightfoot, “Preparedness and Response to Bioterrorism,” *Journal of Infection*, vol. 43, pp. 104–110, Sep. 2001.

[3] P. Cunniff, “Official Methods of Analysis of AOAC International,” 16th ed. AOAC Intern Inc, Washington, pp. 46–48.

[4] R. W. Phillips, D. Abbott, “High-throughput enzyme-linked immunoabsorbant assay (ELISA) electrochemiluminescent detection of botulinum toxins in foods for food safety and defence purposes,” *Food Addit Contam Part A*, vol. 25, pp. 1084-1088, Sep. 2008.

[5] B. Klaubert, N. Vujtovic-Ockenga, R. Wermter, K. Schad, L. MeyerL, “Determination of botulinum toxins after peptic sample pre-treatment by multidimensional nanoscale liquid chromatography and nano-electrospray ion-trap mass spectrometry,” *J Chromatogr B*, vol. 877, pp. 1084-1092, Apr. 2009.

[6] A. Woolfitt, H. Moura, S. Kalb, C. P. Quinn, J. R.Barr, “Quantitative mass spectrometry for bacterial protein toxins-a sensitive, specific, high-throughput tool for detection and diagnosis,” *Molecules*, vol. 16, pp. 2391-2413, 2011.

[7] D. R. Franz, P. B. Jahrling, A. M. Friedlander, et al “Clinical recognition and management of patients exposed to biological warfare agents,” *JMMA*, vol. 278, pp. 399.411, Aug. 1997.

[8] J. B. Tucker, “Toxic Terror: Assessing the Terrorist Use of Chemical and Biological Weapons,” Cambridge, Mass: MIT Press, 2000.

[9] S. WuDunn, J. Miller, W. J. Broad, “How Japan germ terror alerted world,” New York Times,May 26, 1998:A1, A10.

[10] S. S. Arnon, R. Schechter, T. V. Inglesby, et al, “Botulinum Toxin as a Biological WeaponMedical and Public Health Management” *JMMA*, vol. 8, pp. 1059-1070, Feb. 2001.

[11] E. Aranda, M/ M. Rodriguez, M. A. Asensio, J. J. Cordoba, "Detection of Clostridium botulinum types A, B, E and F in foods by PCR and DNA probe," *Lett Appl Microbiol*, vol. 25, pp. 186-190, 1997.

[12] F. Anniballi, B. Auricchio, E. Delibato, M. Antonacci, D. Medici, L. Fenicia, "Multiplex real – time PCR SYBR Green for detection and typing of group III Clostridium botulinum," *Vet Microbiol*, vol. 154, pp. 332-338, 2012.

[13] M. Lindstrom, H. Korkeala, "Laboratory diagnostics of botulism," *Clin Microbiol Rev*, vol. 19, pp. 398-314, 2006.

[14] L. M. Wein and Y. Liu, "Analyzing a bioterror attack on the food supply: The case of botulinum toxin in milk," *PNAC*, vol. 102, pp. 9984-9989, July 2005.

[15] G. Deng and G. Sanyal, "Applications of mass spectrometry in early stages of target based drug discovery," *J. Pharm. Biomed. Anal.*, vol. 40, pp. 528-538, Feb. 2006.

[16] T. Grenda, E. Kukier, K. Kwiatek, "Methods and difficulties in detection of Clostridium botulinum and its toxins" *Polish Journal of Veterinary Sciences*, vol. 17, pp. 195-205, 2014.

[17] S. S. Sridharamurthy, A. K. Agarwal, D. J. Beebe and H. Jiang, "Dissolvable membranes as sensing elements for microfluidics based biological/chemical sensors," *Lab on a Chip*, vol. 6, pp. 840-842, May 2006.

[18] M. L. Frisk, W. H. Tepp, G. Lin, E. A. Johnson, and D. J. Beebe, "Substrate-Modified Hydrogels for Autonomous Sensing of Botulinum Neurotoxin Type A," *Chem. Mater*, vol. 44, no. 19, pp. 5842-5844, 2007.

[19] X. Wu, C. Li, G. Lin, X. Huang, W. H. Tepp, E. A. Johnson, and H. Jiang, "Microfluidic Detection of Botulinum Neurotoxin Type A Utilizing

Polyacrylamide Hydrogels," *IEEE SENSORS JOURNAL*, vol. 15, pp. 1091-1097, Feb. 2015.

[20] X. Wu et al., "A microfluidic sensor of botulinum neurotoxin type A utilizing SNAP-25 incorporated responsive hydrogel," *IEEE Sensors,* Baltimore, MD, USA, Nov. 2013, pp. 629–632.

[21] R. Wolthuis, D. McCrae, E. Saaski, J. Hartl, G. Mitchell, "Development of a medical fiber-optic pH sensor based on optical absorption," *IEEE Trans. Biomed.*, vol. 39, pp. 531-537, 1992.

[22] S. Tierneya, S. Voldenb, B. T. Stokkea, "Glucose sensors based on a responsive gel incorporated as a Fabry-Perot cavity on a fiber-optic readout platform," *Biosensors and Bioelectronics*, vol. 24, pp. 2034-2039, 2009.

[23] N. Massad-Ivanir, G. Shtenberg, T. Zeidman, and E. Segal, "Construction and Characterization of Porous SiO2/Hydrogel Hybrids as Optical Biosensors for Rapid Detection of Bacteria," *Adv. Funct. Mater.*, vol. 20, pp. 2269-2277, 2010.

[24] C. Lin, L. Jiang, H. Xiao, Y. Chai, S. Chen, and H. Tsai, "Fabry–Perot interferometer embedded in a glass chip fabricated by femtosecond laser," *OPTICS LETTERS*, vol. 34, No. 16, pp. 2408-2410, Aug. 2009.

[25] J. Villatoro, V. Finazzi, G. Coviello, and V. Pruneri, "Photonic-crystal-fiber-enabled micro-Fabry-Perot interferometer," *IEEE Trans. Opt. Lett.*, vol. 34, pp. 2441-2443, 2009.

[26] B. Schyrr, S. Boder-Pasche, R. Ischer, R. Smajda, G. Voirin, "Fiber-optic protease sensor based on the degradation of thin gelatin films," Sensing and Bio-Sensing Research, vol. 3, pp. 65-73, Mar. 2002.

[27] B. Qi, G. R. Pickrell, J. C. Xu, P. Zhang, Y. H. Duan, W. Peng, Z. Y. Huang, W. Huo, H. Xiao, R. G. May, and A. Wang, “Novel data processing techniques for dispersive white light interferometer,” Opt. Eng. 42(11), 3165–3171 (2003).

CHAPTER 5. BIOLOGICAL/CHEMICAL SENSING SYSTEM BASED ON DEGRADABLE HYDROGEL WITH FIBER OPTICS AND MICROFLUIDICS

5.1 Introduction

In the previous chapter, we had developed PAAm-based sensor systems with microfluidics or fiber optics to detect biological/chemical agents. In this system, the hydrogel has been used as sacrificial structures by decomposition in the presence of a stimulus, which is the target agent needing to be detected. In order to let the hydrogel response to the stimulus, the cross-linker used in the hydrogel should be responsible to and could be degraded by the target stimulus. After the degradation of the hydrogel by the related stimulus, the physical features, such as morphology and refractive index, will change. Therefore, through monitoring these physical changes, the related stimulus can be detected. Based on this mechanism, various different chemical/biological agents could be detected by integrating various different related cross-linkers to the hydrogel. In our research, two different cross-linkers were integrated to the hydrogel, N, N' – bis(Acryloyl) crystamine and modified SNAP 25-mer peptide. These two hydrogels were used to detect DTT and BoNT respectively.

Firstly, by screening the morphology changes of the hydrogel resulting from the decomposition by the related stimulus, the basic idea was confirmed. Then, we introduced the microfluidics to improve the sensitivity and detecting speed, because the microfluidics could be used to remove the degraded hydrogel to increase the decomposition reaction speed. Later, we introduced the fiber optics to further enhance

the sensitivity and detecting speed. Here, the fiber optics was used to monitor the refractive index change resulting from the decomposition of the hydrogel by related stimulus. Comparing to screening the morphology change of the hydrogel, monitoring refractive index by fiber optics can offer much higher sensitivity and bring much fast detecting speed, because a tiny refractive index could be observed far more earlier to a visible morphology change. In this chapter, we take BoNT-responsive hydrogel as a model, and combined the fiber optics and microfluidics together to further improve the sensitivity and detecting speed.

5.2 Experimental

5.2.1 Fabrication of sensing device

The sensing system combined Fabry Perot interferometer (FPI) and microfluidic structure together. The FPI part was fabricated firstly before being combined with the microfluidics structure. The fabrication of the sensing device is shown in Fig. 5.1. First, four glass slides were glued together by ultra-violet (UV) glue after being exposed to UV light with an intensity of 25 mW/cm^2 for 1 min (Fig. 5.1(a)). Second, the end-section of the output fiber of the fiber optics connector (FOC; PLC-1X2, Fibertronics, Inc., FL, USA) was cut with an optical fiber cutter, followed by polishing using 5 different polishing films successively to smoothen its surface. Third, the prepared FOC was fixed on a glass slide by six rectangular solid polydimethylsiloxane (PDMS) blocks with the end face of the FOC positioned out of the side face by around 500 μm. The sides of the six PDMS blocks were parallel to the long side of the glass slide, which is also the direction of the fiber. The structure was then applied liquid PDMS and placed on a hotplate at 90℃ for 60 min to cure

(Fig. 5.1(b)). Fourth, the components from step 1 and step 3 were combined using PDMS as adhesive (Fig. 5.1(c)). The process of combining the two was carefully performed under a microscope. The end of the fiber should be parallel to the opposite glass surface. It is important that the distance is around 100 μm between the end-section of the fiber and the corresponding opposite glass surface. If the distance is too large, the measured signal would be too weak; if the distance is too short, there would not be enough hydrogel between the two surfaces. Fifth, the two glass slides (the green ones in Fig. 5.1(d)) were adhered to the device using PDMS (Fig. 5.1(d)), and the distance of the two glasses is 2 mm. The end section surface and the glass surface thus formed an FPI cavity (the green area in Fig. 5.1(a)). The liquid pre-hydrogel would be injected into the cavity very carefully to make sure that the hydrogel was just located between the end surface of the optic fiber and the opponent glass surface (the green cuboid area in Fig. 5.1(g)). Sixth, a photopolymerizable prepolymer, isobornyl acrylate (IBA), was used to fabricate the IBA microfluidic structure mold on a glass slide as in Fig. 5.1(e). Seventh, the liquid PDMS was used to cover the IBA microfluidic structure mold fabricated in the last step, and it was placed on a hotplate at 90℃ for 60 min to cure. Then the PDMS copied the IBA shape in the PDMS to form the microfluidic structure in the PDMS (see Fig. 5.1(f)). Actually, the steps 6 and 7 were made at the same time with the previous 5 steps. After step 7 finished, the hydrogel was injected to the FPI cavity between the ending surface of the optic fiber and the opponent glass surface. Now it is ready to finish step 8. Eighth, UV glue was coated on the bottom surface with the exception of the channel area of the PDMS fabricated in step 7, before it was exposured to UV light (25 mW/cm^2, 250s). Then,

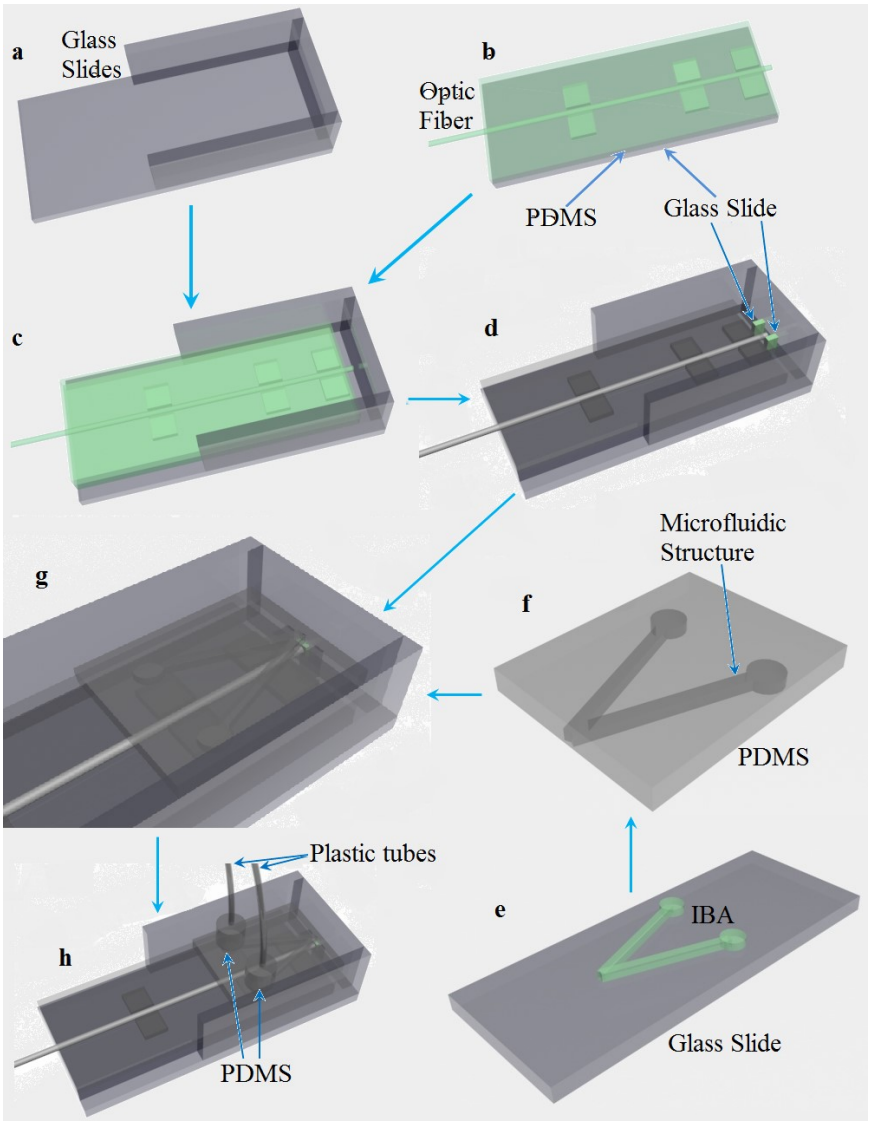

Fig. 5.1: The fabrication process of the sensing device. (a) Four glass slides are glued together. (b) The optic fiber is fixed on a glass slide with PDMS (in green). (c) The parts in (a) and (b) are combined using PDMS. (d) Two glass slides (in green) are glued to the device with PDMS. (e) IBA microfluidic structure mold. (f) Microfluidic structure in PDMS. (g) Bonding the microfluidic structure with FPI structure together, and polymerized the hydrogel in the FPI cavity area. (h) Connect microfluidic structure of the sensing device to outside by two plastic tubes.

the microfluidic structure PDMS was glued to the device fabricated in step 5, and at same time the hydrogel was polymerized and cross-linked (see Fig. 5.1(g)). Finally, two PDMS cylinder was bonded to the device, and the whole device was connected to outside part by two metal tubes and two long plastic tubes (see Fig. 5.1(h)). Here, the hydrogel we used is BoNT-responsive hydrogel, which is same as the one in chapter 2 and 3.

5.2.2 Experimental Setup

The photo of the sensing system setup is shown in Fig 5.2. In this setup, an OSA (AQ6370d, Yokogawa, Japan) was used to detect the interference spectrum of the reflected light. The light source (PLC-1X2, Fibertronics, Inc., FL, USA) was built into the OSA, which delivered wide-spectrum near-infrared light with the wavelength of between 1475 and 1485 nm. The resolution of the OSA was set at 0.5 nm, and each data was the result of averaging 5 measurements. In the Fig 5.3(c), one output of the fiber optic coupler (FOC) was connected to the built-in light source in the OSA. The other output of the FOC was connected to the input of the OSA for measurement. The input of the FOC was integrated into the sensing device during the fabrication, as shown in Fig. 5.2 (a). The microfluidic structure was connected to outside by two tubes (see Fig. 5.2(b)). One tube was connected to the inlet of the sensing device, and was used to inject liquid sample to micro-channel of the sensing system. The other end of the tube was connected to the syringe on the syringe pump (Cole-Parmer Multi-Syringe Pumps, Cole-Parmer, IL, USA). The other tube was connected to the outlet of the micro-channel of the sensing device used to take the waste liquid out to a waste container. The whole sensing device was kept in an incubator at a temperature

of 37±0.3 ℃. In order to avoid vibration of the device, which would induce inaccurate measurement of the highly-sensitive FPI, the incubator was placed on solid ground.

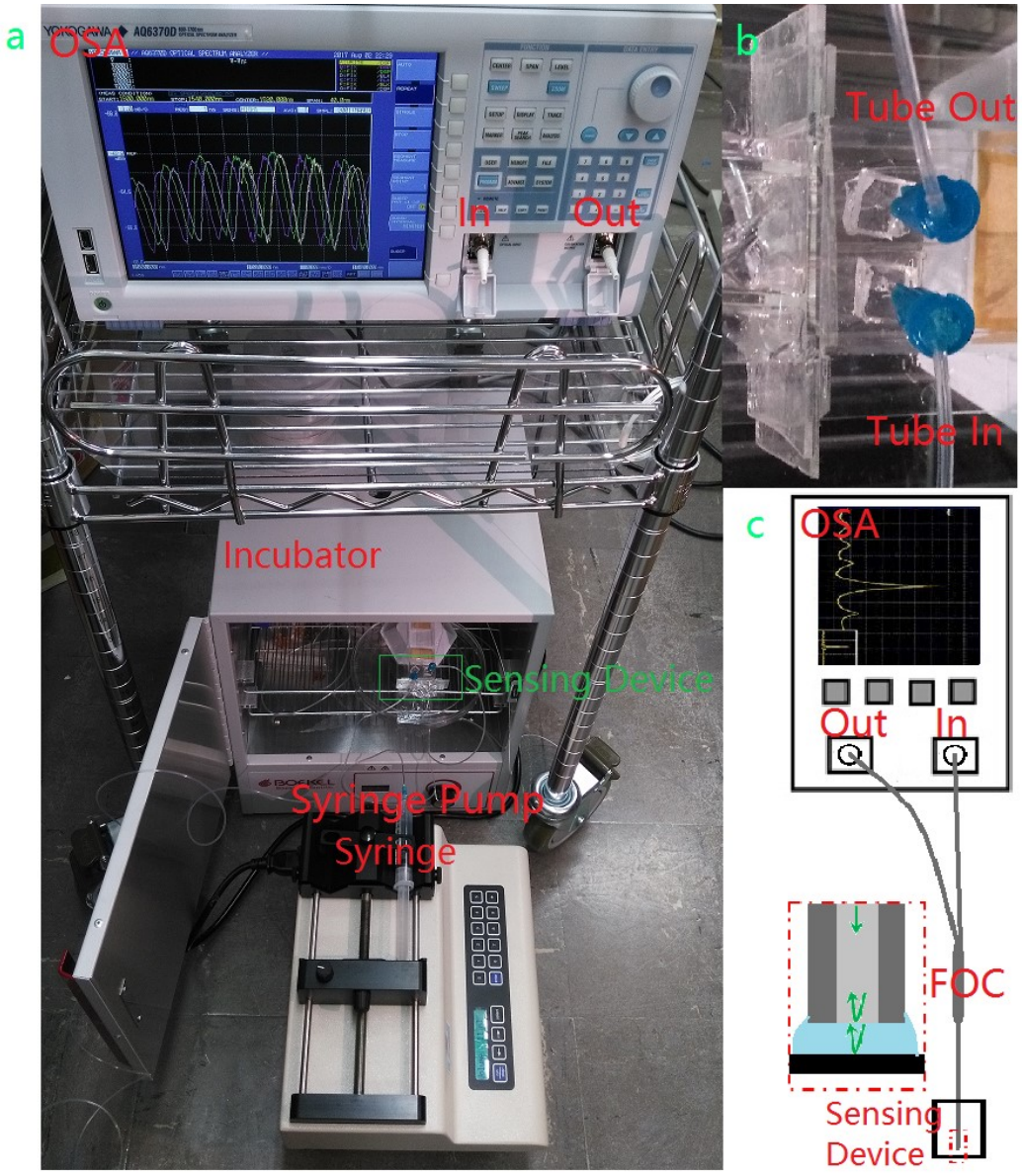

Fig. 5.2: Experimental setup of the sensing system. (a) Photo of the sensing system setup. (b) The enlarge view of the green rectangle area in (a). (c) Schematic diagram of the fiber optic part setup.

5.3 Result and Discussion

In this experiment, the sensing device was tested by DI water and light chain of BoNT (LC) respectively. In addition, we made two sensing devices: one was tested by liquid sample with flow rate of 0; while the other was tested with liquid flow rate of 0.1 ml/min, and the syringe was replaced every one hour.

The sensing system was tested by DI water and 4.5 ug/ml LC respectively. The Fig. 5.3 shows the results tested by DI water and LC (4.5 μg/ml), but there is no liquid flow in the micro-channel. In Fig. 5.3(a), the system was tested by DI water, and it shows the spectrum blue-shifts by around 1.2 nm from 30 mins to 24 hours. In Fig. 5.3(b), the system was tested by 4.5 μg/ml LC, and it shows the spectrum blue-shifts by around 2.2 nm from 30 mins to 24 hours. The LC can cleave the hydrogel in the sensing system, before it brought more blue-shift than the shift resulting from the DI water. The Fig. 5.4 also shows the results tested with DI water and 4.5 μg/ml LC, where we used the syringe pump to keep a fixed flow rate of 0.1 ml/min in the micro-channels. In Fig. 5.4(a-b), the system was tested by DI water, and it shows that the spectrum blue-shifts by around 9.6 nm from 30 mins to 24 hours. In Fig. 5.4(c-e), the system was tested with a flow of 4.5 μg/ml LC at the flow rate is 0.1 ml/min, and it shows the spectrum blue-shifts by around 14.4 nm from 30 mins to 24 hours. The existence of LC brought about 4.8 nm more blue-shift, in comparison with the existence of only DI water. The liquid flow brought more blue-shift in comparison with that without flow. By combining microfluidics with fiber optics, LC of 4.5 μg/ml was detected in 24 hours, while the previous method only with microfluidics in chapter 3 took 90 hours to detect the same concentration of LC. Therefore, it was

approved that the combination of microfluidics and fiber optics could enhance the detect speed. In addition, we thought the combination could also increase the sensitivity of the sensing system.

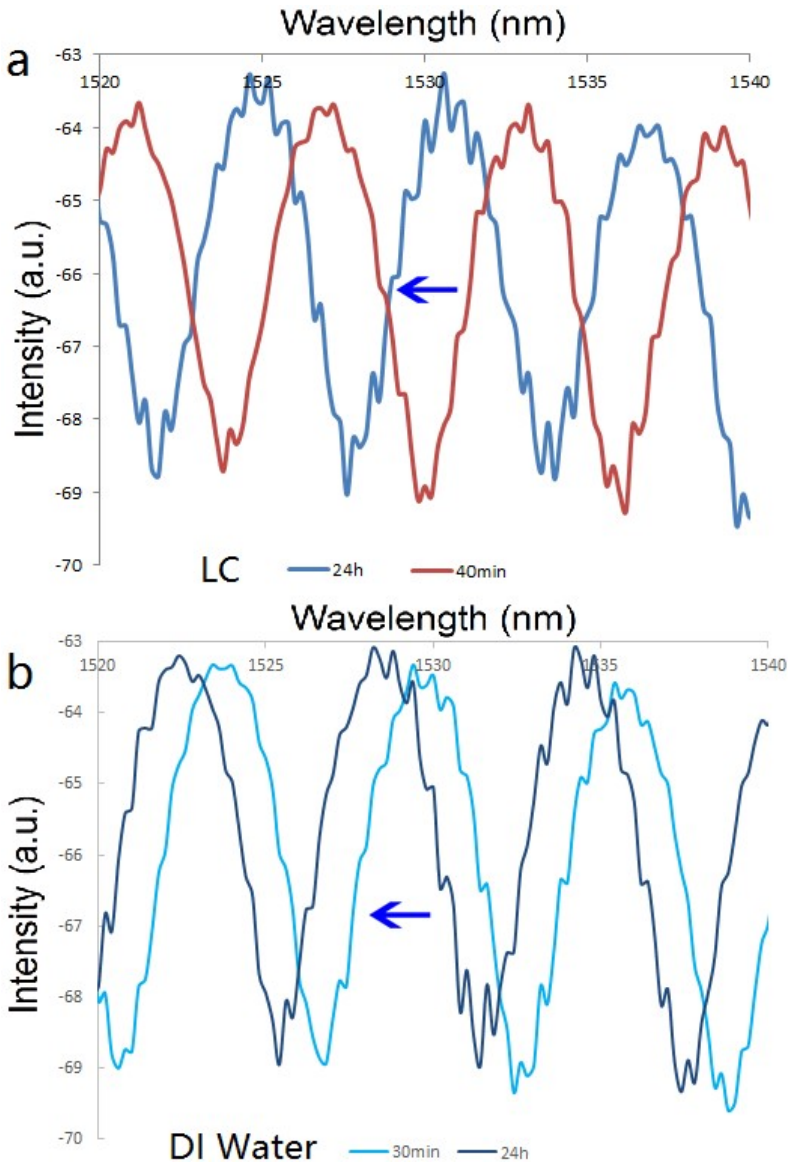

Fig. 5.3: Result tested by DI water and 4.5 μg/ml LC. (a) the interfering spectrum blue-shifts around 1.2 nm; (b) the interfering spectrum blue-shifts around 2.2 nm.

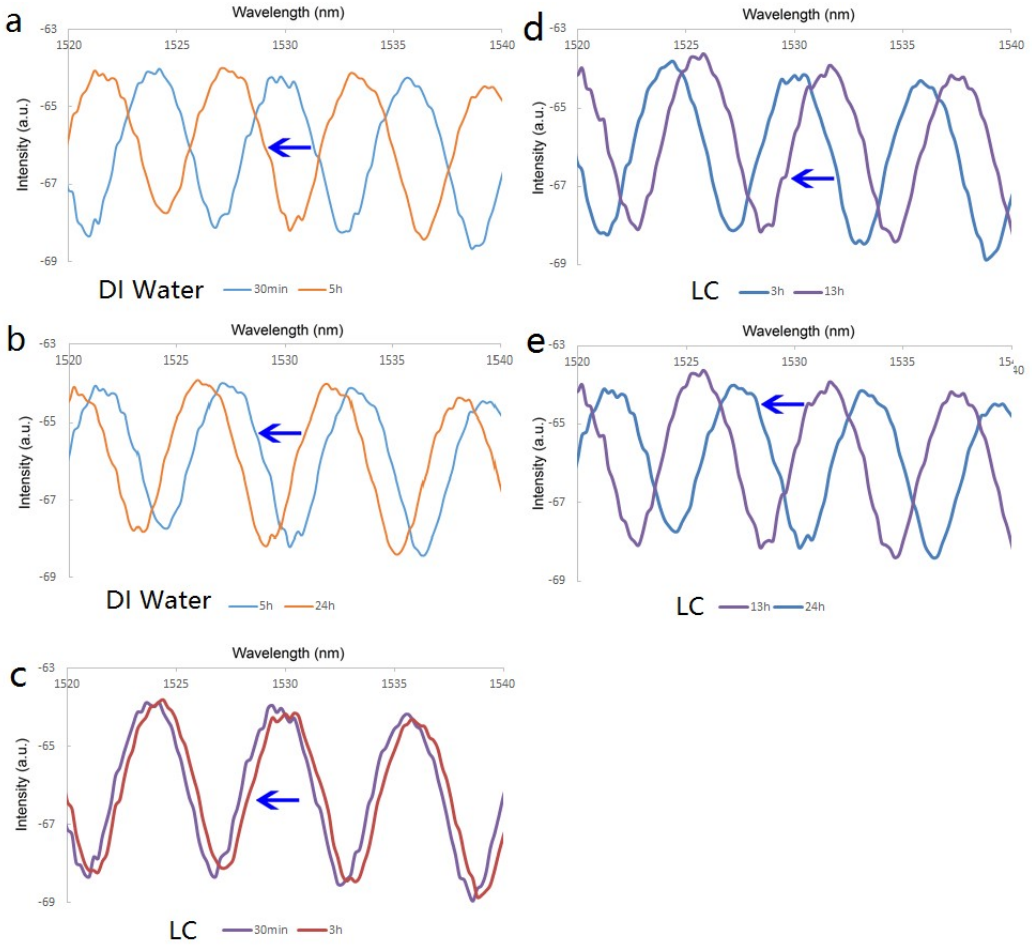

Fig. 5.4: Result tested by DI water and 4.5 µg/ml LC. (a-b) the interfering spectrum blue-shifts around 9.6 nm; (c-e) the interfering spectrum blue-shifts around 14.4 nm.

In addition, during the first 30 mins treated by sample solutions, the spectrum red-shifted for either DI water or LC. Besides, there was no much different for red-shift extent between the DI water and LC. We attributed this red-shift mostly to the temperature change. Especially, R. Barer et al. [1] and H. Zhao et al. [2] exploited the refractive index changing resulting from the existence of protein, and found that the change depended on the concentration of the LC. According to these works, we calculated that the refractive index change would be around 10-5 – 10-6. According to

the simulation in chapter 4, the refractive index change could only bring about around 10-2 – 10-3 nm red-shift, which is less than influence of the temperature vibration and matches our result. In order to double check the influence of the LC (4.5 μg/ml) to the refractive index, we designed another experiment. Specifically, we did not put hydrogel in the FPI cavity (the green cuboid area in Fig. 5.1(g)), but only injected a little water into the FPI area, before injected LC (4.5 μg/ml) very slowly at 0.01 ml/min. In this process, the refractive index in the FPI cavity area would change from the refractive index of the DI water to the refractive index of LC (4.5 μg/ml). If there is only very tiny refractive index change, such as 0.001, it could bring about the red-shift around 2 nm, which is a huge shift. But half an hour later, we did not find any visible shift (see Fig. 5.5).

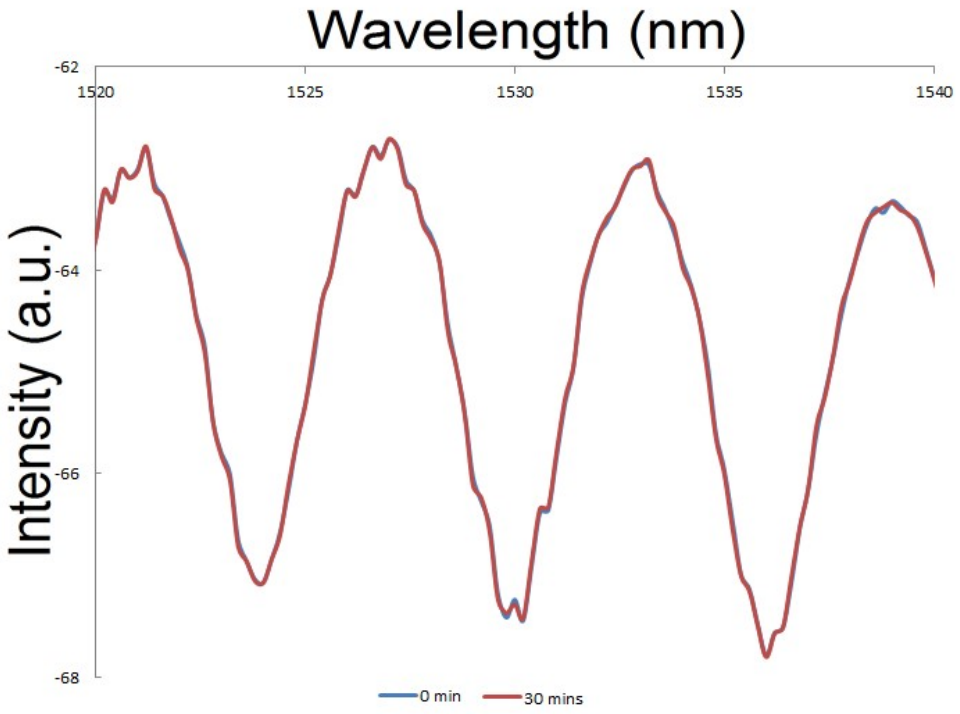

Fig. 5.5: The influence to the refractive index resulting from the LC of 4.5 μg/ml.

5.4 Conclusion

In this chapter, by combining the fiber optics with microfluidics, we fundamentally confirmed the combination can increase the detecting speed for our biological/chemical sensing system based on degradable hydrogel. We also believe it could enhance the sensitivity of our sensing system. Specifically, the LC of 4.5 μg/ml was detected in 24 hours. In comparison with the previous detecting time of 90 hours, the detecting speed was enhanced by around 4 times. By continuing the research, we believe it could further enhance the sensitivity and detecting speed of our sensing system.

5.5 Reference

[1] R. Barer, S. Tkaczyk, *Nature*, p821-822, v173, 1954.

[2] H. Zhao, P. H. Brown, P. Schuck, *Biophisical Journal*, p2309-2317, v100, 2011.

CHAPTER 6. SUMMARY AND FUTURE WORK

6.1 Summary

In this dissertation, we developed a prototype of PAAm-based sensor platform which could be used to detect chemical- and bio- agent with low-cost, easy-to-use, fast screening, and in-site detecting tool. By changing the crosslinker of the hydrogel, various agents could be detected. We also introduced microfluidics, fiber-optics together to improve the sensitivity of the sensor. So far, we had realized detecting chemical agent, DTT, and especially the most natural toxic substrate, BoNT.

First, we checked our idea fundamentally to confirm if the PAAm-based hydrogel could be used to detect chemical- and bio-agent. The PAAm-based hydrogel could be degraded by target agent. After the degradation of the hydrogel, the hydrogel could be solved by water, before the status of the hydrogel changed from solid to liquid, while the morphology of the hydrogel changed. We selected DTT and BoNT as two examples to test this idea. The DTT-responsive hydrogel was cleaved by DTT, while the degraded hydrogel could not be totally solved by water. The BoNT-responsive hydrogel could be cleaved by BoNT, although the degradation of the hydrogel was not very clear. However, when we flushed the BoNT treated BoNT-responsive hydrogel, some floccular materials came out of the hydrogel, which was a very important phenomenon. In order to make the morphology change of the hydrogel resulting from cleaving by target agent clearer and easier to be observed, and to improve the sensitivity, we introduced some types of solid powder (such carbon powder, carbon nanotube, graphene et al), dye, photonic crystal into the hydrogel. Among these materials used in the hydrogel, only the carbon powder worked well and

really improved the sensitivity. However the carbon powder only worked well for DTT-responsive hydrogel, not well for BoNT-responsive hydrogel. Especially, regarding to adding carbon powder to the BoNT-responsive hydrogel, we got one really good result that the 4.5 μg/mL BoNT (LC) was detected in 10 hours. However, the result was very hard to be repeated, because it was really hard to control the adding of the carbon powder to BoNT-responsive hydrogel. Later, we found the phenomenon of floccular materials during flushing the BoNT-responsive hydrogel. It was a very important phenomenon that could be used to improve the sensitivity of our sensor. The floccular materials resulted from the cleavage of the hydrogel and could cover the un-cleaved hydrogel, thus could block the contact between the un-cleaved hydrogel and target agent to hinder the cleavage reaction. If we could take the floccular materials away, we would increase the cleavage reaction and improve the sensitivity. Therefore, we flushed the hydrogel with DI water every four hours, and really found the flushing increased the degradation of the hydrogel. Based on this idea, we introduced the microfluidic system into our sensor platform latterly.

Second, a new microfluidics-based PAAm hydrogel sensor incorporating a modified SNAP-25 peptide for the detection of BoNT/A was developed. The new modified SNAP 25 peptide used in the hydrogels possesses an optimized sequence and conjugation sites for the APN crosslinker to anchor and a potential false alarm by DTT was removed. These gels could be degraded in trypsin, indicating that the modified SNAP 25 peptide was crosslinked into the hydrogel and was accessible to the enzyme. The degradation of the gels when exposed to the LC of BoNT/A depends on the concentration of LC, gel size, and reaction time. The BoNT/A can be detected by direct observation of the morphology change of the hydrogel. The best response of

the BoNT/A sensing hydrogel we achieved was within 22 h at 45 μg/mL of LC, and the lowest LC concentration of 4.5 μg/ in 90 h, with hydrogel post 200 μm in diameter and 50 μm in thickness. The hydrogels remained intact in both control buffer and DTT solutions. The non-response to DTT due to the removal of the disulfide bonds in the crosslinker is an improvement in comparison with prior art, since it eliminates potential false alarms due to cleavage of the disulfide bonds linking the peptide to the APN by DTT, a necessary reducing agent used to fully activate the BoNT/A in vitro tests. The newly designed SNAP-25 25-mer contributed greatly to the high sensitivity, specificity, and accuracy of sensing. The result shows the promise for this hydrogel to be used to detect bio-active BoNT/A.

Third, the detecting mechanism above was only based on naked human eyes, and the hydrogel needed to be nearly totally cleaved by target agent to allow that obvious changed could be observed by human naked eyes. Once the target agent contacted the hydrogel, the change of the hydrogel would start. Therefore, we tried to find another way to observe the change of the hydrogel based on the cleavage by target agent.We introduced the fiber-optics to further improve the sensitivity of our device. The optic fiber FPI device significantly improved the detection sensitivity and efficiency of biological and chemical sensors based on the degradation of hydrogels. The hydrogels that we used in this work was PAAm hydrogel. The disulfide bond in the crosslinker of the PAAm hydrogel can be cleaved by a solution containing DTT, resulting in optical property changes in the hydrogel, although they are not visually observable. By introducing the interfering optics shown in this work, such changes can be detected as the evidence of hydrogel cleavage. Our FPI device increased the detection sensitivity of DTT by 2000 times, and greatly reduced the detection period by several

times, comparing with prior work [1]. We tested our device with DTT solutions with different concentrations. Spectral shift in the interference spectra that combines both red and blue shifts were observed. Such unique spectral shifting process is related to the DTT diffusion and hydrogel cleavage processes, which provides high specificity as well as the capability to determine the concentration of the target agent. We demonstrated a low concentration of detection of 50 μM of DTT within 36 min. In future, we will explore to further improve the sensitivity and the detection speed by reducing the thickness of the hydrogel to accelerate the liquid diffusion and hydrogel reaction process. The centimeter-sized FPI sensors are promising for high-precision, ultra-sensitive and fast in-field detection of biological and chemical agents.

Finally, by combining the fiber optics with microfluidics, we fundamentally confirmed the combination can increase the detecting speed for our biological/chemical sensing system based on degradable hydrogel. We also believe it could enhance the sensitivity of our sensing system. Specifically, the LC of 4.5 μg/ml was detected in 24 hours. In comparison with the previous detecting time of 90 hours, this detecting speed was enhanced by around 4 times. By continuing the research, we believe it could further enhance the sensitivity and detecting speed of our sensing system.

6.2 Future Work

First, we planned to test our devices for long-time preservation in different real food matrices to study the effect of other bioactive compounds, and to validate our sensor using the whole toxin (full-length toxin rather than the LC alone). Second, we will optimize the microfluidic structures to remove the cleaved floccules hydrogel

more efficiently. Third, we will detect more chemical- and bio-agents by changing the cross-linker. Fourth, adding other materials, such as carbon powder, could really improve the sensitivity. However, its repeatability is very poor. Thus we will continue exploring to optimize the method of adding carbon powder or use other materials. After that, we will optimize the hydrogel itself to allow that the target agent could enter into the hydrogel easily and to increase the cleavage reaction. Finally, we will continue to optimize the fiber optical structure.

6.3 Reference

[1] S. S. Sridharamurthy, A. K. Agarwal, D. J. Beebe and H. Jiang, “Dissolvable membranes as sensing elements for microfluidics based biological/chemical sensors,” *Lab on a Chip*, vol. 6, pp. 840-842, May 2006.